وزارة التعليم العالي والبحث العلمي

UNIVERSITE BADJI MOKHTAR
BADJI MOKHTAR UNIVERSITY

جامعة باجي مختار - عنابة

Faculté des Sciences
Département de Physique

Année 2015

THESE

présentée en vue de l'obtention du diplôme de

DOCTORAT EN SCIENCES

Etude de la mobilité par la méthode quantique pour le cas d'un gaz de molécules de carbone ionisées diffusant dans un gaz rare

Option: Matière et Rayonnement

par

Lamia AISSAOUI

Directeur de thèse:	Moncef BOULEDROUA	Professeur	Université Badji Mokhtar, Annaba

Devant le Jury

Président:	Kamel ALIOUA	Professeur	Université Chérif Messadia, Souk-Ahras
Examinateurs:	Salim HOUAMER	Professeur	Université Ferhat Abbas, Sétif-1
	Abdelaziz MANSOURI	Professeur	Université Ferhat Abbas, Sétif-1
	Réda ATTALLAH	Professeur	Université Badji Mokhtar, Annaba
	Med Tahar BOUAZZA	Professeur	Université Badji Mokhtar, Annaba

ملخص

يكرس البحث في هذا العمل على الحسابات العددية لمعلمات النقل : التنقل والانتشار للجملة CHe^+. لإنجاز هذه المهمة، قمنا أولا ببناء منحنيات الطاقة الكمونية الموافقة لتفاعل الحالة الأساسية $C^+(^2P°)$ والحالة المثارة $C^+(^4P)$ مع الحالة الأساسية للهليوم $He(^1S)$ بواسطة البرنامج MOLPRO. ثم استخدمنا كل طاقات التفاعل الكمونية من اجل حساب المقاطع الفعالة الكمية والكلاسيكية. أخيرا أجرينا حساب معاملات التنقل والنشر باستعمال النظرية الحركية المتطورة : نظرية درجات الحرارة الثلاث. تظهر نتائج معامل التنقل المحققة مدى فاعلية منحنيات الطاقة الكمونية التي كونها، وتكشف أيضا قابلية المقاطع الفعالة الكمية مع نظرية درجات الحرارة الثلاث في اطار تحسين نتائج التنقل.

Résumé

La recherche de ce travail est consacrée aux calculs numériques des paramètres de transport : la mobilité réduite et la diffusion du système CHe^+. Pour accomplir cette tâche, nous avons d'abord construit les courbes d'énergie potentielle correspondant à l'interaction de l'état fondamental $C^+\left(^2P^\circ\right)$ et de l'état excité métastable $C^+\,(^4P)$ avec l'état fondamental de l'hélium $He\,(^1S)$ qui sont obtenus avec le programme MOLPRO. Ensuite, nous avons utilisé ces potentiels d'interaction dans le calcul des sections efficaces de transport quantiques et classiques. Enfin, nous avons calculé les coefficients de mobilité et de diffusion en utilisant la théorie cinétique élaborée : théorie de trois températures. Les résultats obtenus de la mobilité montrent la fiabilité de notre construction des courbes d'énergie potentielle et illustrent également la viabilité des sections efficaces de transport quantiques avec la théorie de trois températures pour améliorer les résultats de la mobilité.

Abstract

The research of this work is devoted to the numerical calculations of the transport parameters : the reduced mobility and diffusion of the CHe^+ system. To accomplish this task, we first constructed the potential-energy curves corresponding to the interactions of the ground $C^+\left(^2P^\circ\right)$ and metastable-excited $C^+\left(^4P\right)$ states with the ground state of helium $He\left(^1S\right)$ which are achieved with the package MOLPRO. Then, we used these interaction potentials in the calculation of the quantum-mechanical and classical transport cross sections. Finally, we computed the mobility and diffusion coefficients by using the high kinetic theory : three temperature theory. The attained results of mobility show the reliability of our constructed potential-energy curves, and reveal also the viability of the quantum-mechanical transport cross sections with the three-temperature theory as to improve the results of mobility.

Acknowledgements

First and foremost, I would like to thank my supervisor Dr **Moncef BOULEDROUA,** Professor at the Faculty of Medicine in Badji Mokhtar University-Annaba, for his continual encouragements and interests throughout the course of this work. His guidance were crucial for the successful completion of this project. I appreciated the richness of his scientific ideas. I sincerely thank him for accepting to supervise my work.

I deeply thank Dr **Kamel ALIOUA,** Professor at Chérif Messadia University of Souk-Ahras, for giving me the honor to be interested in my work, agreeing to judge it, and presiding the Jury. I also thank him for helping me to carry out some parts of this work.

I am also very thankful to Drs **Salim HOUAMER** and **Abdelaziz MANSOURI,** both Professors at Sétif-1 University, for agreeing to honor with their presence in my thesis Jury.

I would like to thank Drs **Réda ATTALLAH** and **Mohamed Tahar BOUAZZA,** Professors at Badji Mokhtar University in Annaba, for accepting to participate in the Jury of this thesis. It is here the most distinguished feelings.

Finally, this work was realized as part of the scientific activities of the Radiation Physics Laboratory (LPR) of the Physics Department at Badji Mokhtar University, Annaba. I thank all his members for their encouragements.

Annaba, May 30, 2015

Lamia AISSAOUI

Contents

List of Tables

List of Figures

Introduction

The behavior of ions in gases is an area of continuing interest. Models of the upper atmosphere, interstellar chemistry, lasers, and many other fields of physics and chemical physics require quantitative information concerning the atomic or molecular ion-neutral gas interaction over a wide range of temperature and/or collision energy.

The theoretical predictions and interpretations of most phenomena involving ions in neutral gases hang on the information we have on the ion-neutral interaction potential. Since the *ab initio* calculations are extremely difficult for most systems, the usually employed methods to get the interaction potentials are the careful analysis of the accurate measurements of a given property that depends on the potential in a well-established way. Nevertheless, since a unique determination of the potential from a measured property is seldom possible, even in principle, a more indirect procedure is usually followed: a mathematical model containing a few parameters is chosen for the potential, and then the parameters are adjusted to obtain agreement with the measured property. Such models are ordinarily selected to reproduce various known asymptotic forms of the true potential and to behave in a qualitatively correct way in intermediate regions. A major step in such a procedure is the calculation of the experimental property from the potential model, a process which may require extensive numerical integration. This approach has a long and successful history for the determination of neutral-neutral potentials. However, until recently the approach has been of very limited utility for ion-neutral potentials. The reason is that the theory requires measurements of the ion mobility in weak electric fields as a function of temperature, and very few good experimental data were available.

It has long been realized that if mobility data covering such a wide range of ion energies could be analyzed accurately, information on the ion-neutral potential could be derived that would span a wide range of ion-neutral separation distances. The difficulty was that an accurate general mobility theory existed only for weak electric fields. For that reason, Viehland and Mason [1,2] have developed a rigorous kinetic theory of the ion mobility that is appropriate for

electric fields of arbitrary strength. Therefore, it is now possible to determine ion-neutral potentials over an extensive range of separation distances by the traditional procedure of adjusting the parameters of potential models.

The main objective of this work comes from the recommendations of Matoba *et al.* [3], who proposed to calculate the mobility of ground and metastable-excited states of C^+ ions moving into a helium buffer gas using the *three*-temperature theory for solving the Boltzmann kinetic equation with *full quantum-mechanical* transport cross sections. These recommendations are suggested to improve the results of the mobility of CHe^+ system.

Therefore, the work described in this thesis is primarily concerned with the determination of the kinetic theory of ion transport in gas, where the successful *two*-temperature theory by Viehland and Mason [1, 2] and the more accurate *three*-temperature theory of Lin *et al.* [4] are both briefly detailed in Chapter 1. Because of the relationship between these kinetic theories and the ion transport properties, we have also determined both ion mobility and ion diffusion, which are calculated in the last Chapter.

The major details of the calculation of the theoretical interaction potentials for the open shell CHe^+ system and of the classical and quantum-mechanical cross sections are outlined in Chapter 2.

Finally, to further investigate the effects of the quantum-mechanical cross sections and the *three*-temperature theory on ion mobility, we introduced the obtained values of the quantum-mechanical diffusion cross sections into the Fortran code GC.F90 [5–7] to compute the mobilities of the ground $C^+\left(2s^2 2p;\ {}^2P^\circ\right)$ and metastable-excited $C^+\left(2s2p^2;\ {}^4P\right)$ ions in a helium $He\left(1s^2;\ {}^1S\right)$ gas at very low temperatures. We conclude this Chapter 3 by comparing and discussing the quantum-mechanical and classical results.

Chapter 1

Theoretical Background of Ion Transport

The foundations of the ion mobility theory have been extensively detailed by several authors and investigators, such as in the books of McDaniel and Mason [8, 9] which both treat the transport phenomena of ions in like and unlike atomic or molecular gases. Their investigations are either theoretical or experimental. In this Chapter, we hence attempt to give succinct details of the ion transport theories that will be needed in the last Chapter.

1.1 Moment equations

Boltzmann's equation is the fundamental kinetic equation for the transport of atomic ions moving through a pure and dilute atomic gas without chemical reactions. It is written as [10,11]

$$\left\{\frac{\partial}{\partial t}+\mathbf{v}\cdot\boldsymbol{\nabla}_r+\frac{q}{m}\left[\mathbf{E}\left(\mathbf{r},t\right)+\mathbf{v}\times\mathbf{B}\left(\mathbf{r},t\right)\right]\cdot\boldsymbol{\nabla}_v\right\}f\left(\mathbf{r},\mathbf{v},t\right)=Jf\left(\mathbf{r},\mathbf{v},t\right), \tag{1.1}$$

where $f\left(\mathbf{r},\mathbf{v},t\right)$ is the ion distribution function, which is implicitly a function of time t, $\mathbf{r}$ is the ion position, $\mathbf{v}$ is the ion velocity in the laboratory frame, and $\mathbf{E}\left(\mathbf{r},t\right)$ and $\mathbf{B}\left(\mathbf{r},t\right)$ are the external electric and magnetic fields, respectively. Boltzmann's collision operator J can be written in a way that allows it to be used with either a classical or a quantum mechanical description of the collision between an atomic ion and a neutral atom as

$$Jf\left(\mathbf{r},\mathbf{v},t\right)=\int\left[f\left(\mathbf{r},\mathbf{v}',t\right)F(\mathbf{V}')-f\left(\mathbf{r},\mathbf{v},t\right)F(\mathbf{V})\right]g\sigma\sin\theta d\theta d\phi d\mathbf{V}, \tag{1.2}$$

with

$$F(\mathbf{V}) = N\left(M/2\pi k_{\mathrm{B}}T\right)^{3/2}\exp\left(-MV^2/2k_{\mathrm{B}}T\right), \tag{1.3}$$

being the neutral distribution function which can be taken as Maxwellian, and

$$g = |\mathbf{v}-\mathbf{V}| = |\mathbf{v}'-\mathbf{V}'|, \tag{1.4}$$

is the relative velocity between an atomic ion velocity, $\mathbf{v}$, and an atomic gas velocity, $\mathbf{V}$. This equation reveals the conservation energy of the pre-collision velocities, $\mathbf{v}$ and $\mathbf{V}$, with the post-collision velocities, $\mathbf{v}'$ and $\mathbf{V}'$. Here, σ is the total differential scattering cross section for ionic atom-neutral atom collisions, T is the gas temperature, N is the atomic gas number density with identical mass M, and k_{B} is Boltzmann's constant. Besides, the ion density, n, is neglected compared to the one of the atomic gas, because of the ionic atom-neutral atom collisions are usually considered as elastic collisions.

With the aim of calculating the transport coefficients of the ions in the drift tube, one requires from the solution of Boltzmann's equation (1.1) to yield f, from which all ion properties can then be acquired. Unfortunately, only trivial solutions to Boltzmann's equation are known. Therefore, Eq. (1.1) is converted into a set of moment equations by multiplying from the left by an arbitrary set of functions $\psi(\mathbf{v})$ and integrated over $\mathbf{v}$ as [10, 11]

$$\frac{\partial}{\partial t}\int \psi f d\mathbf{v} + \int \psi \mathbf{v}\cdot\boldsymbol{\nabla}_r f d\mathbf{v} + \frac{q}{m}\int \psi\left[\mathbf{E}\left(\mathbf{r},t\right) + \mathbf{v}\times\mathbf{B}\left(\mathbf{r},t\right)\right]\cdot\boldsymbol{\nabla}_v f = \int \psi J f d\mathbf{v}. \tag{1.5}$$

We neglect the effect of boundaries and transients by adopting the same assumptions made in the analysis of the experimental drift tube data [10, 11], namely, those properties other than the ion number density n does not vary with position and the time scale for the variation of all macroscopic properties except n is much longer than the mean time between collisions. These suppositions let certain terms in the moment equations (1.5) to be dropped, after some mathematical manipulations and the use of the equation of continuity. [2, 9]. Thus, one gets four terms that can be expressed in terms of the moments defined by the relation [10–12]

$$\overline{\psi}\left(\mathbf{r},t\right) = \frac{1}{n\left(\mathbf{r},t\right)}\int f\left(\mathbf{r},\mathbf{v},t\right)\psi(\mathbf{v})d\mathbf{v}, \tag{1.6}$$

where the other moments of $f(\mathbf{r},\mathbf{v},t)$ vary much less rapidly with position and time than does

the ion number density [10–12]

$$n(\mathbf{r},t)=\int f(\mathbf{r},\mathbf{v},t)\,d\mathbf{v}. \tag{1.7}$$

By using Eqs. (1.5), (1.6), and (1.7), we get the following expression

$$\frac{\partial}{\partial t}n(\mathbf{r},t)\,\overline{\psi}+\boldsymbol{\nabla}_r\cdot n(\mathbf{r},t)\,\overline{\psi\mathbf{v}}-\frac{q}{m}n(\mathbf{r},t)\,\overline{(\mathbf{E}+\mathbf{v}\times\mathbf{B})\cdot\boldsymbol{\nabla}_v\psi}=n(\mathbf{r},t)\,N\overline{J^{\dagger}\psi}. \tag{1.8}$$

In the case where $\psi(\mathbf{v})=1$, Eq. (1.8) simplifies to the equation of continuity given by [10–12]

$$\frac{\partial}{\partial t}n(\mathbf{r},t)+\boldsymbol{\nabla}_r\cdot n(\mathbf{r},t)\,\overline{\mathbf{v}}=0, \tag{1.9}$$

which is a straightforward expression of conservation of ions in a system where reactions cannot occur. It can also be used to eliminate the time derivative of the ion number density from Eq. (1.8). After making a minor rearrangement and dropping explicit indication of the dependence of every quantity upon position and time, Eq. (1.8) becomes [10–12]

$$\frac{\partial}{\partial t}\overline{\psi}-\frac{q}{m}\overline{(\mathbf{E}+\mathbf{v}\times\mathbf{B})\cdot\boldsymbol{\nabla}_v\psi}-\overline{J^{\dagger}\psi}=R\left(\overline{\psi}\right), \tag{1.10}$$

where

$$R\left(\overline{\psi}\right)=\left(\overline{\psi}\overline{\mathbf{v}}-\overline{\psi\mathbf{v}}\right)\cdot\boldsymbol{\nabla}_r\ln n+\left(\overline{\psi}\boldsymbol{\nabla}_r\cdot\overline{\mathbf{v}}-\boldsymbol{\nabla}_r\cdot\overline{\psi\mathbf{v}}\right). \tag{1.11}$$

Eq. (1.10) is exact and has the same level of mathematical rigor as Boltzmann's equation (1.1), from which it was derived.

From the inverse encounter property of the collision operator for ion-atom collisions, it can be shown that, without indicating dependences upon $\mathbf{r}$ and t,

$$\overline{J^{\dagger}\psi}=-\frac{1}{n}\int f(\mathbf{v})\,F(\mathbf{V})\left[\psi(\mathbf{v})-\psi(\mathbf{v}')\right]g\sigma(g,\theta_c)\sin\theta_c d\theta_c d\phi_c d\mathbf{V}d\mathbf{v}. \tag{1.12}$$

The negative sign reflects simply a preference for having the difference in the integrand between the pre-collision value and the post-collision value, rather than the reverse.

For more general ion-neutral gas systems, most techniques for solving Boltzmann's equation are special cases of the weighted residuals method that may be considered as based upon three choices. The first choice is the ion velocity function $f_0(\mathbf{v})$ that represents a *zero-order* estimate of the unknown distribution function $f(\mathbf{r},\mathbf{v},t)$. The second is a set of *trial functions* $\phi_{l,m,r}(\mathbf{v})$,

where three indices are needed because of the three-dimensional nature of ion velocity $\mathbf{v}$. The *zero-order distribution function* and the trial function are used together to expand $f(\mathbf{r},\mathbf{v},t)$. The third choice is a set of *weighting functions* $\Psi_{l,m,r}(\mathbf{v})$ used to convert the kinetic equation into a set of coupled, linear, and algebraic equations as

$$f(\mathbf{r},\mathbf{v},t) = n(\mathbf{r},t)\, f_0(\mathbf{v}) \sum_{l,m,r} c_{l,m,r}(\mathbf{r},t)\, \Psi_{l,m,r}(\mathbf{v}), \tag{1.13}$$

where

$$(\Psi_{l,m,r}, \Psi_{l',m',r'}) = \int f_0(\mathbf{v})\, \Psi^*_{l,m,r}(\mathbf{v})\, \Psi_{l',m',r'}(\mathbf{v})\, d\mathbf{v} = \delta_{l,l'}\delta_{m,m'}\delta_{r,r'}N_{l,m,r}. \tag{1.14}$$

Here, the asterisk indicates a complex conjugate and the normalization constants $N_{l,m,r}$ depend upon the particular basis functions being used. There is no error introduced by making these assumptions as long as we use all possible values of the indices and the basis functions form a complete set in velocity space, i.e., as long as the difference between the right-hand side of Eq. (1.13) and any piecewise continuous function of the velocity converges to zero as the upper limit on the sums becomes infinite [10–12].

1.1.1 Two-temperature theory

The tow-temperature theory was performed to overcome the high field divergence problems of the one-temperature theory. The success of this theory has been attained in describing the ion mobility in drift-tube experiments [1] by using a *zero-order approximation* to the ion distribution function containing an ion kinetic temperature T_i and a neutral atomic temperature T. Hence, the approach for solving Boltzmann's equation for ion swarms in neutral gases is based on [12]

$$f_0^{(2T)}(\mathbf{v}) = \left(\frac{m}{2\pi k_{\mathrm{B}} T_i}\right)^{3/2} \exp\left(-\frac{m\mathbf{v}^2}{2k_{\mathrm{B}}T_i}\right), \tag{1.15}$$

where m and $\mathbf{v}$ are the ion mass and ion velocity in the laboratory frame, respectively. The basis functions for this theory are chosen to be Burnett functions, namely, [13, 14]

$$\Psi^{(2T)}_{l,m,r}(\mathbf{v}) = W^l S^{(r)}_{l+1/2}\left(W^2\right) Y^m_l\left(\hat{W}\right), \tag{1.16}$$

where

$$\hat{W} = \left(\frac{m}{2k_{\mathrm{B}}T_i}\right)^{1/2} \mathbf{v}. \tag{1.17}$$

Here, the indices l and r are non-negative indices that indicate a particular Sonine (generalized Laguerre) polynomial $S_{l+1/2}^{(r)}\left(W^2\right)$. The indices l and m are coupled together to indicate a particular (normalized) complex spherical harmonic $Y_l^m\left(\hat{W}\right)$ of the angles W. Therefore,

$$N_{l,m,r}^{(2T)} = \frac{\Gamma\left(l+r+3/2\right)}{4\pi r!\Gamma\left(3/2\right)}, \tag{1.18}$$

and

$$c_{0,0,0}^{(2T)} = \left(4\pi\right)^{1/2}. \tag{1.19}$$

The two-temperature theory converges well only once the mass of the ion is less than that of the neutral. The reason is that for heavy ions in a light gas, the ion distribution function becomes anisotropic and skewed in the field direction, and diffusion is more sensitive than mobility to such anisotropy.

a) Moment equation for velocity

Putting $\psi\left(\mathbf{v}\right) = \mathbf{v}_z$ into Eq. (1.10) leads to

$$\frac{\partial}{\partial t}\overline{\mathbf{v}_z} - \frac{q}{m}\overline{\left(\mathbf{E}+\mathbf{v}\times\mathbf{B}\right)_z} - \overline{J^\dagger \mathbf{v}_z} = R\left(\overline{\mathbf{v}_z}\right). \tag{1.20}$$

After using Eqs. (1.3), (1.12), (1.13), and (1.15), we find that

$$\overline{J^\dagger \mathbf{v}_z} = -N\sum_{l,m,r} c_{l,m,r}^{(2T)}\left(\Psi_{l,m,r}, J^\dagger \mathbf{v}_z\right)^*, \tag{1.21}$$

where $\left(\Psi_{l,m,r}, J^\dagger \mathbf{v}_z\right)$ can be calculated by using the notations of section 6.2 of Ref. [9]

$$\left(A, J^\dagger B\right) = \left(\frac{m}{2\pi k_{\mathrm{B}}T_i}\right)^{3/2}\left(\frac{M}{2\pi k_{\mathrm{B}}T}\right)^{3/2}\int \exp\left(-\frac{m\mathbf{v}^2}{2k_{\mathrm{B}}T_i} - \frac{M\mathbf{V}^2}{2k_{\mathrm{B}}T}\right) A^*\left(\mathbf{v}\right) \times \left[B\left(\mathbf{v}\right) - B\left(\mathbf{v}'\right)\right] g\sigma\left(g,\theta_c\right)\sin\theta_c d\theta_c d\phi_c d\mathbf{V} d\mathbf{v}. \tag{1.22}$$

In two-temperature theory, we have

$$\Psi_{1,0,0}^{(2T)}\left(\mathbf{v}\right) = \left(\frac{3}{4\pi}\right)^{1/2}\left(\frac{m}{2\pi k_{\mathrm{B}}T_i}\right)^{1/2}\mathbf{v}_z. \tag{1.23}$$

We therefore find that

$$\overline{J^{\dagger}\mathbf{v}_z} = -N\left(\frac{4\pi}{3}\right)^{1/2}\left(\frac{2\pi k_{\mathrm{B}}T_i}{m}\right)^{1/2}\sum_{l,m,r} c_{l,m,r}^{(2T)}\left(\Psi_{l,m,r},\Psi_{1,0,0}^{(2T)}\right)^{*} \tag{1.24}$$

$$= -N\left(\frac{4\pi}{3}\right)^{1/2}\left(\frac{2\pi k_{\mathrm{B}}T_i}{m}\right)^{1/2}\sum_{l,m,r} c_{1,0,r}^{(2T)}N_{1,0,r}^{(ZT)}a_{0,r}\left(1\right). \tag{1.25}$$

Eq. (1.25) arises because Boltzmann's collision operator is a scalar operator, so its matrix elements with respect to Burnett functions must be real, diagonal in the l and m indices, and independent of the m indices.

From Eq. (1.23), it can be seen that Eq. (1.25) is a special case of the general formula

$$\overline{J^{\dagger}\Psi_{l',m',r'}^{(2T)}\left(\mathbf{v}\right)} = -N\sum_{l,m,r} c_{l',m',r}^{(2T)}N_{l',m',r}^{(2T)}a_{r',r}\left(l'\right). \tag{1.26}$$

And from Eqs. (1.6), (1.13), and (1.23), we can obtain another general formula as

$$\overline{\Psi_{l',m',r'}^{(2T)}\left(\mathbf{v}\right)} = c_{l',m',r'}^{(2T)}N_{l',m',r'}^{(2T)}. \tag{1.27}$$

If we separate in Eq. (1.25) the term of $r=0$ from the other terms, insert the expression into Eq. (1.20), and make use of Eqs. (1.26) and (1.27), we get

$$\frac{\partial}{\partial t}\overline{\mathbf{v}_z} - \frac{q}{m}\overline{\left(\mathbf{E}+\mathbf{v}\times\mathbf{B}\right)_z} + Na_{0,0}\left(1\right)\overline{\mathbf{v}_z}$$
$$= R\left(\overline{\mathbf{v}_z}\right) - N\left(\frac{4\pi}{3}\right)^{1/2}\left(\frac{2k_{\mathrm{B}}T_i}{m}\right)^{1/2}\sum_{r>0} c_{1,0,r}^{(2T)}N_{1,0,r}^{(2T)}a_{0,r}\left(1\right). \tag{1.28}$$

In the context of the two-temperature theory, Eq. (1.28) is called *moment equation for velocity* along the z direction. It is exact if no approximations or truncations are made on the right-hand side. Note, however, that knowledge of higher order moments must be available before the right-hand side is completely specified and thus before the equation can be solved for $\mathbf{v}_z$, just like knowledge of $\mathbf{v}$ must be available before the equation of continuity can be solved for the ion number density. This is a general aspect of the moment method for solving Boltzmann's equation: each equation involves one or more higher order moments and, then, some approximations must be made in order to truncate the system.

From Eq. (1.28), we can take the general expression for the *collision frequency for momentum-transfer* $\zeta(T_{eff})$, that is, $Na_{0,0}\left(1\right)$ within the context of the two-temperature theory. By using

table $(6-2-1)$ of Ref. [9], we get

$$\zeta(T_{eff}) = N a_{0,0}(1) \tag{1.29}$$

$$= \frac{8N}{3}\frac{M}{m+M}\left(\frac{2k_{\mathrm{B}}T_{eff}}{\pi\mu}\right)^{1/2}\overline{\Omega}^{(1,1)}(T_{eff}), \tag{1.30}$$

where

$$T_{eff} = \frac{mT + MT_i}{m+M}, \tag{1.31}$$

is the effective temperature that characterizes the kinetic energy of an ion-neutral gas collision in the centre-of-mass frame and μ is the ion-neutral reduced mass. Note that $\zeta(T_{eff})$ has a microscopic definition, since the momentum-transfer collision integral, also called collision integral, $\overline{\Omega}^{(1,1)}(T_{eff})$ is given by

$$\begin{aligned}\overline{\Omega}^{(1,1)}(T_{eff}) &= \left(\frac{3}{4\pi}\right)\int_{-\infty}^{+\infty}\int_{-\infty}^{+\infty}\int_{-\infty}^{+\infty}\exp\left(-\gamma_x^2-\gamma_y^2-\gamma_z^2\right)\gamma_z^2\gamma Q_d\left(k_{\mathrm{B}}T_{eff}\gamma^2\right)d\gamma_x d\gamma_y d\gamma_z \\ &= \int_0^{+\infty}\exp\left(-\gamma^2\right)Q_d\left(k_{\mathrm{B}}T_{eff}\gamma^2\right)\gamma^5 d\gamma,\end{aligned} \tag{1.32}$$

with $\gamma^2 = \epsilon/k_{\mathrm{B}}T$. The collision integral can be calculated as a function of T_{eff} from the knowledge of only the ion and neutral masses and the ion-neutral interaction potential energy as a function of the internuclear separation [9]. Consequently, Eq. (1.28) can be rewritten as

$$\frac{\partial}{\partial t}\overline{\mathbf{v}_z} - \frac{q}{m}\overline{(\mathbf{E}+\mathbf{v}\times\mathbf{B})_z} + \zeta(T_{eff})\overline{\mathbf{v}_z} = R\left(\overline{\mathbf{v}_z}\right) + \left[\zeta(T_{eff})\overline{\mathbf{v}_z} + \overline{J^\dagger \mathbf{v}_z}\right], \tag{1.33}$$

which can more easily be obtained by adding $\zeta(T_{eff})\overline{\mathbf{v}_z}$ to both sides of Eq. (1.20). We can also obtain the same form for the x and y directions, with the obvious change of subscript.

b) Moment equation for energy

By inserting the special function $\psi(\mathbf{v}) = \frac{1}{2}mv^2$ into Eq. (1.10), we obtain

$$\frac{\partial}{\partial t}\overline{\frac{1}{2}mv^2} - q\mathbf{E}\cdot\overline{\mathbf{v}} - \overline{J^\dagger\left(\frac{1}{2}mv^2\right)} = R\left(\overline{\frac{1}{2}mv^2}\right), \tag{1.34}$$

with

$$\overline{(\mathbf{E}+\mathbf{v}\times\mathbf{B})\cdot\boldsymbol{\nabla}_v\left(\frac{1}{2}mv^2\right)} = m\overline{(\mathbf{E}+\mathbf{v}\times\mathbf{B})\cdot\mathbf{v}} = m\mathbf{E}\cdot\overline{\mathbf{v}}. \tag{1.35}$$

Here, the magnetic field does not directly affect the ion kinetic energy. From Eq. (1.16), we can note that

$$\overline{J^{\dagger}\left(\frac{1}{2}mv^{2}\right)}=(4\pi)^{1/2}\,k_{\mathrm{B}}T_{i}\left[\frac{3}{2}\overline{J^{\dagger}\Psi_{0,0,0}^{(2T)}\left(\mathbf{v}\right)}-\overline{J^{\dagger}\Psi_{0,0,1}^{(2T)}\left(\mathbf{v}\right)}\right]. \tag{1.36}$$

We use Eq. (1.26) to get

$$\overline{J^{\dagger}\psi_{l',m',r'}^{(2T)*}\left(\mathbf{v}\right)}=-N\sum_{l,m,r}c_{l',m',r}^{(2T)*}N_{l',m',r}^{(2T)}a_{r',r}\left(l'\right), \tag{1.37}$$

since $N_{l',m',r}^{(2T)}$ and $a_{r',r}\left(l'\right)$ are real [9] and, for all values of r in Eq. (1.37), the coefficients $c_{l',m',r}^{(2T)}$ must be real if $\Psi_{l',m',r'}^{(2T)}\left(\mathbf{v}\right)$ is real as well, as in Eq. (1.36). Hence,

$$\overline{J^{\dagger}\left(\frac{1}{2}mv^{2}\right)}=(4\pi)^{1/2}\,Nk_{\mathrm{B}}T_{i}\sum_{r}c_{0,0,r}^{(2T)}N_{0,0,r}^{(2T)}\left[\frac{3}{2}a_{0,r}\left(0\right)-a_{1,r}\left(0\right)\right], \tag{1.38}$$

where $a_{0,r}\left(0\right)=0$ is given in Table $(6-2-1)$ of Ref. [9]. This means that both Eqs. (1.33) and (1.38) combine to get

$$\frac{\partial}{\partial t}\overline{\frac{1}{2}mv^{2}}-q\mathbf{E}\cdot\overline{\mathbf{v}}-v_{0}-v_{1}=R\left(\overline{\frac{1}{2}mv^{2}}\right)+\sum_{r>1}v_{r}, \tag{1.39}$$

with

$$v_{r}=(4\pi)^{1/2}\,Nk_{\mathrm{B}}T_{i}c_{0,0,r}^{(2T)}N_{0,0,r}^{(2T)}a_{1,r}\left(0\right). \tag{1.40}$$

Specifically, we want to consider the first two cases of Eq. (1.40). By using the matrix elements from Table $(6-2-1)$ of [9], we find that

$$v_{0}=-\frac{2m}{m+M}\left[\frac{3}{2}k_{\mathrm{B}}T_{i}-\frac{3}{2}k_{\mathrm{B}}T\right]\zeta(T_{eff}) \tag{1.41}$$

and

$$v_{1}=\frac{2m}{m+M}\left[\frac{3}{2}k_{\mathrm{B}}T_{i}-\overline{\frac{1}{2}mv^{2}}\right]\zeta(T_{eff})\left[1+\frac{1}{2}\left\{6C^{*}\left(T_{eff}\right)-5\right\}\frac{M}{m+M}\frac{T_{i}-T}{T_{eff}}\right]. \tag{1.42}$$

Here, $C^{*}\left(T_{eff}\right)$ is a ratio of two collision integrals [9] of the type given in Eq. (1.32).

The Combination of Eqs. (1.39), (1.41), and (1.42) gives

$$\frac{\partial}{\partial t}\overline{\frac{1}{2}mv^{2}}-q\mathbf{E}\cdot\overline{\mathbf{v}}+\frac{2m\zeta(T_{eff})}{m+M}\left[\overline{\frac{1}{2}mv^{2}}-\frac{3}{2}k_{\mathrm{B}}T+\widetilde{S}\right]=R\left(\overline{\frac{1}{2}mv^{2}}\right)+\sum_{r>1}v_{r}, \tag{1.43}$$

where

$$\widetilde{S} = \frac{1}{2}\left\{6C^*\left(T_{eff}\right) - 5\right\}\frac{M}{m+M}\frac{T_i - T}{T_{eff}}\left[\overline{\frac{1}{2}mv^2} - \frac{3}{2}k_{\mathrm{B}}T_i\right]. \tag{1.44}$$

The new quantity $\widetilde{S}$ is zero in most versions of the two-temperature theory. Thus, Eq. (1.43) can be rewritten as

$$\begin{aligned}\frac{\partial}{\partial t}\overline{\frac{1}{2}mv^2} - q\mathbf{E}\cdot\overline{\mathbf{v}} + \frac{2m\zeta(T_{eff})}{m+M}\left[\overline{\frac{1}{2}mv^2} - \frac{3}{2}k_{\mathrm{B}}T\right] \\ = R\left(\overline{\frac{1}{2}mv^2}\right) + \frac{2m\zeta(T_{eff})}{m+M}\left[\overline{\frac{1}{2}mv^2} - \frac{3}{2}k_{\mathrm{B}}T\right] + \overline{J^{\dagger}\left(\frac{1}{2}mv^2\right)},\end{aligned} \tag{1.45}$$

which is, like Eq. (1.33), exact until making approximations to the right-hand side. Eq. (1.45) is called *moment equation for energy* in the context of the two-temperature theory.

By using the relationship between the ion kinetic energy and the ion temperature,

$$\overline{\frac{1}{2}mv^2} = \frac{3}{2}k_{\mathrm{B}}T_i, \tag{1.46}$$

and Eq. (1.31), we can turn Eq. (1.45) into a *moment equation for the effective temperature* as

$$\begin{aligned}\frac{\partial}{\partial t}\left[\frac{3}{2}k_{\mathrm{B}}\left(T_{eff} - T\right)\right] - \frac{qM}{m+M}\mathbf{E}\cdot\overline{\mathbf{v}} + \frac{2m\zeta(T_{eff})}{m+M}\left[\frac{3}{2}k_{\mathrm{B}}\left(T_{eff} - T\right)\right] \\ = \frac{M}{m+M}\left[R\left(\overline{\frac{1}{2}mv^2}\right) + \frac{2m\zeta(T_{eff})}{m+M}\left[\overline{\frac{1}{2}mv^2} - \frac{3}{2}k_{\mathrm{B}}T\right] + \overline{J^{\dagger}\left(\frac{1}{2}mv^2\right)}\right].\end{aligned} \tag{1.47}$$

Here, the right-hand side is expected to be small when the right-hand side of Eq. (1.33) is also small. Note that from this result, when the ions are much heavier than the neutral atoms, the influence of the electric field term is small and the rate of change of the effective temperature is dominated by the collision frequency for momentum transfer in the two-temperature theory. The reverse is true when the ions are much lighter than the neutral atoms.

1.1.2 Three-temperature theory

The two-temperature theory succeed to solve the convergence problems that resulted by requiring the ion temperature to be identical to the dilute gas. However, it failed to calculate, with high accuracy, the ion diffusion coefficients for systems with high ion-atom mass ratio at high field strengths. It means its treatment is not adequate to deal with the ion diffusion through gases, a process which is inherently anisotropic, whereas Eq. (1.15) is intrinsically isotropic.

Therefore, the three-temperature theory was made [4] as a reason to overcome the problem of the two-temperature theory where its zero-order ion distribution function is chosen to be an *anisotropic* function

$$f_0^{(3T)}(\mathbf{v}) = \left(\frac{m}{2\pi k_{\mathrm{B}} T_T}\right)\left(\frac{m}{2\pi k_{\mathrm{B}} T_L}\right)^{1/2} \exp\left(-\frac{m(v_x^2+v_y^2)}{2k_{\mathrm{B}}T_T} - \frac{m\left(v_z-v_d\right)^2}{2k_{\mathrm{B}}T_L}\right) \tag{1.48}$$

$$= \left(\frac{m}{2\pi k_{\mathrm{B}} T_T}\right)\left(\frac{m}{2\pi k_{\mathrm{B}} T_L}\right)^{1/2} \exp\left(-W_x^2 - W_y^2 - W_z^2\right), \tag{1.49}$$

where

$$W_i = \left(\frac{m}{2k_{\mathrm{B}} T_T}\right)^{1/2} v_i, \tag{1.50}$$

with $i = x, y$ and

$$W_z = \left(\frac{m}{2k_{\mathrm{B}} T_L}\right)^{1/2} \left(v_z - v_d\right). \tag{1.51}$$

Here, v_d is the magnitude of the ion drift velocity along z, the direction of the electric field, while T_T and T_L are the ion kinetic temperatures *transverse* (perpendicular) and *longitudinal* (parallel) to the field, respectively. The basis functions that correspond to Eq. (1.49) are products of three *Hermite* polynomials,

$$\Psi_{l,m,r}^{(3T)}(\mathbf{v}) = H_l(W_x)\, H_m(W_y)\, H_r(W_z), \tag{1.52}$$

and their normalization is such that

$$N_{l,m,r}^{(3T)} = 2^{l+m+r} l!m!r! \tag{1.53}$$

with

$$c_{0,0,0}^{(3T)} = 1. \tag{1.54}$$

The three-temperature theory generally gives good results for all the ion transport coefficients but at the expense of more complicated calculations and of some loss of simple physical interpretation of the results, as compared to the two-temperature theory.

a) Moment equation for velocity

We consider once again Eq. (1.10) for the special function $\psi(v) = \mathbf{v}_z$

$$\frac{\partial}{\partial t}\overline{\mathbf{v}_z} - \frac{q}{m}\overline{(\mathbf{E}+\mathbf{v}\times\mathbf{B})_z} + \zeta_z(T_{eff,x}, T_{eff,y}, T_{eff,z})\overline{\mathbf{v}_z}$$
$$= R\left(\overline{\mathbf{v}_z}\right) - N\left(\frac{2k_{\mathrm{B}}T_z}{m}\right)^{1/2}\sum_{l,m,r}\left(1-\delta_{l,0}\delta_{m,0}\delta_{r,1}\right)a\left(0;0;1\mid l;m;r\right)N_{1,0,r}^{(3T)}c_{1,0,r}^{(3T)}, \quad (1.55)$$

where the general notation, $a\left(p;q;r\mid s;t;u\right)$, of $a\left(0;0;1\mid l;m;r\right)$ is given as [9]

$$a\left(p;q;r\mid s;t;u\right) = \frac{1}{N_{s,t,u}^{(3T)}}\left(\frac{m}{2\pi k_{\mathrm{B}}T_x}\right)^{1/2}\left(\frac{m}{2\pi k_{\mathrm{B}}T_y}\right)^{1/2}\left(\frac{m}{2\pi k_{\mathrm{B}}T_z}\right)^{1/2}\left(\frac{M}{2\pi k_{\mathrm{B}}T}\right)^{1/2}$$
$$\times\int\exp\left(-\frac{mv_x^2}{2k_{\mathrm{B}}T_x}-\frac{mv_y^2}{2k_{\mathrm{B}}T_y}-\frac{mv_z^2}{2k_{\mathrm{B}}T_z}-\frac{MV^2}{2k_{\mathrm{B}}T}\right)$$
$$\times\Psi_{s,t,u}^{(3T)}\left(\mathbf{v}\right)\left[\Psi_{p,q,r}^{(3T)}\left(\mathbf{v}\right)-\Psi_{p,q,r}^{(3T)}\left(\mathbf{v}'\right)\right]g\sigma\sin\theta d\theta d\phi d\mathbf{V}d\mathbf{v}, \quad (1.56)$$

with $a\left(p;q;r\mid s;t;u\right)=0$ if $p+s+t$ or $r+u$ is odd. This leads to the final sum shown in Eq. (1.55) with l and m must be even and r odd.

The collision frequency for momentum transfer along the direction z and in the context of the three-temperature theory is given as

$$\zeta_z(T_{eff,x}, T_{eff,y}, T_{eff,z}) = Na\left(0;0;1\mid 0;0;1\right). \quad (1.57)$$

Based on Eqs. (1.55) and (1.57), and likewise the two-temperature theory, the *moment equation for velocity* can be written as

$$\frac{\partial}{\partial t}\overline{\mathbf{v}_i} - \frac{q}{m}\left(\mathbf{E}+\overline{\mathbf{v}}\times\mathbf{B}\right)_i + \zeta_i(T_{eff,x}, T_{eff,y}, T_{eff,z})\overline{\mathbf{v}_i}$$
$$= R\left(\overline{\mathbf{v}_i}\right) + \left[\zeta_i(T_{eff,x}, T_{eff,y}, T_{eff,z})\overline{\mathbf{v}_i} + \overline{J^{\dagger}\mathbf{v}_i}\right], \quad (1.58)$$

where $\zeta_i\left(T_{eff,x}, T_{eff,y}, T_{eff,z}\right)$ is the collision frequency for momentum transfer along the direction i. It is given as

$$\zeta_i\left(T_{eff,x}, T_{eff,y}, T_{eff,z}\right) = \frac{8N}{3}\frac{M}{m+M}\left(\frac{3}{4\pi^{3/2}}\right)$$
$$\times\int\int\int\exp\left(-\gamma_x^2-\gamma_y^2-\gamma_z^2\right)\gamma_i^2 gQ_d\left(\frac{1}{2}\mu g^2\right)d\gamma_x d\gamma_y d\gamma_z, \quad (1.59)$$

with

$$\frac{1}{2}\mu g^2 = \gamma_x^2 k_{\rm B} T_{eff,x} + \gamma_y^2 k_{\rm B} T_{eff,y} + \gamma_z^2 k_{\rm B} T_{eff,z} \tag{1.60}$$

and

$$T_{eff,i} = \frac{mT + MT_i}{m+M} \tag{1.61}$$

$$\gamma_i^2 = \frac{\epsilon}{k_{\rm B} T_i}. \tag{1.62}$$

with $i = x$, y, or z. Eq. (1.59) reduces to Eq. (1.30) when the three ion temperatures are set equal to T_i.

A qualitative difference between Eq. (1.58) and Eq. (1.33) is that the collision frequencies are different for the three directions in the apparatus. These differences arise because the average ion energies and, hence, the mean times between collision are different in the various directions. They also arise because there is a net correlation between the ion velocities and energies in the various directions [15].

b) Moment equation for energy

By inserting the special function $\psi(\mathbf{v}) = \frac{1}{2}mv_z^2$ into Eq. (1.10), one can get

$$\frac{\partial}{\partial t}\overline{\frac{1}{2}mv_z^2} - qE_z\overline{v_z} + qB_y\overline{v_x v_z} + qB_x\overline{v_y v_z} - \overline{J^\dagger\left(\frac{1}{2}mv_z^2\right)} = R\left(\overline{\frac{1}{2}mv_z^2}\right). \tag{1.63}$$

Note that the terms involving the magnetic field do not cancel, but they would do so if Eq. (1.63) were added to similar equations for the kinetic energies along the x and y directions. Note also that in terms of the basis functions given by Eq. (1.52),

$$\overline{J^\dagger\left(\frac{1}{2}mv_z^2\right)} = \frac{1}{2}k_{\rm B}T_z\left[\frac{1}{2}\overline{J^\dagger\Psi_{0,0,2}^{(3T)}(\mathbf{v})} + \overline{J^\dagger\Psi_{0,0,0}^{(3T)}(\mathbf{v})}\right]. \tag{1.64}$$

From Eqs. (1.3), (1.12), (1.13), (1.49), and (1.58), it may be shown that

$$\overline{J^\dagger\Psi_{l',m',r'}^{(3T)}(\mathbf{v})} = -N\sum_{l,m,r} c_{l,m,r}^{(3T)} N_{l,m,r}^{(3T)} a\left(l',m',r';l,m,r\right). \tag{1.65}$$

Thus, we can use Eqs. (1.64) and (1.65) to write Eq.(1.63) as

$$\frac{\partial}{\partial t}\overline{\frac{1}{2}mv_z^2} - qE_z\overline{v_z} + qB_y\overline{v_x v_z} + qB_x\overline{v_y v_z} + \frac{1}{4}Nk_{\mathrm{B}}T_z \times \sum_{l,m,r} c_{l,m,r}^{(3T)} N_{l,m,r}^{(3T)} \left[a\left(0,0,2;l,m,r\right) + 2a\left(0,0,0;l,m,r\right)\right] = R\left(\overline{\frac{1}{2}mv_z^2}\right), \quad (1.66)$$

where $a\left(0,0,0;l,m,r\right)$ is zero for all values of l, m, and r. Since the only values of $a\left(0,0,2;l,m,r\right)$ that do not vanish for the Maxwell model are $a\left(0,0,2;0,0,0\right)$ and $a(0,0,2;0,0,2)$, we can separate these terms from the sum in Eq. (1.66) to obtain the result

$$\frac{\partial}{\partial t}\overline{\frac{1}{2}mv_z^2} - qE_z\overline{v_z} + qB_y\overline{v_x v_z} + qB_x\overline{v_y v_z} + \frac{1}{4}Nk_{\mathrm{B}}T_z\left[c_{0,0,0}^{(3T)}N_{0,0,0}^{(3T)}a\left(0,0,2;0,0,0\right) + c_{0,0,2}^{(3T)}N_{0,0,2}^{(3T)}a\left(0,0,2;l,m,r\right)\right] = R\left(\overline{\frac{1}{2}mv_z^2}\right) - \frac{1}{4}Nk_{\mathrm{B}}T_z \times \sum_{l,m,r}\left(1-\delta_{l,0}\delta_{m,0}\delta_{r,0}-\delta_{l,0}\delta_{m,0}\delta_{r,2}\right)c_{l,m,r}^{(3T)}N_{l,m,r}^{(3T)}a\left(0,0,2;l,m,r\right). \quad (1.67)$$

From Eqs. (1.6) and (1.13), and from the orthogonality of the basis functions, we find that

$$\overline{\frac{1}{2}mv_z^2} = \frac{1}{2}k_{\mathrm{B}}T_z\left[\frac{1}{2}c_{0,0,2}^{(3T)}N_{0,0,2}^{(3T)} + c_{0,0,0}^{(3T)}N_{0,0,0}^{(3T)}\right]. \quad (1.68)$$

Then, from Eqs. (1.68), (1.53), and (1.54), we can also write

$$\frac{1}{2}k_{\mathrm{B}}T_z c_{0,0,2}^{(3T)}N_{0,0,2}^{(3T)} = \overline{\frac{1}{2}mv_z^2} - \frac{1}{2}k_{\mathrm{B}}T_z. \quad (1.69)$$

Since T_z is ordinarily chosen so as to omit the right-hand side of Eq. (1.69), we can drop from both sides of Eq. (1.67) the term that involves $c_{0,0,2}^{(3T)}$. This gives

$$\frac{\partial}{\partial t}\overline{\frac{1}{2}mv_z^2} - qE_z\overline{v_z} + qB_y\overline{v_x v_z} + qB_x\overline{v_y v_z} + \frac{1}{4}Nk_{\mathrm{B}}T_z a\left(0,0,2;0,0,0\right) = R\left(\overline{\frac{1}{2}mv_z^2}\right) - \frac{1}{4}Nk_{\mathrm{B}}T_z \times \sum_{l,m,r}\left(1-\delta_{l,0}\delta_{m,0}\delta_{r,0}\right)c_{l,m,r}^{(3T)}N_{l,m,r}^{(3T)}a\left(0,0,2;l,m,r\right), \quad (1.70)$$

since

$$\frac{1}{4}Nk_{\mathrm{B}}T_z a\left(0,0,2;0,0,0\right)=\frac{2m}{m+M}\zeta_z(T_{eff,x},T_{eff,y},T_{eff,z})\left[\frac{1}{2}k_{\mathrm{B}}\left(T_z-T\right)\right]$$
$$+\zeta_z(T_{eff,x},T_{eff,y},T_{eff,z})\frac{[0;0;0\mid 0;0;2]}{[0;0;1\mid 0;0;1]}\left[\frac{1}{2}k_{\mathrm{B}}T_{eff,z}\right]. \quad (1.71)$$

Here, the ratio of irreducible collision integrals is obtained from the supplementary data file as

$$\frac{[0;0;0\mid 0;0;2]}{[0;0;1\mid 0;0;1]}=\frac{\int\exp\left(-\gamma^2\right)\gamma_z^2\left(2\gamma_z^2T_{eff,z}-\gamma_x^2T_{eff,x}-\gamma_y^2T_{eff,y}\right)Q_v\left(\frac{1}{2}\mu g^2\right)gd\gamma}{3\int\exp\left(-\gamma^2\right)\gamma_z^2T_z^{(eff)}Q_d\left(\frac{1}{2}\mu g^2\right)gd\gamma}. \quad (1.72)$$

Based on Eq. (1.71), the *moment equation for energy* in Eq. (1.70), can be written as

$$\frac{\partial}{\partial t}\overline{\frac{1}{2}mv_z^2}-qE_z\overline{v_z}+qB_y\overline{v_xv_z}+qB_x\overline{v_yv_z}+\frac{2m}{m+M}\zeta_z(T_{eff,x},T_{eff,y},T_{eff,z})\left[\frac{1}{2}k_{\mathrm{B}}\left(T_z-T\right)\right]$$
$$+\zeta_z(T_{eff,x},T_{eff,y},T_{eff,z})\frac{[0;0;0\mid 0;0;2]}{[0;0;1\mid 0;0;1]}\left[\frac{1}{2}k_{\mathrm{B}}T_{eff,z}\right]$$
$$=R\left(\overline{\frac{1}{2}mv_z^2}\right)+\overline{J^{\dagger}\frac{1}{2}mv_z^2}+\frac{2m}{m+M}\zeta_z(T_{eff,x},T_{eff,y},T_{eff,z})\left[\frac{1}{2}k_{\mathrm{B}}\left(T_z-T\right)\right]$$
$$+\zeta_z(T_{eff,x},T_{eff,y},T_{eff,z})\frac{[0;0;0\mid 0;0;2]}{[0;0;1\mid 0;0;1]}\left[\frac{1}{2}k_{\mathrm{B}}T_{eff,z}\right]. \quad (1.73)$$

The qualitative differences between Eq. (1.73) and the two-temperature equivalent equation, Eq. (1.45), are the terms involving $[0;0;0|0;0;2]$ and the magnetic field terms. It may be shown that $[0;0;0|0;0;2]$ vanishes in the special case where the three ion temperatures are identical, i.e., when the three-temperature theory is reduced to the two-temperature theory. The magnetic field terms require knowledge of a moment of a product of two different velocity components. Proceeding in exactly the same manner as above leads to the moment equation

$$\frac{\partial}{\partial t}\overline{v_xv_y}-\frac{q}{m}E_x\overline{v_y}-\frac{q}{m}\overline{v_x}E_y-\frac{q}{m}\frac{2B_z}{m}\left(\overline{\frac{1}{2}mv_x^2}+\overline{\frac{1}{2}mv_y^2}\right)$$
$$+\frac{q}{m}B_x\overline{v_xv_z}+\frac{q}{m}B_y\overline{v_yv_z}+\varsigma_{xy}(T_{eff,x},T_{eff,y},T_{eff,z})\overline{v_xv_y}$$
$$=R\left(\overline{v_xv_y}\right)+\overline{J\left(v_xv_y\right)}+\varsigma_{xy}(T_{eff,x},T_{eff,y},T_{eff,z})\overline{v_xv_y}. \quad (1.74)$$

The new quantity

$$\varsigma_{xy}(T_{eff,x},T_{eff,y},T_{eff,z})=\frac{2MN}{m+M}\frac{1}{3\pi^{3/2}}\int\int\int\exp\left(-\gamma^2\right)\gamma_x^2\gamma_y^2Q_v\left(\frac{1}{2}\mu g^2\right)gd\gamma, \quad (1.75)$$

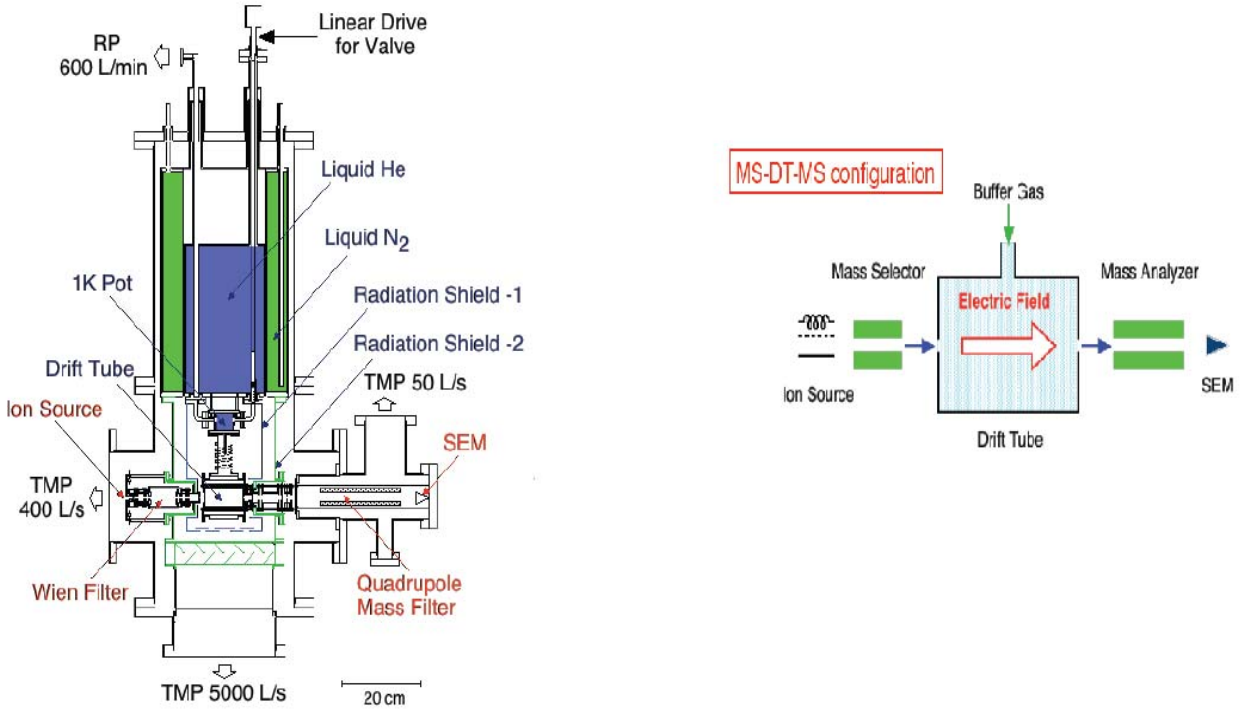

Figure 1-1: Drift tube mass spectrometer (DT-SM).

is the collision frequency for correlated velocities along the x and y directions in the three-temperature theory.

1.2 Ion drift tube transport properties

The drift tube mass spectrometer, shown in Fig. 1-1, is one of the very powerful techniques for studying ion-atom/molecule collisions at very low collision energies, from sub-milli to a few electron volts. It is generally used for measuring the ion transport properties in gases, such as mobility and diffusion coefficients and also the reaction rate constants. The drift-tube techniques succeeded to separate the different electronic states of ions, likewise the metastable-excited state. Hence, we will be able to obtain the detailed information about the interaction potential between the metastable-excited ion and the gas molecule.

Based on the field cases of ion drift tube, we have given the appropriate definitions of ion mobility and ion diffusion in neutral gas.

1.2.1 Ion mobility

Most of the measurements in drift tube are made at steady state, so that the time derivatives in the moment equations can be dropped. On the average, the ions move only along the z axis, and their average speed along this direction is usually written as v_d. In such apparatus, the first approximations of Eqs. (1.33) and (1.47) are, respectively,

$$v_d = \frac{qE}{m\zeta(T_{eff})}, \tag{1.76}$$

and

$$\frac{2}{M}\zeta(T_{eff})\left[\frac{3}{2}k_{\mathrm{B}}\left(T_{eff}-T\right)\right] = \frac{qE}{m}v_d. \tag{1.77}$$

The ion mobility K is defined by

$$v_d = KE, \tag{1.78}$$

while the reduced mobility K_0 is defined in terms of Loschmidt's constant N_0 as

$$N_0 K_0 = NK. \tag{1.79}$$

Usually, the mobility coefficient is expressed, if p is in torrs and T in kelvins, as [9]

$$K_0 = \left(\frac{p}{760}\right)\left(\frac{273.15}{T}\right)K. \tag{1.80}$$

Both Eqs. (1.76) and (1.77) can be solved for the effective temperature at steady state by eliminating $\zeta(T_{eff})$. This gives

$$\epsilon_{eff} = \frac{3}{2}k_{\mathrm{B}}T_{eff} = \frac{3}{2}k_{\mathrm{B}}T + \frac{1}{2}Mv_d^2. \tag{1.81}$$

Eq. (1.81) is valid only for ions in pure neutral gases. The expressions for neutral gas mixtures, which are considerably more complex [18] and Eqs. (1.76) and (1.81) are the desired expressions–in first approximation–for the drift velocity and effective temperature in drift tube in terms of experimental parameters and microscopic properties.

Eqs. (1.31) and (1.81) give the Wannier formula as

$$\frac{3}{2}k_{\mathrm{B}}T_i = \frac{3}{2}k_{\mathrm{B}}T + \frac{1}{2}mv_d^2 + \frac{1}{2}Mv_d^2. \tag{1.82}$$

This equation shows that the ion energy in the laboratory frame consists of three pieces: thermal energy, kinetic energy that the ions have absorbed from the external field and are exhibiting as motion along the field axis, and kinetic energy that the ions have similarly absorbed, but that has been transformed into a random motion due to collisions with the neutrals.

The success achieved with the first approximation for drift tube means that this approximation can be used to find a better way of describing the change of the mobility as the field strength increases in DTMS. Eq. (1.81) shows that there is essentially one independent variable T_{eff} rather than the two ordinarily considered T and E/N. This was first noted in [1]. Since Eq. (1.81) is equivalent to

$$\frac{3}{2}k_{\mathrm{B}}T_{eff} = \frac{3}{2}k_{\mathrm{B}}T + \frac{1}{2}MN_0^2\left(E/N\right)^2 K_0^2, \tag{1.83}$$

from this equation, we can calculate T_{eff} within the experimental quantities of E/N and by using only a simple algebra.

1.2.2 Ion diffusion

At *zero* field, the ion-gas diffusion occurs at the same rate in directions parallel and perpendicular to the electric field. Hence, the diffusion coefficient, D, is directly related to the mobility, K, by the familiar Einstein (or Nemst-Townsend) relationship

$$D = \left(\frac{k_{\mathrm{B}}T}{q}\right)K. \tag{1.84}$$

Here, q is the ionic charge. However, at a *non-zero* field, the diffusion D increases more much rapidly than the mobility K and becomes anisotropic. As a result, diffusion tensor takes place at different components transverse, D_T, and longitudinal, D_L, to the field as

$$D_T = \left(\frac{k_{\mathrm{B}}T_T}{q}\right)K\left[1+\Delta_T\left(\frac{K'}{2+K'}\right)\right] \tag{1.85}$$

$$D_L = \left(\frac{k_{\mathrm{B}}T_L}{q}\right)K\left[1+\left(1+\Delta_L\right)K'\right], \tag{1.86}$$

where

$$K' = \frac{d\ln K_0}{d\ln\left(E/N\right)}. \tag{1.87}$$

The value of K' can be calculated from the experimental data by a numerical differentiation, but it is easier to find it from the differentiation of Eq. (1.83) as

$$1 + K' = \left[1 - 2\left(\frac{T_{eff} - T}{T_{eff}}\right)\frac{d\ln K_0}{d\ln T_{eff}}\right]^{-1}. \tag{1.88}$$

Eqs. (1.85) and (1.86) are called *generalized* Einstein relations which have been elaborated from the three-temperature theory by Waldman and Mason [19]. These authors have introduced the small correction parameters Δ_T and Δ_L which depend primarily on the ion-atom mass ratio $m/(m+M)$.

The ion temperatures T_T and T_L are given by

$$k_{\mathrm{B}}T_{T,\,L} = k_{\mathrm{B}}T + \delta_{T,L}\left(1 + \beta_{T,L}K'\right)Mv_d^2, \tag{1.89}$$

where

$$\delta_T = \frac{4m - (2m - M)\breve{A}}{4m + 3M\breve{A}} \tag{1.90}$$

$$\delta_L = \frac{(m+M)\breve{A}}{4m + 3M\breve{A}}, \tag{1.91}$$

with $\breve{A}$ being a dimensionless ratio of collision integrals occurring in the three-temperature theory [9, 19]. Its numerical value depends on the T_{eff} and the ion-atom potential [20].

The determination of $\beta_{T,L}$ is still only on a semiempirical basis in which $\beta_T = 0$ and using semiempirical tabulated values for β_L. As a first approximation, β_L depends only on the ion-atom mass ratio $m/(m+M)$ [20].

Chapter 2

CHe^+ System

The main part for the evaluation of the transport properties of ions in gases, such as mobility and diffusion, is to know accurately the expressions of the transport cross sections and collision integrals, which are strongly related to the ion-neutral interaction potential. Thus, an accurate interaction potential is necessary for the theoretical calculations of the ion mobility. In this case, not only the interaction potentials of the ground state should be known, but also those related to the metastable-excited state of the CHe^+ system.

Therefore, in the following sections, we give the details of the constructions of the potential-energy curves *via* which the ground $C^+(2s^22p;\ ^2P^\circ)$ and metastable-excited $C^+(2s2p^2;\ ^4P)$ ions interact with ground-state helium $He(1s^2;\ ^4S)$. Then, we describe two approaches to calculate the *diffusion* cross sections, which will be used in Chapter 3 devoted to the computation of the CHe^+ mobility.

2.1 Interaction potentials

To find out the exact interaction potential $V(R)$ between two atomic species, the task is almost impossible. Instead, mathematical models that mimic this potential in a reasonable way provide good tools to test the kinetic theories *via* the mobility measurements. So, the ion-atom potentials should be known in the *long* (or *attractive*), *intermediate,* and *short* (or *repulsive*) regions for the requisite calculations.

2.1.1 Short-range potential

The short-range ion-atom potential can be expressed by the Born-Meyer relationship [21]

$$V_{\mathrm{SR}}(R) = \alpha \exp(-\beta R), \tag{2.1}$$

with α and β are two constant parameters and R is the internuclear distance. This form is suggested by approximate quantum-mechanical calculations, since the short-range interactions are purely quantal. In some cases, to simplify the mathematical calculation, $V_{\mathrm{SR}}(R)$ is represented as an inverse power function

$$V_{\mathrm{SR}}(R) \approx \frac{B}{R^n}, \tag{2.2}$$

where the constants n and B are adapted empirically to the experimental data of the interactions. But, in general, there are no simple known methods by which the short-range parameters α and β (or B and n) can be estimated from properties of the isolated ions and atoms [9]. According to Mason and McDaniel [9], the best known methods to estimate the short-range parameters α and β is the correlation scheme which is based on models and empirical observations of V_{SR} for various systems from various sources.

2.1.2 Long-range potential

The long-range interaction potential can be written as the sum of three parts

$$V_{\mathrm{LR}}(R) = V_{\mathrm{pol}}(R) + V_{\mathrm{dis}}(R) + V_{\mathrm{ele}}(R), \tag{2.3}$$

with

- $V_{\mathrm{pol}}(R)$: the polarization potential which arises primarily from the interaction of the ionic charge with the multipole moments induced in the neutral atom;

- $V_{\mathrm{dis}}(R)$: the dispersion potential which is fundamentally quantum-mechanical in nature, but has a simple semiclassical interpretation; and

- $V_{\mathrm{ele}}(R)$: the electrostatic potential that arises from the interactions between the charge on the ion and the permanent multipole moments of the neutral.

According to the theoretical calculations of each part of these different potentials, the long-range potential function in Eq. (2.3) ends up in the mathematical form [32, 33]

$$V_{\mathrm{LR}}(R) = -\left(\frac{C_4}{R^4} + \frac{C_6}{R^6} + \frac{C_8}{R^8}\right), \tag{2.4}$$

where

$$C_4 = \frac{1}{2}\alpha_d \tag{2.5}$$

$$C_6 = \frac{1}{2}\alpha_q \tag{2.6}$$

$$C_8 = \frac{1}{2}\alpha_o \tag{2.7}$$

are the dispersion coefficients correlated to the dipole α_d, quadrupole α_q, and octupole α_o polarizabilities of the neutral atom, respectively. In this case, the dominant ion-neutral interaction is usually the inverse fourth power term R^{-4} which accounts for the attraction between the charge on the ion and the dipole that induces in the polarizable neutral. The coefficients C_4, C_6, and C_8 are often known rather accurately from the knowledge of the polarizabilities. Furthermore, Mason and McDaniel [9] described some methods for estimating C_6 that end up with the expression

$$\alpha_q \approx \frac{3}{2}\alpha_d^2 \frac{h\nu}{e^2 f}, \tag{2.8}$$

where $h\nu$ is the oscillator frequency or some mean excitation energy and f is the oscillator strength. The usual simple guess takes $h\nu$ equal to the ionization potential I and $f = 1$, which yields

$$\alpha_q \approx 0.104\alpha_d^2 I. \tag{2.9}$$

The units of α_q and α_d are here in $\mathrm{\AA}^5$ and $\mathrm{\AA}^3$, respectively, and I in eV. It has been realized that the estimation methods of C_6 is seldom known as accurately as C_4. The addition of the long-range attraction energy $-C_6/R^6$ to $-C_4/R^4$ causes a minimum to develop at lower temperatures and the further energy $-C_4/R^4$ suppresses eventually both the maximum and the minimum.

At low temperatures and weak electric field, the mobility is dominated by the long-range polarization attraction energy $-C_4/R^4$ of Eq. (2.4). It approaches the polarization limit as

$T \to 0$. This limit of the mobility is at the standard gas density

$$K_{\rm pol} = \frac{13.853}{\sqrt{\mu\alpha_d}}, \tag{2.10}$$

with μ being the reduced mass of the ion-neutral species. The mobility is in this case in units of $\mathrm{cm^2\,V^{-1}\,s^{-1}}$.

2.1.3 Intermediate data points

It is well-known from quantum chemistry that the ground-state carbon $\mathrm{C^+}\left(2s^22p;\ ^2\mathrm{P^\circ}\right)$ ion and the ground-state $\mathrm{He}\,(1s^2)$ neutral atom approach each other, with a relative motion of energy ϵ, along one of the *doublet* molecular states $^2\Pi$ and $^2\Sigma$. However, the metastable-excited $\mathrm{C^+}\,(2s2p^2;\ ^4\mathrm{P})$ ion and the ground-state $\mathrm{He}\,(1s^2)$ atom approach each other through one of the excited *quartet* molecular states $^4\Sigma^-$ and $^4\Pi$. Consequently, we have to generate in this work with *ab initio* methods the ion-atom potential-energy curves of four individual and distinct molecular states: $^2\Pi$, $^2\Sigma$, $^4\Sigma^-$, and $^4\Pi$. Since the spin-orbit effects are small for light atoms, as it is the case for carbon, they are not here taken into account.

In order to determine the potential curves of the above doublet and quartet states, we have chosen the Dunning *correlation consistent polarized valence quintuple zeta* (cc-pV5Z) basis for both C and He atoms [22]. The calculations yield the value 5.351 eV of the $\mathrm{C^+}(^2\mathrm{P^\circ} \longrightarrow {}^4\mathrm{P})$ transition energy, which is very close to the recommended value 5.335 eV by *National Institute of Standards and Technology* (NIST) [23] and to the numerical results 5.307 eV of Matoba *et al.* [3] and 5.32 ± 0.18 eV of Hughes and von Nagy-Felsobuki [24]. We have further performed the *multireference configuration interaction* (MRCI) method [25, 26], using reference functions derived from the *state-averaged complete active space self-consistent field* (SA-CASSCF) approach [27, 28]. Among the seven electrons of the $\mathrm{CHe^+}$ system, two are frozen and the remaining ones are considered as active. The active space contains the following orbitals: 5σ corresponding to $\mathrm{C}(2s; 3p_0; 3s; 4p_0)$ and $\mathrm{He}(1s)$ and 4π corresponding to $\mathrm{C}(2p_\pm; 3s_\pm)$. These 9 active orbitals are distributed among the irreducible representations a_1, b_1, b_2, and a_2 of the C_{2v} symmetry as follows: 5, 2, 2, and 0. To estimate the effect of higher-order excitations, we have introduced the Davidson correction [29]. The *basis-set superposition error* (BSSE) has also been introduced via the counterpoise correction technique [30]. The $\mathrm{C^+He}$ electronic potential curves are determined for the $^2\Pi$, $^2\Sigma$, $^4\Sigma^-$, and $^4\Pi$ states in the range of internuclear distances $1.0 \le R \le 20.8$. We have performed all the calculations with the quantum-chemistry package

MOLPRO [31].

2.1.4 CHe^+ potential-energy curves

For the requisite calculations, the four ion-atom potential curves have to be known in the long, intermediate, and short regions of R. We hence adopted the data points we have generated above to construct smooth and reliable $C^+\left(^2P^\circ\right)$ He and $C^+\left(^4P\right)$ He potential-energy curves. In the short-range region, i.e., for $R \leq 1.0$, the ion-neutral interaction potential $V_{SR}(R)$ was computed by using Eq. (2.1). The adopted values of constant parameters α and β are listed for each molecular state in Table 2.2. For $R \geq 20.8$, the extension is chosen at large distances of the analytical form [32,33] where $V_{LR}(R)$ is given by Eq. (2.4). Since the leading R^{-4} term is important in shaping the common long-range forms of all the ion-atom interaction potentials and in fixing the C^+He polarization limit, $K_{\rm pol} \simeq 17.66\,{\rm cm^2\,V^{-1}\,s^{-1}}$, by Eq. (2.10).

In the calculations of CHe^+ potential energy curves, we employed the theoretical value $\alpha_{\rm d} \simeq 1.384$ of Łach *et al.* [34]. Experimental measurements performed by Schmidt *et al.* [35] confirmed this value, which is also very close to the NIST dipole polarizability $\alpha_{\rm d} \simeq 1.404$ [23]. Complete and useful compilations of calculated and measured dipole polarizabilities of helium and many other systems can be found in Masili and Starace [36] and Mitroy *et al.* [37]. The two remaining polarizabilities, $\alpha_{\rm q} \simeq 2.445$ and $\alpha_{\rm o} \simeq 10.620$, are taken from the recent theoretical work of Kar and Ho [38], which are identical to the figures already produced by Yan *et al.* [39]. In addition, Matoba *et al.* [3] used the same dipole polarizability $\alpha_{\rm d} = 0.205\,{\rm \AA}^3$ for all the C^+He molecular states. In contrast, they utilized different values of $\alpha_{\rm q}$ and $\alpha_{\rm o}$ which they deduced from analytical fittings of the different potentials. Their values of $\alpha_{\rm q}$ and $\alpha_{\rm o}$ are listed in Table 2.3.

The constructed C^+He potential-energy curves are shown in Fig. 2-1 and some of their data points are reported from $R = 1$ to $R = 10$ in Table 2.4. The potential curves are also compared in Fig. 2-1 with some data points provided in Matoba *et al.* [3]. The agreement between both potential sets, mainly for the lower states, is in general quite good. To further characterize quantitatively our computed and constructed potentials, we list in Table 2.5 the internuclear separations σ at which $V(\sigma) = 0$, as well as the equilibrium distances R_e and potential depths D_e, both contrasted with previous published data. We also give in Table 2.6 their *rotationless*-vibrational energy levels, where the calculations showed that the $^2\Pi$, $^2\Sigma$, $^4\Sigma^-$, and $^4\Pi$ states

Table 2.1: Data points derived from the calculated interaction potentials with the BSSE *ab initio* method of the ground and metastable-excited C^+He molecular states. All the data are given in a.u.

Distance	$C^+\left(^2P^\circ\right)+He$		$C^+\left(^4P\right)+He$	
R	$^2\Sigma$	$^2\Pi$	$^4\Sigma^-$	$^4\Pi$
1.0	−38.8239	−38.9172	−38.9479	−38.3916
1.2	−39.4591	−39.5612	−39.5795	−39.0333
1.4	−39.7646	−39.8832	−39.8840	−39.3345
1.6	−39.9069	−40.0475	−40.0272	−39.5282
1.8	−39.9678	−40.1342	−40.0903	−39.7092
2.0	−39.9884	−40.1826	−40.1138	−39.8318
2.2	−40.0252	−40.2117	−40.1186	−39.9139
2.4	−40.0947	−40.2305	−40.1154	−39.9684
2.6	−40.1459	−40.2432	−40.1091	−40.0040
2.8	−40.1826	−40.2518	−40.1022	−40.0273
3.0	−40.2087	−40.2576	−40.0959	−40.0425
3.2	−40.2270	−40.2614	−40.0904	−40.0525
3.4	−40.2397	−40.2639	−40.0860	−40.0592
3.6	−40.2485	−40.2655	−40.0826	−40.0636
3.8	−40.2545	−40.2664	−40.0800	−40.0666
4.0	−40.2586	−40.2669	−40.0779	−40.0686
4.2	−40.2612	−40.2671	−40.0764	−40.0699
4.4	−40.2630	−40.2671	−40.0753	−40.0708
4.6	−40.2641	−40.2671	−40.0744	−40.0713
4.8	−40.2649	−40.2669	−40.0738	−40.0716
5.0	−40.2653	−40.2668	−40.0732	−40.0718
5.2	−40.2655	−40.2666	−40.0729	−40.0719
5.4	−40.2656	−40.2665	−40.0726	−40.0719
5.6	−40.2657	−40.2663	−40.0723	−40.0719
5.8	−40.2657	−40.2662	−40.0722	−40.0718
6.0	−40.2656	−40.2661	−40.0719	−40.0718
6.4	−40.2655	−40.2659	−40.0718	−40.0717
6.8	−40.2655	−40.2658	−40.0716	−40.0716
7.0	−40.2654	−40.2657	−40.0716	−40.0715
8.0	−40.2653	−40.2655	−40.0714	−40.0714
9.0	−40.2652	−40.2655	−40.0713	−40.0713
10.0	−40.2652	−40.2654	−40.0713	−40.0713
12.8	−40.2652	−40.2654	−40.0712	−40.0713
16.8	−40.2652	−40.2654	−40.0712	−40.0712
20.8	−40.2652	−40.2654	−40.0712	−40.0712

Table 2.2: Adopted short-range parameters, that appear in Eq. (2.1), in the construction of the ground and metastable-excited C^+He potential-energy curves. All the data are in a.u.

Short-range parameters	C^+He states			
	$^2\Pi$	$^2\Sigma$	$^4\Sigma^-$	$^4\Pi$
α	33.54	28.63	51.67	23.89
β	3.230	3.004	3.847	2.663

Table 2.3: Constant parameters adopted for the construction of the ground and metastable-excited C^+He potentials in both short- and long-range regions. All these data (in a.u.) are taken from Matoba *et al.* [3].

Molecular states	Short range		Long range	
	α	β	C_6	C_8
$^2\Sigma^+$	3.76924	1.46937	3.28353	24.3240
$^2\Pi$	20.5114	2.84693	9.09081	31.5853
$^4\Sigma^-$	310.868	5.29863	10.50999	209.8915
$^4\Pi$	3.87397	1.23193	5.949524	62.33395

can hold 7, 5, 19, and 5 vibrational levels, respectively.

2.2 Transport cross sections

The *transport* cross sections $Q^{(l)}$ are the key relation between the ion-neutral interaction potential and the transport coefficients. In general, the numerical calculation of the transport cross sections are usually accomplished over wide ranges of the relative kinetic energy ϵ for collisions between two structureless particles and for many values of l $(l \geq 1)$. The first transport cross sections $Q^{(1)} \equiv Q_d$ is known as the *diffusion* (or *momentum-transfer*) cross sections. However, for $l = 0$, the cross section corresponds to the isotropic part of the elastic cross sections and the associated collisions do not affect the ion transport because of the isotropy of these collisions.

In the case of ion-atom elastic collisions, the transport cross sections provide us with full information on the exchange probability of the impulsion and the energy during an elastic collision. The general expression of $Q^{(l)}$ is given by [9]

$$Q^{(l)}(\epsilon) = 2\pi \int_0^{\pi} \left(1 - \cos^l \theta\right) \sigma\left(\theta, \epsilon\right) \sin\theta d\theta, \tag{2.11}$$

where $\sigma\left(\theta, \epsilon\right)$ is the *differential* cross section for elastic scattering, through an angle θ, by the

Table 2.4: Data points derived from the constructed interatomic potentials of the ground and metastable-excited C^+He molecular states. The numbers in parentheses indicate powers of ten. All the data are given in a.u.

Distance	$C^+\left(^2P^\circ\right)+He$		$C^+\left(^4P\right)+He$	
R	$^2\Pi$	$^2\Sigma$	$^4\Sigma^-$	$^4\Pi$
1.0	+1.3271	+1.4192	+1.1031	+1.6327
1.5	+0.2793	+0.4073	+9.4923(−2)	+0.5829
2.0	+7.9249(−2)	+0.2723	−4.5776(−2)	+0.2302
2.5	+2.5362(−2)	+0.1382	−4.3557(−2)	+7.9152(−2)
3.0	+5.9367(−3)	+5.4191(−2)	−2.6429(−2)	+2.6370(−2)
3.5	−6.1676(−4)	+1.9212(−2)	−1.4091(−2)	+8.2620(−3)
4.0	−2.1468(−3)	+5.8192(−3)	−7.2897(−3)	+1.9001(−3)
4.5	−2.0167(−3)	+1.1453(−3)	−3.8766(−3)	−1.9463(−4)
5.0	−1.5226(−3)	−2.5992(−4)	−2.1814(−3)	−7.0990(−4)
5.5	−1.0722(−3)	−5.5073(−4)	−1.3093(−3)	−7.0169(−4)
6.0	−7.4407(−4)	−5.1325(−4)	−8.3500(−4)	−5.6522(−4)
6.5	−5.2161(−4)	−4.0862(−4)	−5.6069(−4)	−4.2790(−4)
7.0	−3.7340(−4)	−3.1133(−4)	−3.9266(−4)	−3.1969(−4)
7.5	−2.7372(−4)	−2.3615(−4)	−2.8462(−4)	−2.4048(−4)
8.0	−2.0540(−4)	−1.8078(−4)	−2.1218(−4)	−1.8353(−4)
8.5	−1.5731(−4)	−1.4042(−4)	−1.6185(−4)	−1.4235(−4)
9.0	−1.2271(−4)	−1.1069(−4)	−1.2583(−4)	−1.1213(−4)
9.5	−9.6598(−5)	−8.8456(−5)	−9.9443(−5)	−8.9581(−5)
10.0	−7.7534(−5)	−7.1560(−5)	−7.9699(−5)	−7.2468(−5)
10.5	−6.2991(−5)	−5.8533(−5)	−6.4662(−5)	−5.9280(−5)
11.0	−5.1713(−5)	−4.8349(−5)	−5.3025(−5)	−4.8974(−5)

Table 2.5: Some of the spectroscopic parameters compared with previous published data. The potential depths D_e are measured with respect to the dissociation limits of the respective *ab initio* C^+He molecular states. The numbers in parentheses are powers of ten.

	$C^+\left(^2P^\circ\right)$He		$C^+\left(^4P\right)$He		
Parameters	$^2\Pi$	$^2\Sigma$	$^4\Sigma^-$	$^4\Pi$	Refs.
σ (Å)	1.905	2.593	0.900	2.381	This work
R_e (Å)	2.196	2.963	1.164	2.752	This work
	2.21	2.99	1.16	2.78	[3]
	2.2330		1.1555		[24]
	2.329	2.978	1.158	2.805	[40]
	2.406		1.168		[41]
	2.504		1.177		[42]
D_e (cm^{-1})	482	122	11.007(3)	162	This work
	468	122	10.691 (3)	159	[3]
	406	147	10.254 (3)	175	[40]
	385		10.248 (3)		[41]

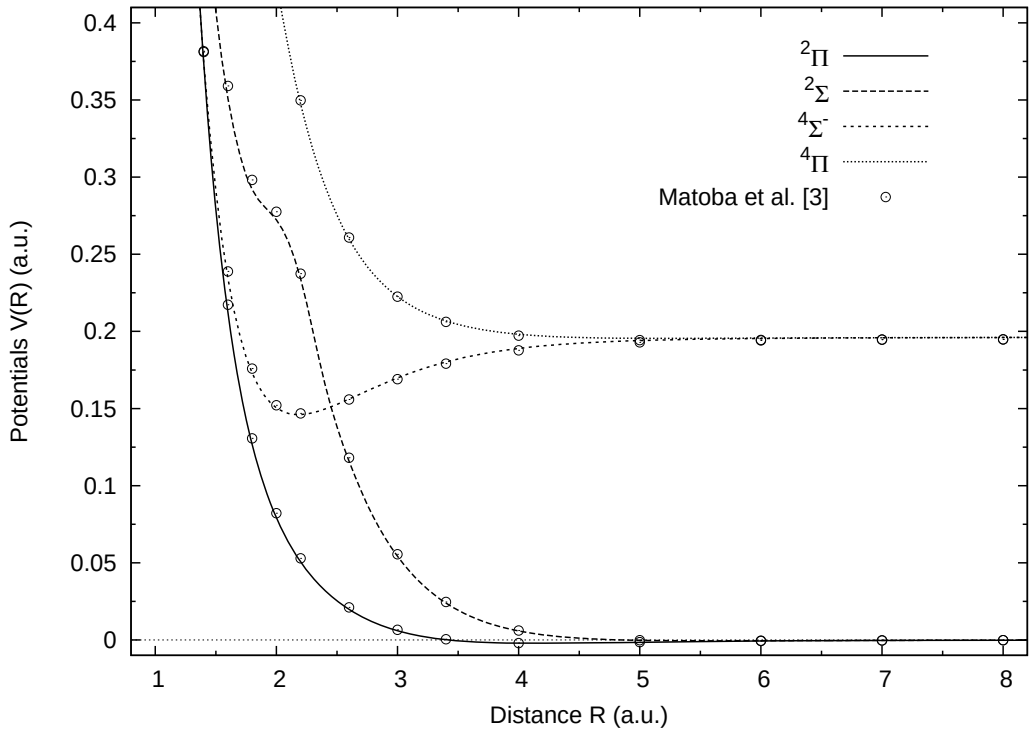

Figure 2-1: The constructed potential-energy curves of the quasimolecular $C^+\left(^2P^\circ\right)He$ and $C^+\left(^4P\right)He$ states. Empty circles represent the data points produced by Matoba *et al.* [3].

Table 2.6: Rotationless-vibrational energy levels (in cm^{-1}) of the doublet and quartet C^+He molecular states.

Level	$C^+\left(^2P^\circ\right)He$		$C^+\left(^4P\right)He$	
v	$^2\Pi$	$^2\Sigma$	$^4\Sigma^-$	$^4\Pi$
0	−312.6197	−75.1408	−9756.0190	−99.5158
1	−184.9595	−26.6879	−8509.1256	−40.2552
2	−92.5661	−7.8367	−7346.0876	−13.2426
3	−36.3233	−1.2937	−6267.3752	−2.9865
4	−11.2541	−0.0431	−5273.1523	−0.2821
5	−2.3101		−4363.4599	
6	−0.1761		−3539.5131	
7			−2803.2954	
8			−2156.5573	
9			−1600.8161	
10			−1136.5718	
11			−762.4773	
12			−474.9170	
13			−267.7434	
14			−131.8062	
15			−53.3043	
16			−16.8371	
17			−3.9306	
18			−0.4114	

ion-neutral interaction potential $V(R)$. This differential cross section is usually defined as

$$\frac{d\sigma}{d\Omega} = I(\Omega)\,\sigma(\theta,\epsilon), \tag{2.12}$$

i.e., the ratio of the number of scattered particles into the solid angle $d\Omega$ by time unit and the incident flux density.

The differential transport cross section is therefore a tool for determining the transport cross section in classical or quantum-mechanical approach.

2.2.1 Classical approach

At high temperatures, the collision of unlike particles can be described classically, except at very small scattering angles. The differential cross section for this approach is calculated by the relationship

$$\sigma(\theta,\epsilon) = \left| \frac{1}{\sin\theta(b,\epsilon)} \sum_i \frac{db_i}{d\theta(b,\epsilon)} \right|, \tag{2.13}$$

where the index i corresponds to the impact parameters b_i for which the absolute value of the angle θ is the same. Therefore, the classical expression of Eq. (2.11) is written as

$$Q^{(l)}(\epsilon) = 2\pi \int_0^\infty \left[1 - \cos^l\theta(b,\epsilon)\right] b\,db. \tag{2.14}$$

Here b is the impact parameter and θ is the scattering angle defined by the expression [9]

$$\theta(b,\epsilon) = \pi - 2b \int_{R_0}^\infty \left[1 - \frac{b^2}{R^2} - \frac{V(R)}{\epsilon}\right]^{-1/2} \frac{dR}{R^2}, \tag{2.15}$$

where the distance of closest approach R_0 is the outermost of

$$1 - \frac{b^2}{R_0^2} - \frac{V(R_0)}{\epsilon} = 0. \tag{2.16}$$

It is through Eq. (2.16) that the position-dependent interaction potential $V(R)$ affects the transport cross sections and, hence, the transport coefficients.

Figure 2-2(a)-(b) displays the individual classical diffusion cross sections for the *doublet* and *quartet* states of the C^+He system. These transport cross sections are viable, but do not consider the quantum effects, such as tunnelling and interference, that give the orbiting resonances in the low-energy cross sections.

The values of the classical transport cross section for both the ground $C^+\left(^2P^\circ\right)-$He and metastable-excited $C^+\left(^4P\right)-$He states were obtained by using the Fortran program PC.F90 of Viehland [43]. Before PC.F90 calculates the transport cross sections from Eq. (2.14), it needs to determinate the orbiting parameters (ϵ, b_o, R_o) to find the possible b_o values corresponding to ϵ. Then, if necessary, it rearranges them so that the b_o values are monotonically increasing. Mathematically, orbiting occurs because of a non-integrable singularity in the integrand of Eq. (2.15). Orbiting can only occur at energies smaller than some critical value ϵ_c that depends upon the interaction potential. This is because larger values of ϵ mean that the ratio $V(R)/\epsilon$ in Eq. (2.16) is negligible compared to $1-(b/R)^2$.

For N values of b_o, Eq. (2.14) can then be written as the sum

$$Q^{(l)}(\epsilon) = \sum_{i=0}^{N} Q_i^{(l)}(\epsilon), \tag{2.17}$$

where, for $1 \leq i \leq N-1$,

$$Q_i^{(l)}(\epsilon) = 2\pi \int_{b_i}^{b_{i+1}} \left[1-\cos^l\theta(b,\epsilon)\right] b db \tag{2.18}$$

and

$$Q_0^{(l)}(\epsilon) = 2\pi \int_{0}^{b_1} \left[1-\cos^l\theta(b,\epsilon)\right] b db \tag{2.19}$$

$$Q_N^{(l)}(\epsilon) = 2\pi \int_{b_N}^{\infty} \left[1-\cos^l\theta(b,\epsilon)\right] b db. \tag{2.20}$$

Hence, due to the fact that the numerical techniques used for calculating the integrals in Eqs. (2.18), (2.19), and (2.20) are different, Viehland *et al.* [43] separated the integral of Eq. (2.14) into three separate integrals. The calculations of the classical transport cross sections in Eqs. (2.18)-(2.20) need three distinctive energy intervals.

a) Region 1: $\epsilon_{\min} \leqslant \epsilon < \epsilon_{\mathbf{c}}$

In the case of the first integral (2.19), the energy is agreed to that orbiting collisions only occur at the upper endpoint of the integral, i.e., when $b = b_1$. The transport cross sections in Eq. (2.19) are therefore expressed as [44]

$$Q_0^{(l)}(\epsilon) = \int_{-1}^{1} f_0^{(l)}(y,\epsilon)\, dy, \tag{2.21}$$

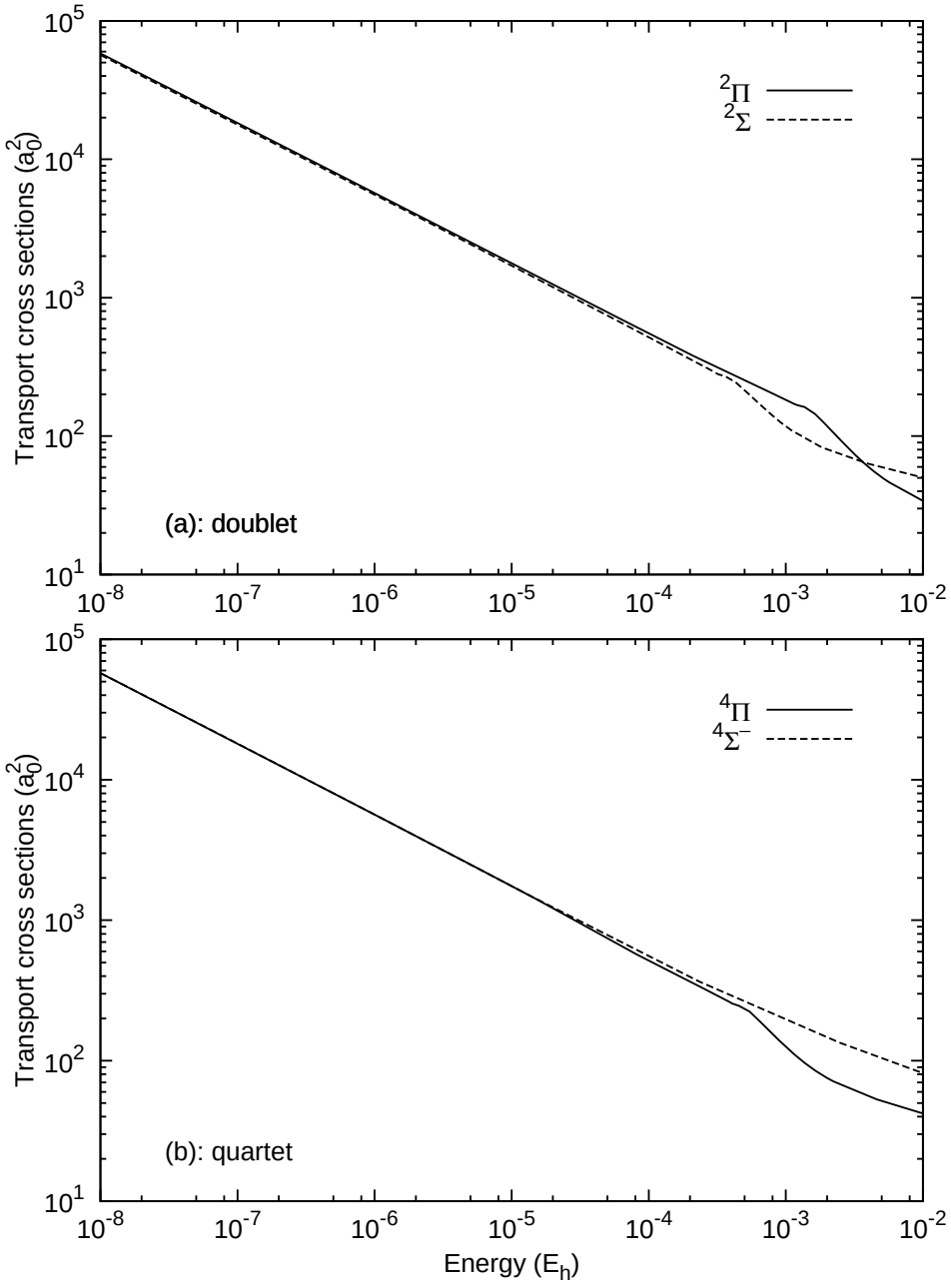

Figure 2-2: Individual *classical* transport cross sections, effective in diffusion, varying with energy. The cross sections are computed: in (a), for doublet states; in (b), for quartet states.

where

$$f_0^{(l)}(y,\epsilon) = \frac{1}{4}\pi^2 b_1^2 \left[1 - \cos^l\theta\left(b^{(1)}(y),\epsilon\right)\right] \sin\left[\frac{\pi}{2}(y+1)\right], \tag{2.22}$$

and

$$b^{(1)}(y) = b_1 \cos\left[\frac{\pi}{4}(y+1)\right]. \tag{2.23}$$

This equation gives the relationship between the variables b and y. The integral in Eq. (2.19) is well suited for Clenshaw-Curtis quadrature, since the integrand is zero at each endpoint but, due to orbiting, varies rapidly near $y = -1$, where many of the quadrature points are concentrated.

Then, in the second integral (2.18), the orbiting collisions occur at both endpoints, b_i and b_{i+1}, and the transport cross sections appearing in this equation are given by [45]

$$Q_i^{(l)}(\epsilon) = 2\pi \int_{R_i}^{R_{i+1}} \left[1 - \cos^l\theta\left(b^{(2)}(R),\epsilon\right)\right] \left[1 - \frac{V(R)}{\epsilon} - \frac{R}{2}\frac{V'(R)}{\epsilon}\right] RdR, \tag{2.24}$$

with $V'(R)$ being the potential first derivative, and

$$b^{(2)}(R) = R\left[1 - \frac{V(R)}{\epsilon}\right]^{1/2}, \tag{2.25}$$

which helps to change the integration variables from the impact parameter to the distance of the closest approach. One may notice that the integral in Eq. (2.24) is more difficult than the one in Eq. (2.19), because it needs to calculate potential derivatives and to define the two endpoints, $b^{(2)}(R_i) = b_i$ and $b^{(2)}(R_{i+1}) = b_{i+1}$, iteratively from Eq. (2.25). However, the most important difficult is that the integrand would have to be evaluated exactly at each endpoint, which is an impossible task.

In order to get out of this task in Eq. (2.24), Viehland *et al.* [43] split the integration into two pieces at $\overline{R}_i = (R_i + R_{i+1})/2$ as to transform the integral in Eq. (2.24) likewise that in Eq. (2.21), i.e.,

$$Q_i^{(l)}(\epsilon) = \int_{-1}^{1} f_i^{(l)}(y,\epsilon)\, dy, \tag{2.26}$$

with $1 \leq i \leq N-1$, and

$$\begin{aligned} f_i^{(l)}(y,\epsilon) &= \frac{1}{8}\pi^2 \overline{R}_i^2 \left(1 - x_i^{(1)}\right) \left[1 - \cos^l\theta\left(b^{(2)}\left(R^{(1)}\left(x^{(1)}(y)\right)\right),\epsilon\right)\right] \\ &\times \left[1 - \frac{V\left(R^{(1)}\left(x^{(1)}(y)\right)\right)}{\epsilon} - \frac{R^{(1)}\left(x^{(1)}(y)\right)}{2}\frac{V'\left(R^{(1)}\left(x^{(1)}(y)\right)\right)}{\epsilon}\right] \\ &\times \sin\left[\frac{\pi}{2}\left(x^{(1)}(y)+1\right)\right] + \frac{1}{8}\pi^2 R_{i+1}^2\left(1 + x_i^{(2)}\right) \\ &\times \left[1 - \cos^l\theta\left(b^{(2)}\left(R^{(2)}\left(x^{(2)}(y)\right)\right),\epsilon\right)\right] \\ &\times \left[1 - \frac{V\left(R^{(2)}\left(x^{(2)}(y)\right)\right)}{\epsilon} - \frac{R^{(2)}\left(x^{(2)}(y)\right)}{2}\frac{V'\left(R^{(2)}\left(x^{(2)}(y)\right)\right)}{\epsilon}\right] \\ &\times \sin\left[\frac{\pi}{2}\left(x^{(2)}(y)+1\right)\right]. \end{aligned} \tag{2.27}$$

Here, $R^{(1)}$ and $x^{(1)}$ describe the variables in the piece below $\overline{R}_i$, that are given by

$$R^{(1)}(x) = \overline{R}_i \sin\left[\frac{\pi}{4}(x+1)\right], \tag{2.28}$$

and

$$x^{(1)}(y) = \frac{1}{2}\left[\left(1 - x_i^{(1)}\right)y + x_i^{(1)} + 1\right], \tag{2.29}$$

with

$$x_i^{(1)} = \frac{4}{\pi}\sin^{-1}\left(\frac{R_i}{\overline{R}_i}\right) - 1. \tag{2.30}$$

However, the variables $R^{(2)}$ and $x^{(2)}$, expressed by

$$R^{(2)}(x) = R_{i+1}\cos\left[\frac{\pi}{4}(x+1)\right] \tag{2.31}$$

and

$$x^{(2)}(y) = \frac{1}{2}\left[\left(1 + x_i^{(2)}\right)y + x_i^{(2)} - 1\right], \tag{2.32}$$

with

$$x_i^{(2)} = \frac{4}{\pi}\cos^{-1}\left(\frac{\overline{R}_i}{R_{i+1}}\right) - 1, \tag{2.33}$$

determine the piece above $\overline{R}_i$. The values of the integrand (2.27) at the endpoints are given by

the expressions of $f_i^{(l)}(-1,\epsilon)$ and $f_i^{(l)}(1,\epsilon)$ as

$$f_i^{(l)}(-1,\epsilon) = \frac{1}{8}\pi^2\overline{R}_i^2\left(1-x_i^{(1)}\right)\left[1-\cos^l\theta\left(b^{(2)}\left(R^{(1)}\left(x_i^{(1)}\right)\right),\epsilon\right)\right] \times\left[1-\frac{V\left(R^{(1)}\left(x_i^{(1)}\right)\right)}{\epsilon}-\frac{R^{(1)}\left(x_i^{(1)}\right)}{2}\frac{V'\left(R^{(1)}\left(x_i^{(1)}\right)\right)}{\epsilon}\right]\sin\left[\frac{\pi}{2}\left(x_i^{(1)}+1\right)\right] \quad (2.34)$$

and

$$f_i^{(l)}(1,\epsilon) = \frac{1}{8}\pi^2 R_{i+1}^2\left(1+x_i^{(2)}\right)\left[1-\cos^l\theta\left(b^{(2)}\left(R^{(2)}\left(x_i^{(2)}\right)\right),\epsilon\right)\right] \times\left[1-\frac{V\left(R^{(2)}\left(x_i^{(2)}\right)\right)}{\epsilon}-\frac{R^{(2)}\left(x_i^{(2)}\right)}{2}\frac{V'\left(R^{(2)}\left(x_i^{(2)}\right)\right)}{\epsilon}\right]\sin\left[\frac{\pi}{2}\left(x_i^{(2)}+1\right)\right]. \quad (2.35)$$

Finally, in the case of the third integral, orbiting occurs at the lower endpoint of the integral, i.e., only when $b = b_N$. Henceforth, the expression of this integral is

$$Q_N^{(l)}(\epsilon) = 2\pi\int_{R_N}^{\infty}\left[1-\cos^l\theta\left(b^{(2)}(R),\epsilon\right)\right]\left[1-\frac{V(R)}{\epsilon}-\frac{R}{2}\frac{V'(R)}{\epsilon}\right]RdR, \quad (2.36)$$

with

$$b^{(2)}(R_N) = b_N \quad (2.37)$$

Following O'Hara *et al.* [44], the integral in Eq. (2.36) can be rehabilitated as

$$Q_N^{(l)}(\epsilon) = \pi^2 R_N^2\int_0^1\left[1-\cos^l\theta\left(b^{(2)}\left(R^{(3)}(x)\right),\epsilon\right)\right] \times\left[1-\frac{V\left(R^{(3)}(x)\right)}{\epsilon}-\frac{R^{(3)}(x)}{2}\frac{V'\left(R^{(3)}(x)\right)}{\epsilon}\right]\frac{\cos(\pi x/2)}{\sin^3(\pi x/2)}dx \quad (2.38)$$

with

$$R^{(3)}(x) = \frac{R_N}{\sin(\pi x/2)}. \quad (2.39)$$

The integrand in Eq. (2.38) has also difficulties to compute it, therefore the program PC.F90 uses the same technique that are made for the integral in Eq. (2.24) by introducing the change of variables

$$x^{(3)}(y) = (1+y)/2, \quad (2.40)$$

as to get

$$Q_N^{(l)}(\epsilon) = \int_{-1}^{1} f_N^{(l)}(y,\epsilon)\, dy, \tag{2.41}$$

with

$$f_N^{(l)}(y,\epsilon) = \frac{1}{2}\pi^2 R_N^2 \int_0^1 \left[1-\cos^l\theta\left(b^{(2)}\left(R^{(3)}\left(x^{(3)}(y)\right)\right),\epsilon\right)\right] \times \left[1-\frac{V\left(R^{(3)}\left(x^{(3)}(y)\right)\right)}{\epsilon}-\frac{R^{(3)}\left(x^{(3)}(y)\right)}{2}\frac{V'\left(R^{(3)}\left(x^{(3)}(y)\right)\right)}{\epsilon}\right] \times \left[\frac{R^{(3)}\left(x^{(3)}(y)\right)}{R_N}\right]^3 \cos\left(\frac{\pi}{2}R^{(3)}\left(x^{(3)}(y)\right)\right). \tag{2.42}$$

b) Region 2: $\epsilon_{\mathbf{c}} \leqslant \epsilon < 3\epsilon_{\mathbf{c}}$

In this region, orbiting does not occur but there is a large negative minimum in the scattering angle. Viehland *et al.,* [43] split the integral at $b = R_c$, where R_c is the orbiting separation corresponding to energy ϵ_c. In each piece, they used Eq. (2.25) to change variables. This gives

$$Q^{(l)}(\epsilon) = 2\pi \int_{\widetilde{R}_0}^{\widetilde{R}_c} \left[1-\cos^l\theta\left(b^{(2)}(R),\epsilon\right)\right]\left[1-\frac{V(R)}{\epsilon}-\frac{R}{2}\frac{V'(R)}{\epsilon}\right] RdR + 2\pi \int_{\widetilde{R}_c}^{\infty} \left[1-\cos^l\theta\left(b^{(2)}(R),\epsilon\right)\right]\left[1-\frac{V(R)}{\epsilon}-\frac{R}{2}\frac{V'(R)}{\epsilon}\right] RdR, \tag{2.43}$$

where $\widetilde{R}_0$ and $\widetilde{R}_c$ are determined from iterative solutions of the equations

$$b^{(2)}\left(\widetilde{R}_c\right) = R_c, \tag{2.44}$$

and

$$V\left(\widetilde{R}_0\right) = \epsilon. \tag{2.45}$$

It is clearly noticeable that there is no trouble with the first integral, so Viehland *et al.* [43] introduced

$$R^{(4)}(y) = \frac{1}{2}\left[\left(\widetilde{R}_c - \widetilde{R}_0\right)y + \widetilde{R}_c + \widetilde{R}_0\right] \tag{2.46}$$

to change the interval to $[-1,1]$ and, to concentrate the quadrature points near the integration endpoints for the second integral, one must use

$$R^{(5)}(x) = \frac{\widetilde{R}_c}{\sin(\pi x/2)}. \tag{2.47}$$

The changing variables defined in Eqs. (2.46) and (2.47) convert Eq. (2.43) into

$$Q^{(l)}(\epsilon) = \int_{-1}^{1} g^{(l)}(y,\epsilon)\, dy, \tag{2.48}$$

where

$$\begin{aligned} g^{(l)}(y,\epsilon) &= \pi\left(\widetilde{R}_c - \widetilde{R}_0\right)\left[1-\cos^l\theta\left(b^{(2)}\left(R^{(4)}(y)\right),\epsilon\right)\right] \\ &\times\left[1-\frac{V\left(R^{(4)}(y)\right)}{\epsilon}-\frac{R^{(4)}(y)}{2}\frac{V'\left(R^{(4)}(y)\right)}{\epsilon}\right]R^{(4)}(y) \\ &+\frac{1}{2}\pi^2\widetilde{R}_c\left[1-\cos^l\theta\left(b^{(2)}\left(R^{(5)}\left(x^{(3)}(y)\right)\right),\epsilon\right)\right] \\ &\times\left[1-\frac{V\left(R^{(5)}\left(x^{(3)}(y)\right)\right)}{\epsilon}-\frac{R^{(5)}\left(x^{(3)}(y)\right)}{2}\frac{V'\left(R^{(5)}\left(x^{(3)}(y)\right)\right)}{\epsilon}\right] \\ &\times\left[\frac{R^{(5)}\left(x^{(3)}(y)\right)}{\widetilde{R}_c}\right]^3\cos\left(\frac{\pi}{2}x^{(3)}(y)\right) \end{aligned} \tag{2.49}$$

From this equation, we can deduce that

$$g^{(l)}(-1,\epsilon) = \left[1+(-1)^l\right]\pi\widetilde{R}_0\left(\widetilde{R}_c-\widetilde{R}_0\right)\left[-\frac{\widetilde{R}_0}{2}\frac{V'\left(\widetilde{R}_0\right)}{\epsilon}\right] \tag{2.50}$$

and

$$g^{(l)}(1,\epsilon) = \pi\widetilde{R}_c\left(\widetilde{R}_c-\widetilde{R}_0\right)\left[1-\cos^l\theta\left(b^{(2)}\left(\widetilde{R}_c\right),\epsilon\right)\right]\left[1-\frac{V\left(\widetilde{R}_c\right)}{\epsilon}-\frac{\widetilde{R}_c}{2}\frac{V'\left(\widetilde{R}_c\right)}{\epsilon}\right]. \tag{2.51}$$

c) Region 3: $3\epsilon_{\mathbf{c}} \leqslant \epsilon < \epsilon_{\max}$

Because orbiting does not also occur in this region, one has to make use of the same techniques for the integration of Eq. (2.14) at b_c, the orbiting impact parameter corresponding to ϵ_c. At small impact parameter, we define a new variable

$$b^{(4)}(y) = \frac{b_c}{2}(y+1) \tag{2.52}$$

and, at large impact parameters, we give another new variable

$$b^{(5)}(y) = \frac{2b_c}{y+1}. \tag{2.53}$$

Likewise the two above regions, Viehland *et al.* [43] transformed the integral in Eq. (2.14) into

$$Q^{(l)}(\epsilon) = \int_{-1}^{1} h^{(l)}(y,\epsilon)\, dy, \tag{2.54}$$

where

$$h^{(l)}(y,\epsilon) = \frac{1}{2}\pi b_c^2 \left[1 - \cos^l\theta\left(b^{(4)}(y),\epsilon\right)\right](y+1) + \pi b_c^2 \left[1 - \cos^l\theta\left(b^{(5)}(y),\epsilon\right)\right]\left[\frac{b^{(5)}(y)}{b_c}\right]^3. \tag{2.55}$$

We can easily show from Eq. (2.55) that $h^{(l)}(-1,\epsilon) = 0$. Hence, we may also show that

$$h^{(l)}(1,\epsilon) = 2\pi b_c^2 \left[1 - \cos^l\theta(b_c,\epsilon)\right]. \tag{2.56}$$

2.2.2 Quantum approach

The quantum-mechanical cross sections are obtained from the differential scattering $\sigma(\theta,\epsilon)$ which has the following form in the framework of the partial plane wave description [46, 47]

$$\sigma(\theta,\epsilon) = \frac{1}{4\kappa^2}\left|\sum_{l=0}^{\infty}(2l+1)\exp(2i\eta_l)\, P_l(\cos\theta)\right|^{2,} \tag{2.57}$$

where l is the orbital angular momentum quantum number, $\kappa = \sqrt{2\mu\epsilon}/\hbar$ is the wave number of the relative motion at energy ϵ, $P_l(\cos\theta)$ are Legendre polynomials, and $\eta_l = \eta_l(\epsilon)$ are the elastic phase shifts, which depend on the angular momentum l and energy ϵ. Hence, the problem of the quantum-mechanical transport cross sections is that the calculation of the phase shift η_l for each value of l is requiring detailed description of the interactions between the ions and the neutral atoms.

a) Phase shift

The phase shifts are usually obtained from the regular solution of the radial wave equation

$$\frac{d^2\psi_l(R)}{d^2R} + \left[\kappa^2 - \frac{2\mu}{\hbar^2}V(R) - \frac{l(l+1)}{R^2}\right]\psi_l(R) = 0. \tag{2.58}$$

The partial wave functions $\psi_l(R)$ must behave, at large distances R, like

$$\psi_l(R) \underset{R\to\infty}{\sim} \sin\left(\kappa R - \frac{l}{2}\pi + \eta_l\right) \tag{2.59}$$

The energy-dependent elastic phase shifts η_l are basically employed in the quantal computation of the transport cross sections.

The phase shifts are typically evaluated by using the approximation of Jeffrey with the modification of Langer as [48]

$$\eta_l = \int_{R_0}^{\infty} \left\{ \kappa^2 - \frac{2\mu V(R)}{\hbar^2} - \frac{(l+1/2)^2}{R^2} \right\}^{1/2} dR - \int_{R_0'}^{\infty} \left\{ \kappa^2 - \frac{(l+1/2)^2}{R^2} \right\}^{1/2} dR, \tag{2.60}$$

the lower limits being the outermost zeros of the respective integrands.

In practice, η_l are computed quantum mechanically up to a certain large value of the orbital angular momentum l^* beyond which the calculations are achieved with the semiclassical approximation [48, 49]

$$\eta_l \approx -\mu \int_{R_0}^{\infty} \frac{V(R)}{\sqrt{(\kappa R)^2 - (l+1/2)^2}} R dR, \tag{2.61}$$

where the lower limit R_0 verifies

$$\kappa R_0 = \left(l + \frac{1}{2} \right). \tag{2.62}$$

In Figs. 2-3 and 2-4, we have illustrated, as an example, the behavior of the quantal phase shifts that correspond to the doublet C^+He molecular states, $^2\Pi$ and $^2\Sigma$, and to the quartet C^+He molecular states, $^4\Pi$ and $^4\Sigma^-$, at the energies 10^{-4} and 10^{-3} hartree, respectively. One may notice from both Figures that, beyond $l^* = 132$ and $l^* = 82$, and respectively $l^* = 119$ and $l^* = 115$, the phase shifts η_l are calculated semiclassically with Eq. (2.61). The semiclassical asymptotes are represented in full solid curves.

b) Quantal diffusion cross section

The quantal expression for the diffusion transport cross section Q_d is obtained by summing over the angular momentum quantum number l [9]

$$Q_d(\kappa) = \frac{4\pi}{\kappa^2} \sum_{l=0}^{\infty} (l+1) \sin^2 \left(\eta_l - \eta_{l+1} \right). \tag{2.63}$$

This Eq. (2.63) shows orbiting resonances when the relative energy ϵ corresponds to a significant increase in the phase shifts η_l.

In Fig. 2-5, we illustrate a comparison of the quantum-mechanical and classical diffusion cross sections for the case of individual doublet and quartet states. It clearly shows that the

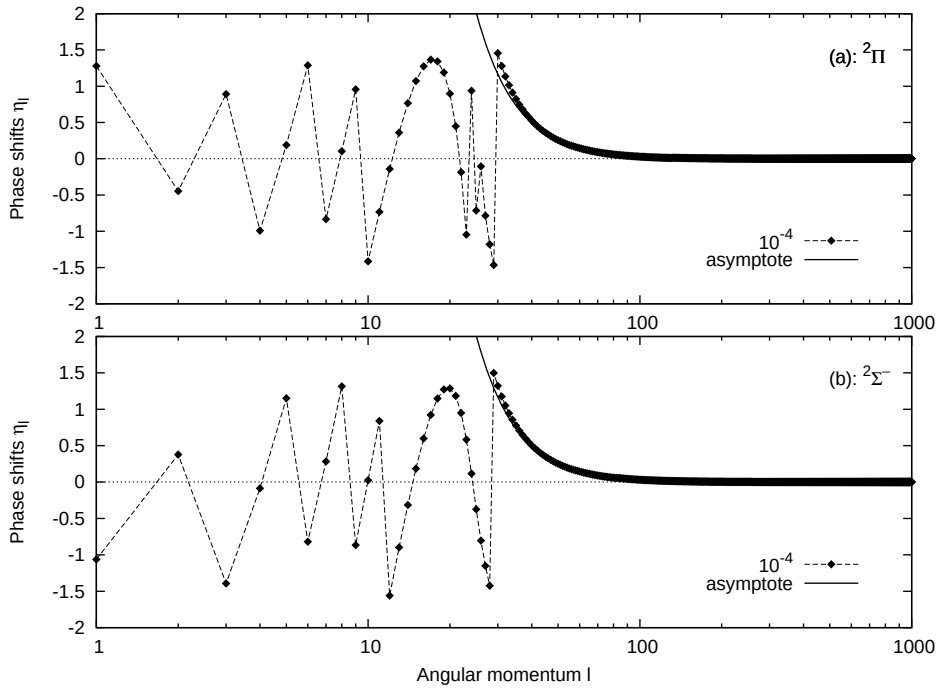

Figure 2-3: Elastic phase shifts obtained at the same energy, $\epsilon = 10^{-4}$ hartree, for two *doublet* C^+He states $^2\Pi$ and $^2\Sigma$.

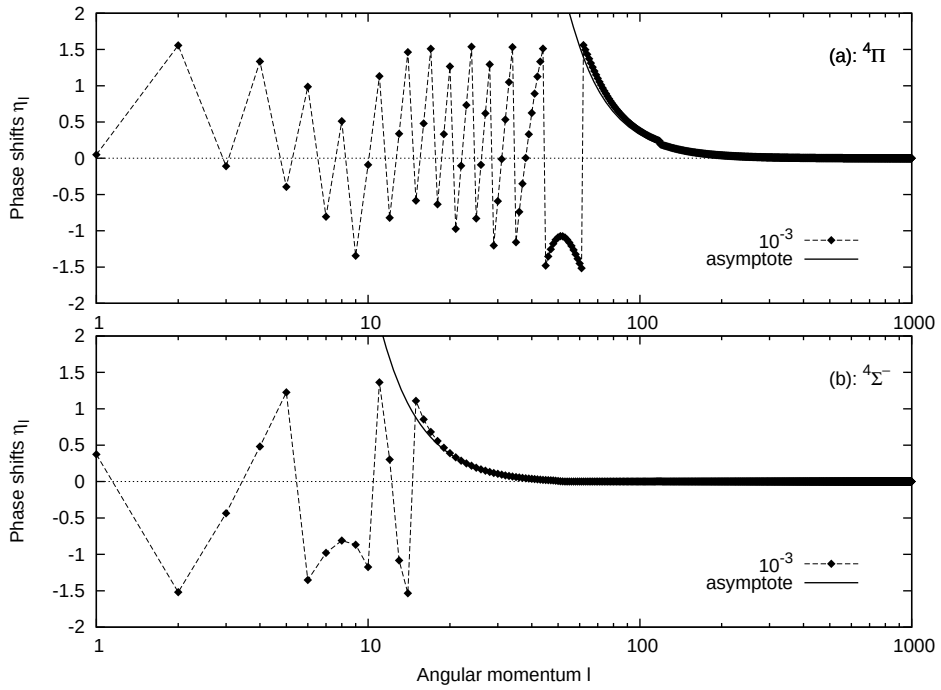

Figure 2-4: Elastic phase shifts obtained at the same energy, $\epsilon = 10^{-3}$ hartree, for two *quartet* C^+He states $^4\Pi$ and $^4\Sigma^-$.

quantal effects are important at lower energies, where the cross sections exhibit undulations with some regular peaks occurring at orbiting resonances. However, at higher energies, the quantum-mechanical diffusion cross sections have the same behavior as the classical diffusion cross sections. One may see that the behavior of the diffusion cross sections depend tightly on the depth of the considered interaction potential and their decrease becomes smooth and sharp beyond the energies corresponding to the well-depth values D_e. In particular, since the $^4\Sigma^-$ curve represents the deepest potential, the slope change occurs in Fig. 2-5(d) at the highest energy superior to $10^{-2}E_\mathrm{h}$.

Moreover, assuming one third of the collisions between C^+ and He occur along the Σ curves and two thirds along the Π curves [9], the average quantum-mechanical diffusion cross sections are therefore given by the statistically weighted sum

$$\overline{Q}_d(\kappa) = \frac{1}{3}Q_d^{\Sigma}(\kappa) + \frac{2}{3}Q_d^{\Pi}(\kappa). \tag{2.64}$$

The average quantum-mechanical cross sections, relative to the doublet and quartet states, are displayed in Fig. 2-6(a) and (b). They are both compared with the semiclassical results of Matoba *et al.* [3], which have linear forms at small energies. This Figure shows also the results of the average quantum-mechanical diffusion cross sections obtained by using the interaction potentials of Matoba *et al.* [3]. At higher energies, both potentials yield very similar behavior of the cross sections, which is not the case at lower energies.

2.3 Zero-field diffusion and mobility coefficients

The diffusion transport cross sections should allow the determination of the temperature-dependent coefficients of diffusion. The knowledge of such measurable parameter may primarily constitute sensitive probes and high-quality assessments for the accuracy of the ion-atom potentials. Indeed, according to the Chapman-Enskog model for the transport theory of *dilute* gases [9, 48], the collision integrals are defined as

$$\Omega_d(T) = \frac{1}{2}\int_0^\infty \frac{\epsilon^2}{(k_\mathrm{B}T)^3}\overline{Q}_d(\epsilon)\exp\left(-\frac{\epsilon}{k_\mathrm{B}T}\right)d\epsilon, \tag{2.65}$$

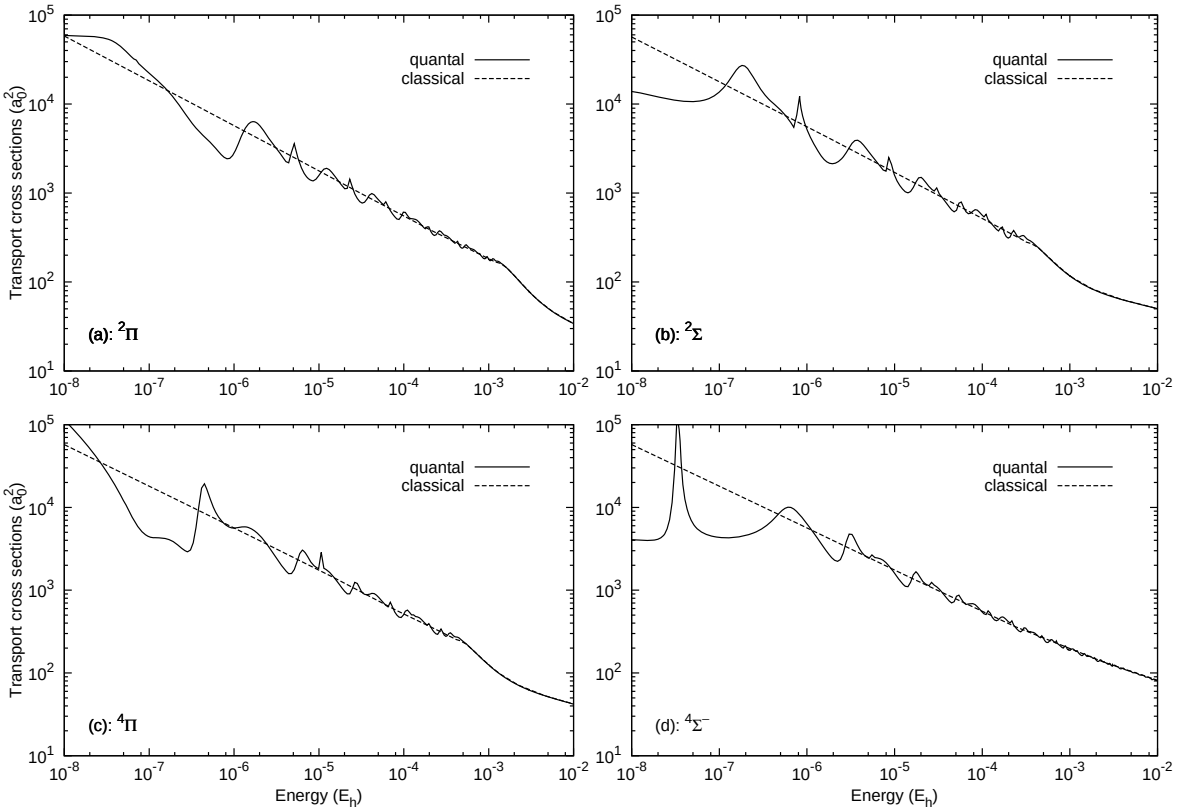

Figure 2-5: Comparison of the individual *quantum-mechanical* transport cross sections, effective in diffusion, with those obtained classically. The cross sections are computed, in (a) and (b), for the *doublet* states and, in (c) and (d), for the *quartet* states.

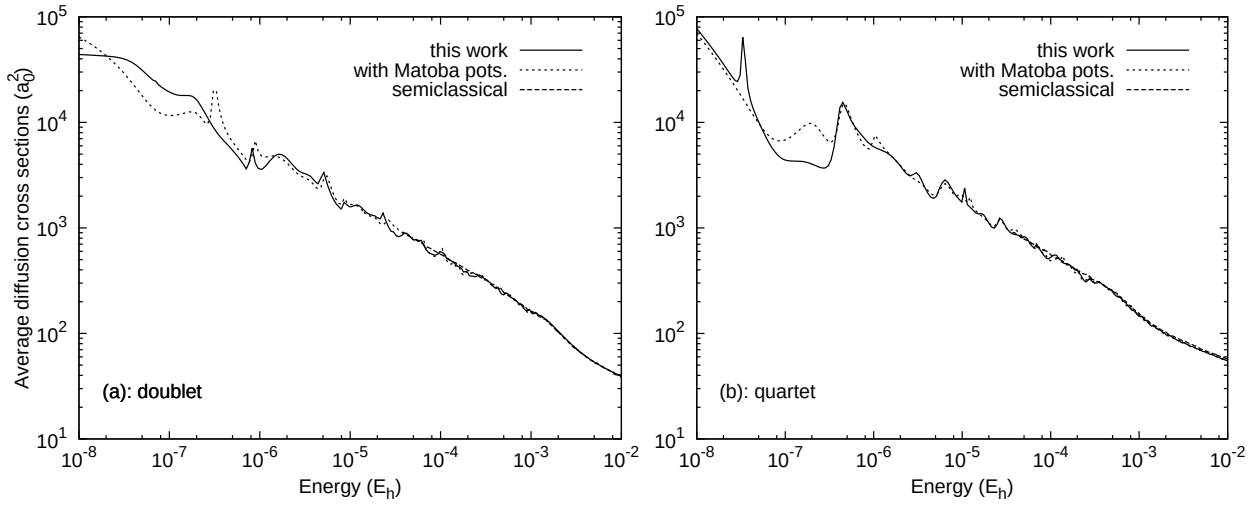

Figure 2-6: Average diffusion cross sections calculated with Eq. (2-6): in (a), for *doublet* states; in (b), for *quartet* states. Both cross sections are compared with the *quantum-mechanical* cross sections determined from the use of Matoba potentials. The *semiclassical* results of Matoba *et al.* [3] are represented in dashed lines.

which lead to the calculation of the *zero-field* mobility from the expression

$$K(T) = \frac{q}{k_{\mathrm{B}}T} D(T) \tag{2.66}$$

with q being the electric charge of the atomic ion and $D(T)$, given by

$$D(T) = \frac{3}{8N}\sqrt{\frac{\pi k_{\mathrm{B}}T}{2\mu}}\frac{1}{\Omega_d(T)}, \tag{2.67}$$

is the temperature-dependent coefficient of diffusion for the zero-field case. The number density N of the helium buffer gas is related to its pressure p by

$$p = N k_{\mathrm{B}} T. \tag{2.68}$$

At this point, one may observe that, numerically, the calculation of K is only possible if the integrand appearing in Eq. (2.65) constitutes a sommable function. Thus, the choice of the whole energy interval, over which the cross sections are computed, should be made to fulfill this requirement. For more illustration, we display in Fig. 2-7 the integrands of the

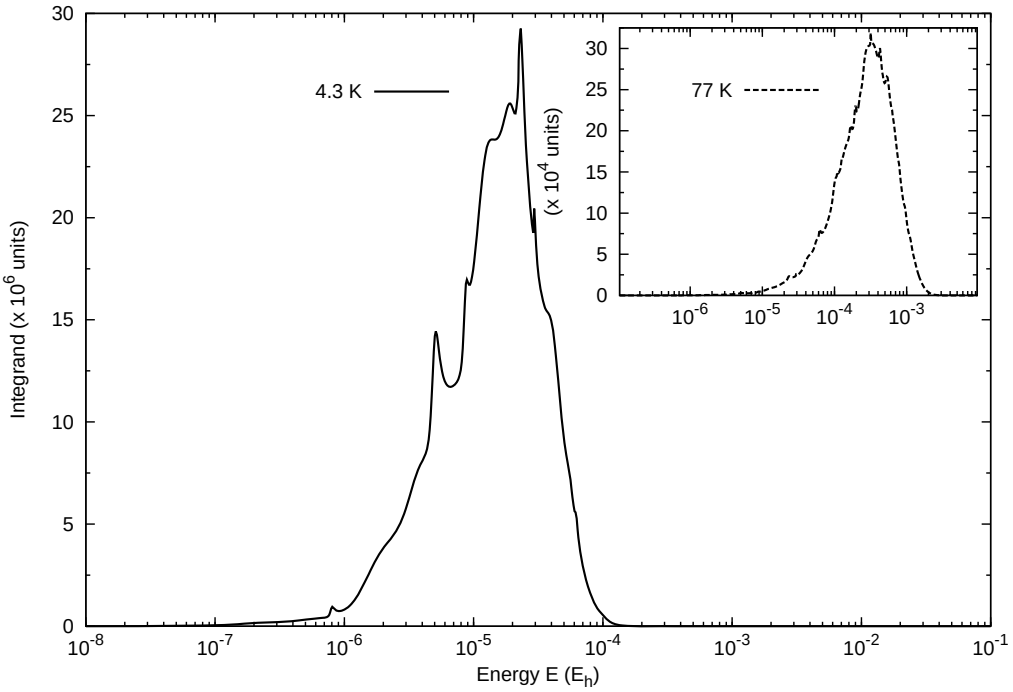

Figure 2-7: Integrands appearing in the collision integrals (2.65), in connection with the asymptotic separation $C^+\left(^2P^\circ\right)$ He, at the gas temperature 4.3 K; in the inset, at 77 K.

collision integrals, in connection with the asymptotic separation $C^+\left(^2P^\circ\right)$ He, at two distinct gas temperatures: 4.3 and 77 K. This Figure shows the required minimum and the maximum values of energy ϵ for each gas temperature. For instance, the energy interval should be $10^{-8} \lesssim \epsilon \lesssim 10^{-3}$ hartree, if the gas temperature is 4.3 K.

As stated above in Eq. (1.80), the mobility coefficient is usually expressed, if p is in torrs and T in kelvins, as

$$K_0(T) = \left(\frac{p}{760}\right)\left(\frac{273.15}{T}\right) K(T), \tag{2.69}$$

known as the *reduced* mobility [9]. The results of the diffusion coefficient D, presented as D times the gas pressure $p = 0.250$ Torr or times the number density N, are listed in Table 2.7 for the case of helium buffer gas at temperature $T = 297$ K. The same Table 2.7 also presents, in the same conditions, the zero-field reduced mobility K_0 of the $C^+\left(^2P^\circ\right)$ and $C^+\left(^4P\right)$ ions moving through helium. In particular, our ground theoretical results are compared to the experimental measurements of Dotan, Fehdenfeld, and Albritton [53]. The comparison shows an excellent agreement between the values, which confirms, once again, the good quality of our generated *ab initio* C^+He potentials.

Table 2.7: Zero-field reduced mobility K_0 and diffusion coefficients D at room temperature $T = 297$ K. The diffusion coefficients are given as D times the pressure $p = 0.250$ torr and times the gas density N. The ground-state results are compared with data from Dotan *et al.* [53].

	$C^+\left(^2P^\circ\right)$ in He		$C^+\,(^4P)$ in He
Coefficients	This work	Dotan *et al.* [53]	This work
pD $\left(\mathrm{cm^2\,Torr\,s^{-1}}\right)$	468	461	463
ND $\left(10^{19}\,\mathrm{cm^{-1}\,s^{-1}}\right)$	1.52	1.50	1.51
K_0 $\left(\mathrm{cm^2\,V^{-1}\,s^{-1}}\right)$	22.1	21.8 ± 1.1	21.9

Chapter 3

Mobility of C^+ Ions in Helium Gas

As a consequence of the relative simplicity at calculating cross sections for closed shell systems, most of the kinetic theory studies of ion transport systems have involved alkali metal cations and halogen anions with inert gases. However, there are few theoretical studies of open-shell atomic systems that are published in literature. As a result, the information contained in the available databases of the transport properties [20, 50, 51] of open-shell atomic systems has largely been neglected. This is mainly due to the difficulties met at calculating the cross sections in which two or more collision channels correlate to the non-interacting collision partners. Similarly, there are a few theoretical studies of electronically excited ion-atom systems [3, 40, 52], although the databases of such systems are equally sparse.

So, in this last Chapter, a detailed review of the ion mobility calculations is given for the open-shell carbon ion, in the ground $C^+\left(^2P^\circ\right)$ and metastable $C^+\left(^4P\right)$ states, interacting with helium, using the three-temperature theory. To accomplish this task, we use the quantum-mechanical diffusion cross sections deduced in the previous Chapter. The obtained results are compared with the published experimental data in Ref. [3].

3.1 Previous works

The mobility of C^+ ions in helium has been of continuing interest in the experimental determination of the ion/molecule rate coefficients of C^+ reactions, which have large astrophysical applications. It is very sensitive to the shape and numerical values of the interaction potential curve between the ion and the neutral gas.

For this reason, several experiments have been performed to measure the mobility of C^+ ions in helium gas, such as the experiments of Dotan *et al.* [53], Thomas *et al.* [54], Peska *et al.* [55],

Twiddy *et al.* [56], Grice *et al.* [40], and more recently of Matoba *et al.* [3]. Furthermore, there have been different theoretical attempts at calculating the mobility of ground and metastable-excited states of C^+ ions in helium gas, such as by Grice *et al.* [40] and Matoba *et al.* [3], which have been obtained by using the classical transport cross sections within the first approximation of the *two*-temperature theory.

The crucial theoretical idea of Grice *et al.* [40] at calculating the mobility of ground $C^+(^2P^\circ)-$He and metastable-excited $C^+(^4P)-$He states at room temperature was based on the relationship between the reduced mobility and the effective collision integral which provides them to give an expression for calculating the average reduced mobility. Their theoretical results were in good agreement with their measured results.

In fact, in recent experiment of Matoba, Tanuma, and Ohtsuki [3] using a very low temperature drift-tube-mass spectrometer at 4.3 and 77 K, they could achieve a condition in which the T_{eff} is low enough for mobility to become very close to $K_{\rm pol}$ of ground and metastable-excited states. Moreover, they also computed the relevant average classical transport cross sections and used them to calculate the mobility. In their published work [3], the authors suggest to improve the calculations by using quantum-mechanical cross sections and a higher-level kinetic theory. Accordingly, we intend to use the *three*-temperature theory and the quantal transport cross sections generated above to determine the mobility of C^+ in He.

3.2 Numerical details

In this section, we introduce the average of the *doublet* and *quartet* diffusion cross sections $\overline{Q}_d(\epsilon)$ for C^+-He system into the Fortran code GC.F90 to compute the mobility of ground $C^+\left(^2P^\circ\right)$ and metastable-excited $C^+\,(^4P)$ states in helium gas [5–7]. This code, which relies on the Gram-Charlier series [6], uses the cross sections into three distinctive energy intervals that were revealed earlier in Chapter 2

$$\begin{aligned} \epsilon_{\rm min} &\leqslant \epsilon < \epsilon_{\rm c} \\ \epsilon_{\rm c} &\leqslant \epsilon < 3\epsilon_{\rm c} \\ 3\epsilon_{\rm c} &\leqslant \epsilon \leqslant \epsilon_{\rm max}. \end{aligned} \tag{3.1}$$

In each interval, the transport cross sections are fitted by means of the Chebyshev expansion coefficients

$$a_i = \frac{2}{\mathcal{N}} \sum_{k=0}^{\mathcal{N}} \widetilde{T}_i \left[\cos\left(\frac{k\pi}{\mathcal{N}} \right) \right] \log \left\{ \overline{Q}_d (\epsilon) \right\}, \tag{3.2}$$

where $\mathcal{N}$ is the number of energies in each region and the tilde sign above the Chebyshev polynomials $\widetilde{T}_i$ indicates that the *first* and *last* terms in the summation are *halved.* The cross sections are given by a finite series of Chebyshev polynomials $\widetilde{T}_i [\xi(\epsilon)]$ in GC.F90 as [43]

$$\log \left\{ \overline{Q}_d (\epsilon) \right\} = \sum_{i=0}^{\mathcal{N}} a_i \widetilde{T}_i [\xi(\epsilon)], \tag{3.3}$$

with $|\xi(\epsilon)| \leqslant +1$ being defined by

$$\xi(\epsilon) = \frac{2\log(\epsilon) - \log(\epsilon_{\max}) - \log(\epsilon_{\min})}{\log(\epsilon_{\max}) - \log(\epsilon_{\min})}, \tag{3.4}$$

where $\epsilon_{\min}$ and $\epsilon_{\max}$ are the limits of each of the above energy intervals.

3.3 Results and discussion

Mobility and diffusion coefficients have been reported for both ground $C^+ \left(^2P^\circ\right)$He and metastable-excited states $C^+ (^4P)$ He. Their calculations were performed at the gas temperatures 297, 4.3, and 77 K. We have first chosen to treat the reduced mobility K_0 at 297 K to confirm the reliability of our CHe^+ interaction potentials, then, to verify the quantum-mechanical results of K_0, at the temperatures of interest, 4.3 and 77 K, with the three-temperature theory. Moreover, we have also used, for more illustrations, the interaction potentials of Ref. [3] in the calculations of mobility.

3.3.1 Room temperature: 297 K

According to the results of several experiments that have been performed to measure the reduced mobilities K_0 of ground and metastable-excited C^+ ions in helium at room temperature $T =$ 297 K or close to it [40, 53–56], we have first chosen to treat K_0 at this temperature to confirm the reliability of our CHe^+ interaction potentials and to verify the results of the quantum-mechanical calculations, with three-temperature theory, of the reduced mobility, K_0, at the temperature of interest, 4.3 and 77 K.

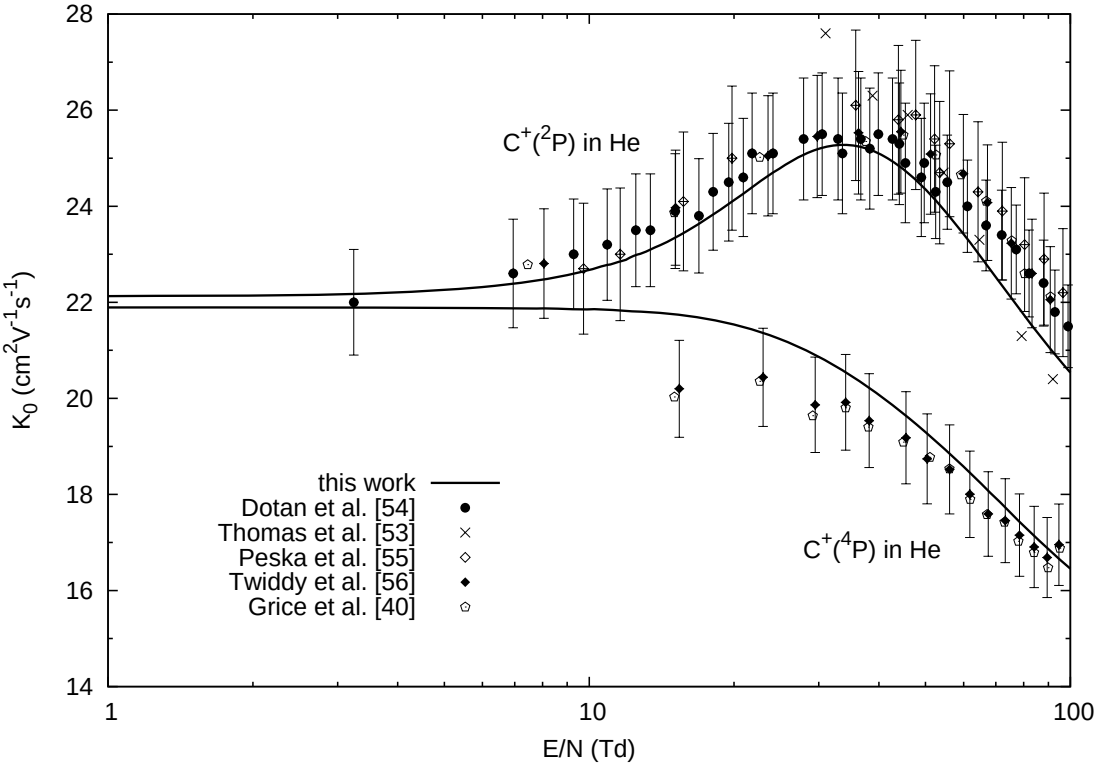

Figure 3-1: Non zero-field mobilities of the $C^+\left(^2P^\circ\right)$ and $C^+\,(^4P)$ ions into He as a function of E/N at room temperature $T \simeq 300\,\mathrm{K}$. They are compared with published data from [40,53–56].

The obtained results, presented in terms of the ratio E/N of the electric field strength to the gas number density, are drawn in Fig. 3-1 as full solid lines. They are compared in the same figure with a bunch of theoretical and experimental data determined at very close temperatures [40, 53–56]. As the ratio E/N goes to zero, the curves show particularly that the lower limits of the reduced mobilities agree quite well with the values 22.1 and $21.9\,\mathrm{cm^2\,V^{-1}\,s^{-1}}$, also confirmed from Table 2.5. Moreover, when the electric field increases in intensity, the present $C^+\left(^2P^\circ\right)$ mobility results reach a maximum that lies between 20 and $50\,\mathrm{Td}$ $(1\,\mathrm{Td} = 10^{-21}\,\mathrm{V\,m^2})$, which is believed typical for mobilities in helium [55]. As already underlined by Dotan *et al.* [53], the zero-field mobilities show they are substantially different from the polarization value $K_{\mathrm{pol}} \simeq 17.66\,\mathrm{cm^2\,V^{-1}\,s^{-1}}$, which suggests that the Langevin approximation is a poor one for ions at room temperature in the rather weakly polarizable helium. The polarization limit is theoretically reached when the gas temperature is low enough, i.e., $T \to 0$ [57].

3.3.2 Low temperatures: 4.3 and 77 K

We have further employed the three-temperature model of Lin *et al.* [4,9,11,43] to generate the mobilities of C^+ into He as a function of the ratio E/N at very low temperatures, namely, 4.3 and 77 K by means of quantum-mechanical transport cross sections. The results are presented in Fig. 3-2(a)-(d). The upper and lower graphs illustrate the calculations and measurements at 4.3 and 77 K, respectively. The solid curves correspond to those in which the present *ab initio* potentials are used, whereas the dashed lines represent the calculated mobilities by inserting the potentials described in Ref. [3]. The polarization limits, $K_{\rm pol} \simeq 17.66\,{\rm cm^2\,V^{-1}\,s^{-1}}$, are shown with horizontal dotted lines. All the present calculations are contrasted with the mobility measurements, known with the accuracy of $\pm 0.2\,{\rm cm^2\,V^{-1}\,s^{-1}}$, carried out by Matoba *et al.* [3] at the prescribed temperatures.

The first column gives the reduced mobility coefficients in connection with the ground $C^+\left(^2P^\circ\right)$ ions moving into helium. As the electric field tends to zero, the curves in Fig. 3-2(a) shows that the mobility approaches the value $18.8\,{\rm cm^2\,V^{-1}\,s^{-1}}$, also found from the zero-field calculations. For higher values of the ratio E/N, the experimental data attain lower values around ~ 10 Td before their increase. Unfortunately, this feature was unable to be imitated numerically by using both potential sets. Furthermore, for the 77 K curves exhibited in Fig. 3-2(b), the agreement of the present results with the experimental data is better, which leads us to assume the accuracy of the quantal collision integrals at a higher temperature is good enough. As the electric strength goes to zero, the reduced mobility appear here too to tend to $19.1\,{\rm cm^2\,V^{-1}\,s^{-1}}$. Tables 3.1 and 3.2 list the main transport parameters as a function of E/N at 4.3 and 77 K, respectively.

The second column displays the variation of K_0 in terms of the ratio E/N of the metastable-excited $C^+\,(^4P)$ ions through helium. In Fig. 3-2(c) and (d), the curves, extrapolated to the zero-field limits, end at the values 18.4 and $19.6\,{\rm cm^2\,V^{-1}\,s^{-1}}$. Tables 3.3 and 3.4 give also the transport parameters as a function of E/N at 4.3 and 77 K, respectively.

3.3.3 Further calculations and comparisons

With the aim of computing the non zero-field mobility of $C^+\left(^2P^\circ\right)$ and $C^+\,(^4P)$ ions through helium gas at cooled temperatures, it is interesting to compare the results generated by the present potentials with those produced by the potentials of Matoba and his collaborators [3]. Both classical and quantal approaches are used, within the frameworks of the three-temperature

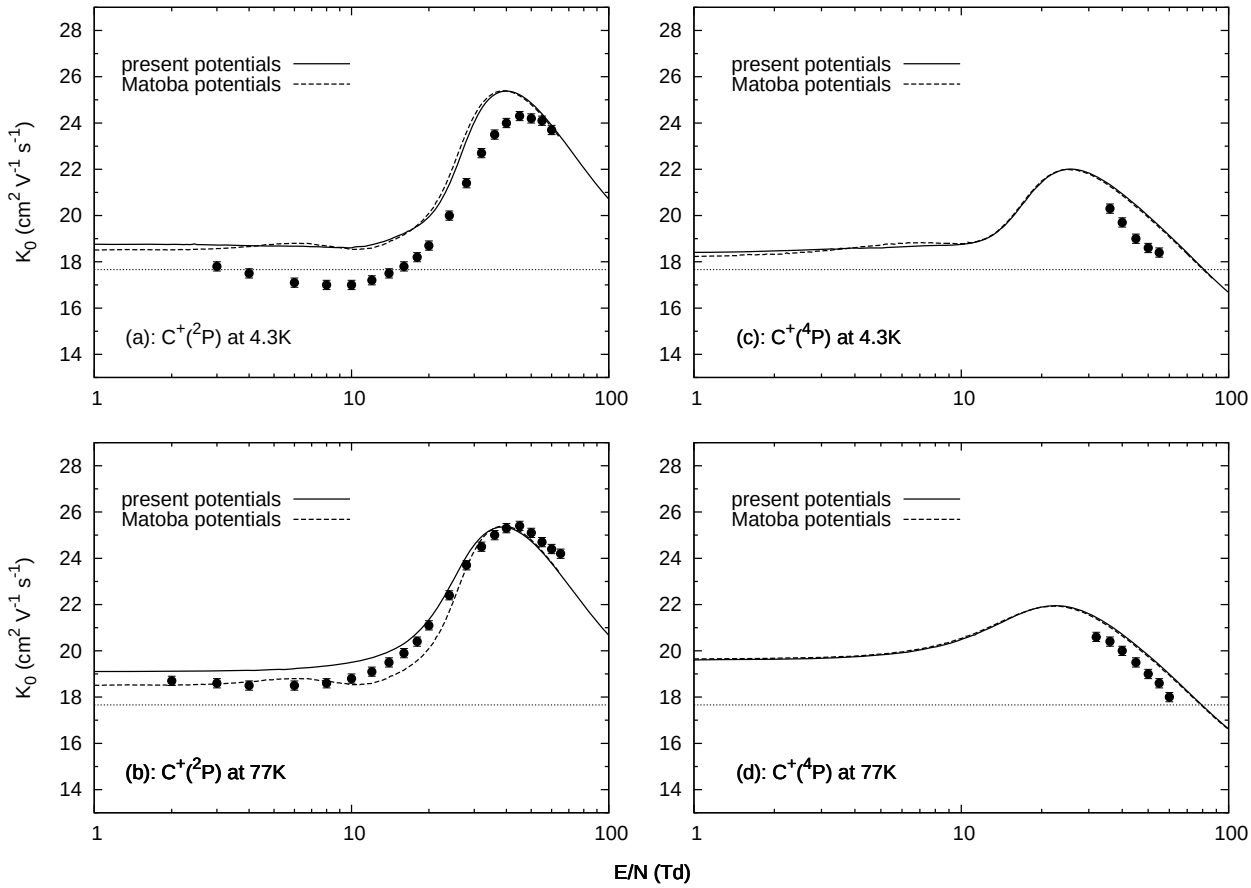

Figure 3-2: Non zero-field mobilities of the $C^+\left(^2P^\circ\right)$ and $C^+\left(^4P\right)$ ions into helium as a function of E/N at two distinct temperatures: in the upper row at $T = 4.3\,\mathrm{K}$, and in the lower row at $T = 77\,\mathrm{K}$. Full circles are the measurements of Matoba *et al.* [3], estimated as ± 0.2. The first column is connected with $C^+\left(^2P^\circ\right)$ moving through He and the second column with $C^+\left(^4P\right)$. The dashed lines represent our calculations with the potentials described in [3]. The horizontal dotted lines represent the polarization limit $K_{\mathrm{pol}} = 17.66\,\mathrm{cm^2\,V^{-1}\,s^{-1}}$.

Table 3.1: Non zero-field transport properties for the ground state $C^+(2P)$ in He at 4.3 K. These values are calculated with our potentials.

E/N	v_d	K_0	T_L	T_T	ND_L	ND_T
(Td)	($m\,s^{-1}$)	($cm^2\,V^{-1}\,s^{-1}$)	(K)		($10^{20}\,m^2\,s^{-1}$)	
0.03	0.001	18.76	4.30	4.30	0.187	0.187
1.47	0.553	18.75	5.76	4.88	0.250	0.212
4.46	1.675	18.68	17.71	9.66	0.766	0.418
8.27	3.095	18.63	50.07	22.61	2.160	0.975
12.90	4.881	18.82	118.12	49.83	5.148	2.172
18.40	7.253	19.61	255.62	104.83	11.605	4.759
24.41	10.566	21.53	537.67	217.64	26.803	10.850
29.21	13.941	23.75	932.92	375.74	51.291	20.658
35.61	18.034	25.19	1558.26	625.87	90.896	36.508
42.31	21.553	25.34	2223.74	892.05	130.483	52.343
50.64	25.253	24.81	3051.12	1222.99	175.238	70.241
60.49	29.007	23.86	4024.52	1612.34	222.285	89.054
71.25	32.667	22.81	5102.91	2043.68	269.475	107.923
81.96	36.067	21.89	6219.47	2490.30	315.226	126.218
91.50	39.040	21.23	7286.37	2917.04	358.065	143.349
102.02	42.258	20.61	8536.40	3417.04	407.258	163.022

Table 3.2: Non zero-field transport properties for the ground state $C^+(2P)$ in He at 77 K. These values are calculated with our potentials.

E/N	v_d	K_0	T_L	T_T	ND_L	ND_T
(Td)	($m\,s^{-1}$)	($cm^2\,V^{-1}\,s^{-1}$)	(K)		($10^{20}\,m^2\,s^{-1}$)	
0.07	0.006	19.10	77.00	77.00	3.405	3.405
1.39	0.126	19.11	78.37	77.55	3.467	3.431
4.52	0.412	19.16	91.50	82.80	4.060	3.674
8.24	0.758	19.37	126.20	96.68	5.659	4.335
12.96	1.220	19.82	204.28	127.91	9.374	5.870
18.59	1.849	20.94	369.39	193.95	17.905	9.401
24.32	2.640	22.86	673.44	315.57	35.642	16.702
29.41	3.416	24.45	1075.10	476.23	60.848	26.953
35.38	4.247	25.27	1620.04	694.20	94.770	40.609
42.29	5.075	25.27	2280.83	958.51	133.421	56.070
50.74	5.947	24.67	3102.39	1287.12	177.211	73.521
60.61	6.831	23.72	4068.94	1673.73	223.477	91.926
71.33	7.693	22.70	5139.75	2102.04	270.172	110.494
81.92	8.493	21.83	6248.46	2545.51	315.744	128.628
91.40	9.193	21.17	7307.85	2969.25	358.255	145.562
101.77	9.951	20.59	8549.09	3465.74	407.444	165.175

Table 3.3: Non zero-field transport properties for the ground state $C^+(4P)$ in He at 4.3 K. These values are calculated with our potentials.

E/N	v_d	K_0	T_L	T_T	ND_L	ND_T
(Td)	($m\,s^{-1}$)	($cm^2\,V^{-1}\,s^{-1}$)	(K)		($10^{20}\,m^2\,s^{-1}$)	
0.03	0.001	18.42	4.30	4.30	0.183	0.183
1.46	0.542	18.44	5.70	4.86	0.243	0.208
4.48	1.675	18.60	17.71	9.66	0.763	0.416
8.22	3.095	18.72	50.07	22.61	2.171	0.980
12.95	4.978	19.12	122.72	51.67	5.432	2.287
18.55	7.851	21.06	298.76	122.08	14.564	5.951
24.38	10.777	21.99	559.22	226.26	28.473	11.520
29.29	12.880	21.88	796.87	321.32	40.363	16.275
35.87	15.392	21.35	1136.28	457.08	56.156	22.589
42.49	17.681	20.70	1497.92	601.73	71.788	28.838
50.69	20.310	19.93	1975.10	792.60	91.142	36.575
60.81	23.330	19.08	2604.73	1044.44	115.092	46.149
71.48	26.273	18.29	3302.28	1323.45	139.802	56.028
82.01	29.007	17.60	4024.52	1612.34	163.949	65.683
91.47	31.399	17.08	4714.62	1888.37	186.391	74.656
101.88	33.987	16.60	5523.20	2211.79	212.220	84.985

Table 3.4: Non zero-field transport properties for the ground state $C^+(4P)$ in He at 77 K. These values are calculated with our potentials.

E/N	v_d	K_0	T_L	T_T	ND_L	ND_T
(Td)	($m\,s^{-1}$)	($cm^2\,V^{-1}\,s^{-1}$)	(K)		($10^{20}\,m^2\,s^{-1}$)	
0.00	0.000	19.59	77.00	77.00	3.492	3.492
1.36	0.126	19.62	78.37	77.55	3.560	3.522
4.38	0.412	19.77	91.50	82.80	4.187	3.789
8.22	0.789	20.20	130.25	98.30	6.091	4.597
12.96	1.294	21.02	220.34	134.33	10.723	6.538
18.57	1.923	21.80	393.49	203.59	19.861	10.276
24.37	2.538	21.92	628.02	297.40	31.878	15.096
29.50	3.033	21.65	863.99	391.79	43.300	19.635
35.38	3.554	21.14	1157.37	509.14	56.650	24.921
42.87	4.164	20.44	1560.12	670.23	73.835	31.720
51.05	4.783	19.72	2033.94	859.75	92.870	39.257
61.15	5.494	18.91	2659.14	1109.83	116.435	48.596
71.77	6.187	18.15	3351.78	1386.87	140.825	58.269
82.16	6.831	17.50	4068.94	1673.73	164.881	67.823
91.62	7.394	16.99	4754.20	1947.82	186.991	76.611
101.81	8.003	16.55	5557.08	2268.97	212.917	86.935

theory, in the calculation of the transport cross sections. The utilization of these cross sections into the Fortran code GC.F90 allows then the comparison of all sets of results.

Since, the reduced mobility has a straightforward relationship with the diffusion cross sections Q_d, we opted here to determine the average reduced mobility from the average relationship

$$\frac{1}{K_0} = \frac{1}{3K_0^{\Sigma}} + \frac{2}{3K_0^{\Pi}}. \tag{3.5}$$

Such an approach of calculations has already been adopted by Grice *et al.* [40].

Figures 3-3 and 3-4 display for comparison the quantum-mechanical and classical results of the reduced mobilities K_0 of ground C^+ ions in helium He at 4.3 and 77 K, respectively. The upper(left-hand-side) plots(graphs) (a) illustrate the calculated reduced mobilities using the interaction potentials generated in the present work, whereas the mobility values represented in the lower(right-hand-side) plots(graphs) (b) are determined with the potential-energy curves as calculated by Matoba *et al.* [3]. Both Figures 3-3 and 3-4 show for $E/N \lesssim 10$ Td slight differences between the quantal and classical K_0 values. As $E/N \to 0$, the mobilities approach close values. However, for higher values of the electric field, more precisely for $E/N \gtrsim 10$ Td, these differences become noticeable. On the other hand, for lower electric field, the mobility coefficients of metastable-excited C^+ ions moving into helium, presented in Figures 3-5 and 3-6, show more distinctive differences between the results due to the present and Matoba potentials. With these two potential sets, as E/N exceeds 30 Td, the quantal and classical results coincide, though they seem at $T = 77$ K closer to the experimental values.

Moreover, as the electric field approaches zero, the classical calculations of K_0 with Matoba potentials yield, at the very low temperature $T = 4.3$ K, results very close to the polarization limit $K_{\rm pol} \simeq 17.66\,{\rm cm^2\,V^{-1}\,s^{-1}}$ than those obtained quantum mechanically. This is clearly demonstrated in Figs. 3-3(b) and 3-5(b).

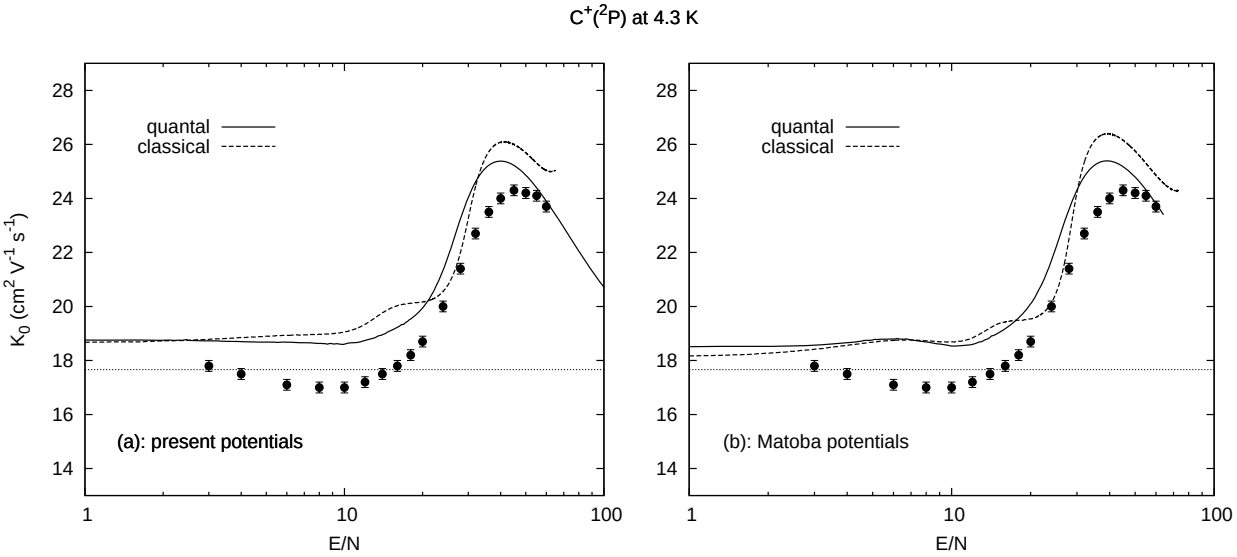

Figure 3-3: Non zero-field mobilities of the $C^+\left(^2P^\circ\right)$ ions in He as a function of E/N at $T = 4.3\,\mathrm{K}$. The quantal and classical mobilities are obtained in (a) with the interaction potentials of the present work and in (b) with those of Matoba *et al.* [3]. Full circles are measurements from [3], estimated as ± 0.2. The horizontal dotted lines represent the polarization limit $K_{\mathrm{pol}} = 17.66\,\mathrm{cm^2\,V^{-1}\,s^{-1}}$.

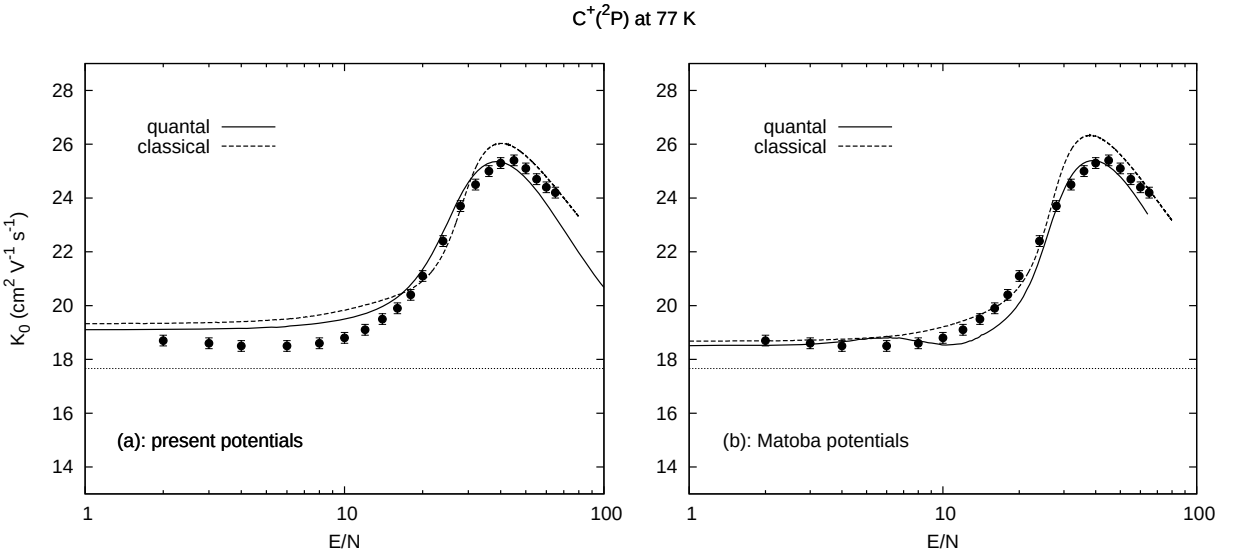

Figure 3-4: Non zero-field mobilities of the $C^+\left(^2P^\circ\right)$ ions in He as a function of E/N at $T = 77\,\mathrm{K}$. The quantal and classical mobilities are obtained in (a) with the interaction potentials of the present work and in (b) with those of Matoba *et al.* [3]. Full circles are measurements from [3], estimated as ± 0.2. The horizontal dotted lines represent the polarization limit $K_{\mathrm{pol}} = 17.66\,\mathrm{cm^2\,V^{-1}\,s^{-1}}$.

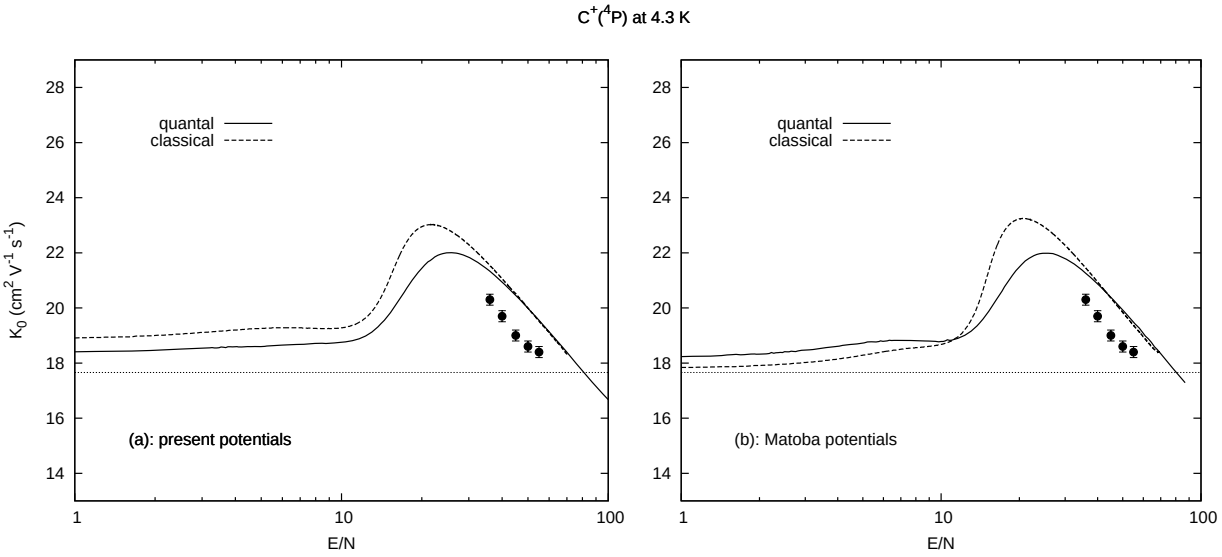

Figure 3-5: Non zero-field mobilities of the C^+ (^4P) ions in He as a function of E/N at $T = 4.3\,\mathrm{K}$. The quantal and classical mobilities are obtained in (a) with the interaction potentials of the present work and in (b) with those of Matoba *et al.* [3]. Full circles are measurements from [3], estimated as ± 0.2. The horizontal dotted lines represent the polarization limit $K_{\mathrm{pol}} = 17.66\,\mathrm{cm^2\,V^{-1}\,s^{-1}}$.

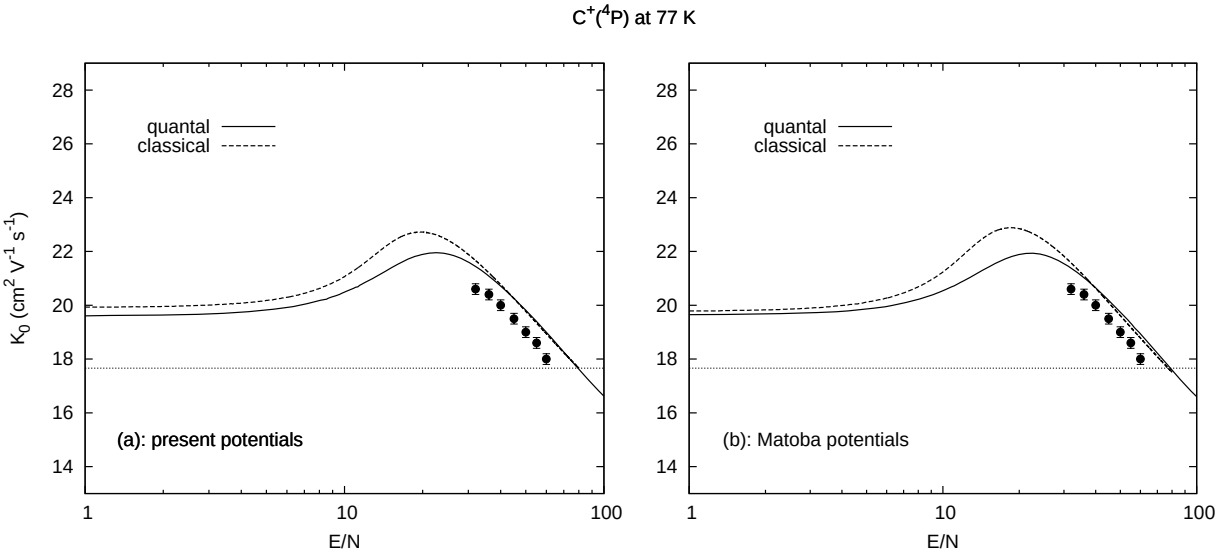

Figure 3-6: Non zero-field mobilities of the C^+ (^4P) ions in He as a function of E/N at $T = 77\,\mathrm{K}$. The quantal and classical mobilities are obtained in (a) with the interaction potentials of the present work and in (b) with those of Matoba *et al.* [3]. Full circles are measurements from [3], estimated as ± 0.2. The horizontal dotted lines represent the polarization limit $K_{\mathrm{pol}} = 17.66\,\mathrm{cm^2\,V^{-1}\,s^{-1}}$.

Conclusion

This thesis succeeded in its main objective based on the recommendations of the recent work of Matoba *et al.* [3]. Ion transport properties of C^+ in He have been calculated at cooled temperatures. The calculations have generally resulted in fairly good agreement with the experiments.

The process of this work is started by the construction of the energy-potential curves corresponding to the dimers which dissociate into $C^+\left(^2P^\circ\right) + He\left(^1S\right)$ and $C^+\left(^4P\right) + He\left(^1S\right)$. The constructed potentials have been made in the three separation domains, depending on the *ab initio* data computed with MOLPRO. The quality and the accuracy of our obtained potentials have been compared and verified with data from the literature, such as the spectroscopic parameters. The obtained results are generally in good agreement with the obtained ones of the other authors, which proves the trustworthiness of our constructions.

Afterward, we have numerically calculated the diffusion cross sections for the doublet $\left(^2\Sigma \text{ and } ^2\Pi\right)$ and quartet $\left(^4\Sigma^- \text{ and } ^4\Pi\right)$ states. These cross sections have followed two different trajectory methods: classical method and quantal method. The classical transport cross sections have been computed with the Fortran code PC.F90 [43]. The obtained results have been compared with the semi-classical transport cross sections of Matoba *et al.* [3].

Finally, we have used the average transport cross sections within the frames of the the three-temperature theory accomplished with the GC.F90 Fortran code [5–7] to determine, at 4.3 and 77 K temperatures, the mobility of C^+ ions in He and to examine their variation with the ratio E/N. These transport parameters have been compared with published measurements of C^+ in He mobilities. The agreement has been found fairly good.

Appendix A

Publication and communication

The main work presented in this thesis has been the subject of a paper, published in *Molecular Physics,* and an international communication. They are both given below.

A.1 Paper

L. Aïssaoui, M. Bouledroua, and K. Alioua, *Mobility of carbon ions* $C^+\left(^2P^\circ\right)$ *and* $C^+\left(^4P\right)$ *in helium computed from quantum-mechanical transport cross sections,* Molecular Physics **113** (2015).

DOI: 10.1080/00268976.2015.1059960

A.2 Communication

M. Bouledroua, L. Aïssaoui, and K. Alioua, *Quantal determination of the mobility of ground and excited* C^+ *ions evolving in a cooled helium gas,* Physical Processes in the Interstellar Medium, Max-Plank Institute for Extraterrestrial Physics 21-25 October 2013, Garching-Munich, Germany.

Molecular Physics, 2015
http://dx.doi.org/10.1080/00268976.2015.1059960

RESEARCH ARTICLE

Mobility of carbon ions $C^+(^2P^\circ)$ and $C^+(^4P)$ in helium computed from quantum-mechanical transport cross sections

Lamia Aïssaoui[a,*], Moncef Bouledroua[b] and Kamel Alioua[b,c]

[a]*Physics Department, Badji Mokhtar University, Annaba, Algeria;* [b]*Laboratoire de Physique des Rayonnements, Badji Mokhtar University, Annaba, Algeria;* [c]*Faculty of Science and Technology, Chérif Messadia University, Souk-Ahras, Algeria*

(*Received 17 April 2015; accepted 2 June 2015*)

On the light of a previous work and its recommendations by Matoba *et al.* [J. Phys. B **41**, 145205 (2008)], this paper proposes to look at the mobility of ground and metastable-excited states of C^+ ions moving into a helium buffer gas. The calculations, based on the three-temperature theory for solving the Boltzmann kinetic equation, are accomplished with quantum-mechanical transport cross sections at the low temperatures 4.3 and 77 K. The obtained mobility results are contrasted with the available theoretical data and experimental measurements, which show acceptable agreements.

Keywords: potential-energy curve; transport cross section; three-temperature theory; mobility

PACS numbers: 34.20.Cf; 51.10.+y; 51.20.+d; 72.20.Fr

1. Introduction

In 2008, Matoba *et al*. [1] studied at Tokyo Metropolitan University (TMU) the mobility of carbon ions in a neutral helium gas, cooled by helium and nitrogen. More specifically, using a drift tube mass spectrometer with a mass-selected-ion-injection system, they measured the mobilities of the ground $2s^2 2p\ ^2P^\circ$ and metastable-excited $2s2p^2\ ^4P$ states of C^+ into He at two low temperatures, 4.3 and 77 K. They further computed the relevant *classical* transport cross sections, which they used to determine the mobilities of C^+ in He, within the first approximation of the *two*-temperature theory set up for solving the Boltzmann equation [2,3], and analysed their behaviour in terms of the ratio E/N of the electric field strength to the gas number density of the neutral gas. In their published work [1], the authors suggest to improve the calculations by using *quantum-mechanical* cross sections and a higher level kinetic theory.

Although the spin-orbit couplings between the interaction potentials are considered negligible at short internuclear distances [1], this study deals with the same ion–atom system and is devoted to the calculation, at the above temperatures, of the mobility of $C^+(^2P^\circ)$ and $C^+(^4P)$ ions diffusing through a dilute buffer gas made of helium. Practically, this work aims at (1) generating with the MOLPRO package new *ab initio* potential-energy curves *via* which *ground* and *metastable-excited* C^+ ions interact with neutral He, (2) computing quantum mechanically the transport cross sections over a larger energy interval to cover low temperatures, and finally (3) determining, with the *three*-temperature theory of the Boltzmann kinetic equation, the *non-zero-field* transport parameters, such as the diffusion and mobility coefficients. The three-temperature theory of gaseous ion transport is an enhanced theoretical treatment, proposed by Lin *et al*. [4] and Viehland and Lin [5], intended to overcome the drawbacks and imperfections of the two-temperature model and to include essentially some anisotropic features [2,3].

The mobility of carbon ions in inert gases is particularly important for the experimental determination of the ion–molecule rate constants of C^+ reactions which have astrophysical interests. It is very sensitive to the shape and numerical values of the interaction potentials occurring between the ion and the neutral. For this reason, several experiments have been realised for measuring the C^+ mobility in helium, such as the measurements of Dotan *et al*. [6], Thomas *et al*. [7], Peska *et al*. [8] , Twiddy *et al*. [9], and more recently of Matoba *et al*. [1].

The main purposes of this investigation are therefore to carry out *full* quantum-mechanical calculations of the transport cross sections, based on the *ab initio* interaction potentials of the ionic dimers, which dissociate asymptotically into $C^+(^2P^\circ) + He(^1S)$ and $C^+(^4P) + He(^1S)$, and to examine theoretically the mobilities of C^+ ions moving in a helium gas by comparing them with the previous experimental and computed data. In order to get the appropriate transport coefficients, the latter task will be fulfilled by implementing the quantal cross sections in the Fortran

* Corresponding author. Email: lamia.aissaoui@aol.com

code GC.F, a more recent version of the older GRAMCHAR.F program, both written by Viehland [10–12].

Unless otherwise specified, atomic units (a.u.) are used throughout this paper; in particular, energies are in hartrees (E_h), distances in bohrs (a_0), and $\hbar = 1$.

2. Potentials

In this section, we expose the *ab initio* methods we used in this work to generate the ion-atom potential-energy curves *via* which the ground $C^+\left(2s^2 2p\ ^2P^\circ\right)$ and metastable-excited $C^+(2s2p^2\ ^4P)$ ions interact with ground-state helium $He(1s^2\ ^1S)$ atoms. Since the spin-orbit effects are small for light atoms, as it is the case with carbon, they are not taken into account here. When a ground $C^+(^2P^\circ)$ ion interacts with helium, both species approach each other through one of the molecular curves $^2\Pi$ or $^2\Sigma$. However, when a metastable-excited $C^+(^4P)$ ion interacts with He, they rather form an excited quasimolecular system in the $^4\Sigma^-$ or $^4\Pi$ state.

In order to determine the potential curves of the above *doublet* and *quartet* states, we have chosen the Dunning *correlation consistent polarised valence quintuple zeta* (cc-pV5Z) basis for both C and He atoms [13]. The calculations yield the value 5.351 eV of the unperturbed $C^+\left(^2P^\circ \rightarrow ^4P\right)$ transition energy, which is very close to the National Institute of Standards and Technology (NIST) recommended value 5.335 eV [14] and to the numerical results 5.307 eV of Matoba *et al*. [1] and 5.32 ± 0.18 eV of Hughes and von Nagy-Felsobuki [15]. Grice *et al*. [16] reported an energy difference close to 5.141 eV, which they compared with the value 5.331 eV determined spectroscopically.

We have further performed the *multireference configuration interaction* method [17,18] using reference functions derived from the *state-averaged complete active space self-consistent field* approach [19,20]. Among the seven electrons of the C^+He system, two are frozen and the remaining ones are considered as active. The active space contains the following orbitals: 5σ, corresponding to C$(2s;\ 3p_0;\ 3s;\ 4p_0)$ and He$(1s^2)$, and 4π, corresponding to C$(2p_\pm; 3p_\pm)$. These nine active orbitals are distributed among the irreducible representations a_1, b_1, b_2, and a_2 of the C_{2v} symmetry as follows: 5, 2, 2, and 0. To estimate the effect of higher order excitations, we have introduced the Davidson correction [21]. The *basis-set superposition error* has also been introduced *via* the counterpoise correction technique [22]. The C^+He electronic potential curves are determined for the $^2\Pi$, $^2\Sigma$, $^4\Sigma^-$, and $^4\Pi$ states in the range of internuclear distances $1.0 \le R \le 20.8$. We have performed all the above calculations with the quantum-chemistry package MOLPRO [23].

For the requisite calculations, the *four* ion-atom potential curves have to be known in the long, intermediate, and short regions of R. We hence adopted the above-generated data points to construct smooth and reliable $C^+(^2P^\circ)$He and $C^+(^4P)$He potential-energy curves. In the short-range region, namely for $R \le 1.0$, the ion–atom potential follows the Born–Meyer relationship [24]

$$V_{SR}(R) = \alpha \exp(-\beta R), \tag{1}$$

with α and β being two constant parameters. Their adopted values are listed for each molecular state in Table 1. For $R \ge 20.8$, the extension is chosen at large distances of the analytical form [25,26]

$$V_{LR}(R) = -\frac{1}{2}\left(\frac{\alpha_d}{R^4} + \frac{\alpha_q}{R^6} + \frac{\alpha_o}{R^8}\right), \tag{2}$$

where $V_{LR}(R)$ is the long-range potential function correlated with the dipole α_d, quadrupole α_q, and octupole α_o polarisabilities of the neutral atom He.

Since the leading R^{-4} term is important in shaping the common long-range forms of all the ion–atom interaction potentials and in fixing the C^+He classical polarisation limit, $K_{pol} \simeq 17.66\ cm^2\ V^{-1}\ s^{-1}$, determined from [2]

$$K_{pol} = \frac{13.853}{\sqrt{\mu\alpha_d}}, \tag{3}$$

with μ being the reduced mass of the colliding species, we employed in the present calculations the theoretical value $\alpha_d \simeq 1.384$ of Łach *et al*. [27]. Experimental measurements performed by Schmidt *et al*. [28] confirmed this value, which is also very close to the NIST dipole polarisability $\alpha_d \simeq 1.404$ [14]. Complete and useful compilations of calculated and measured dipole polarisabilities of helium and many other systems can be found in Masili and Starace [29] and Mitroy *et al*. [30]. The two remaining polarisabilities, $\alpha_q \simeq 2.445$ and $\alpha_o \simeq 10.620$, are taken from the recent theoretical work of Kar and Ho [31], which are identical to the figures already produced by Yan *et al*. [32]. In their investigations, based on the classical momentum-transfer theory, Matoba *et al*. [1] used the same dipole polarisability $\alpha_d = 0.205$ Å^3 for all the C^+He molecular states they generated with the *multi-configuration self-consistent field* and *multi-reference singly and doubly excited configuration interaction* calculations. In contrast, they utilised different values of α_q and α_o which they deduced from analytical fittings of different potentials.

Table 1. Adopted short-range parameters, that appear in Equation (1), in the construction of the ground and metastable-excited C^+He potential-energy curves. All the data are in a.u.

Short-range	C^+He states			
parameters	$^2\Pi$	$^2\Sigma$	$^4\Sigma^-$	$^4\Pi$
α	33.54	28.63	51.67	23.89
β	3.230	3.004	3.847	2.663

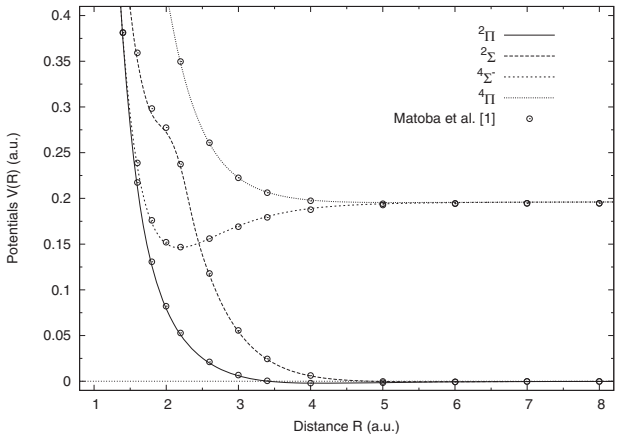

Figure 1. The present constructed potential-energy curves of the quasimolecular $C^+(^2P^\circ)$He and $C^+(^4P)$He states. Empty circles represent the data points produced by Matoba *et al*. [1].

The constructed C^+He potential-energy curves are shown in Figure 1 and some of their data points are reported from $R = 1$ to $R = 10$ in Table 2. The potential curves are also compared in Figure 1 with some data points provided in Matoba *et al*. [1]. The agreement between both potential sets, mainly for the lower states, is in general quite good. To further characterise quantitatively our computed and constructed potentials, we list in Table 3 the internuclear separations σ at which $V(\sigma) = 0$, as well as the equilibrium distances R_e and potential depths D_e, both contrasted with the previous published data. We also give in Table 4 their *rotationless*-vibrational energy levels, where the calculations showed that the $^2\Pi$, $^2\Sigma$, $^4\Sigma^-$, and $^4\Pi$ states can hold 7, 5, 19, and 5 vibrational levels, respectively.

3. Zero-field transport properties

Once determined at all internuclear separations R, the four electronic interaction potentials are inserted separately into the radial wave equation [35]

$$\frac{d^2\psi_l(R)}{dR^2} + \left[\kappa^2 - 2\mu V(R) - \frac{l(l+1)}{R^2}\right]\psi_l(R) = 0 \tag{4}$$

to determine numerically the radial wave functions $\psi_l(R)$ of the colliding species, forcing them to behave asymptotically like [35]

$$\psi_l(R) \underset{R\to\infty}{\sim} \sin\left(\kappa R - \frac{l}{2}\pi + \eta_l\right). \tag{5}$$

In both equations, l is the orbital angular momentum quantum number and $\kappa = \sqrt{2\mu\epsilon}$ is the wave number of relative motion at energy ϵ. The energy-dependent *elastic* phase shifts η_l are basically employed in the quantal computation of the transport cross sections [36]. In practice, η_l are computed quantum mechanically up to a certain large value of

Table 2. Data points derived from the constructed interatomic potentials of the ground and metastable-excited C^+He molecular states. The numbers in parentheses indicate powers of 10. All the data are given in a.u.

Distance	$C^+(^2P^\circ)$ + He		$C^+(^4P)$ + He	
R	$^2\Pi$	$^2\Sigma$	$^4\Sigma^-$	$^4\Pi$
1.0	+1.3271	+1.4192	+1.1031	+1.6327
1.5	+0.2793	+0.4073	+9.4923(−2)	+0.5829
2.0	+7.9249(−2)	+0.2723	−4.5776(−2)	+0.2302
2.5	+2.5362(−2)	+0.1382	−4.3557(−2)	+7.9152(−2)
3.0	+5.9367(−3)	+5.4191(−2)	−2.6429(−2)	+2.6370(−2)
3.5	−6.1676(−4)	+1.9212(−2)	−1.4091(−2)	+8.2620(−3)
4.0	−2.1468(−3)	+5.8192(−3)	−7.2897(−3)	+1.9001(−3)
4.5	−2.0167(−3)	+1.1453(−3)	−3.8766(−3)	−1.9463(−4)
5.0	−1.5226(−3)	−2.5992(−4)	−2.1814(−3)	−7.0990(−4)
5.5	−1.0722(−3)	−5.5073(−4)	−1.3093(−3)	−7.0169(−4)
6.0	−7.4407(−4)	−5.1325(−4)	−8.3500(−4)	−5.6522(−4)
6.5	−5.2161(−4)	−4.0862(−4)	−5.6069(−4)	−4.2790(−4)
7.0	−3.7340(−4)	−3.1133(−4)	−3.9266(−4)	−3.1969(−4)
7.5	−2.7372(−4)	−2.3615(−4)	−2.8462(−4)	−2.4048(−4)
8.0	−2.0540(−4)	−1.8078(−4)	−2.1218(−4)	−1.8353(−4)
8.5	−1.5731(−4)	−1.4042(−4)	−1.6185(−4)	−1.4235(−4)
9.0	−1.2271(−4)	−1.1069(−4)	−1.2583(−4)	−1.1213(−4)
9.5	−9.6598(−5)	−8.8456(−5)	−9.9443(−5)	−8.9581(−5)
10.0	−7.7534(−5)	−7.1560(−5)	−7.9699(−5)	−7.2468(−5)
10.5	−6.2991(−5)	−5.8533(−5)	−6.4662(−5)	−5.9280(−5)
11.0	−5.1713(−5)	−4.8349(−5)	−5.3025(−5)	−4.8974(−5)

Table 3. Some of the spectroscopic parameters compared with the previous published data. The potential depths D_e are measured with respect to the dissociation limits of the respective *ab initio* C^+He molecular states. The numbers in parentheses are powers of 10.

	$C^+(^2P^\circ)$He		$C^+(^4P)$He		
Parameters	$^2\Pi$	$^2\Sigma$	$^4\Sigma^-$	$^4\Pi$	Refs.
σ (Å)	1.905	2.593	0.900	2.381	This work
R_e (Å)	2.196	2.963	1.164	2.752	This work
	2.21	2.99	1.16	2.78	[1]
	2.2330		1.1555		[15]
	2.329	2.978	1.158	2.805	[16]
	2.406		1.168		[33]
	2.504		1.177		[34]
D_e (cm^{-1})	482	122	11.007(3)	162	This work
	468	122	10.691(3)	159	[1]
	406	147	10.254(3)	175	[16]
	385		10.248(3)		[33]

the orbital angular momentum l^* beyond which the calculations are achieved with the semiclassical approximation [35,36]

$$\eta_l \approx -\mu \int_{R_0}^{\infty} \frac{V(R)}{\sqrt{(\kappa R)^2 - (l+1/2)^2}} R\, dR, \qquad (6)$$

where the lower limit R_0 verifies the relationship $\kappa R_0 = (l + 1/2)$. Figure 2 illustrates, as an example, the behaviour of two different data sets of the quantal phase shifts that correspond to the C^+He molecular states $^2\Pi$ and $^4\Sigma^-$ at the energies 10^{-4} and 10^{-3} hartree, respectively. One may notice from Figure 2(a) and 2(b) that, beyond $l^* = 115$ and $l^* = 132$, the phase shifts η_l are calculated semiclassically with Equation (6). The semiclassical asymptotes are presented in full solid curves.

Table 4. Rotationless-vibrational energy levels (in cm^{-1}) of the doublet and quartet C^+He molecular states.

Level	$C^+(^2P^\circ)$He		$C^+(^4P)$He	
v	$^2\Pi$	$^2\Sigma$	$^4\Sigma^-$	$^4\Pi$
0	−312.6197	−75.1408	−9756.0190	−99.5158
1	−184.9595	−26.6879	−8509.1256	−40.2552
2	−92.5661	−7.8367	−7346.0876	−13.2426
3	−36.3233	−1.2937	−6267.3752	−2.9865
4	−11.2541	−0.0431	−5273.1523	−0.2821
5	−2.3101		−4363.4599	
6	−0.1761		−3539.5131	
7			−2803.2954	
8			−2156.5573	
9			−1600.8161	
10			−1136.5718	
11			−762.4773	
12			−474.9170	
13			−267.7434	
14			−131.8062	
15			−53.3043	
16			−16.8371	
17			−3.9306	
18			−0.4114	

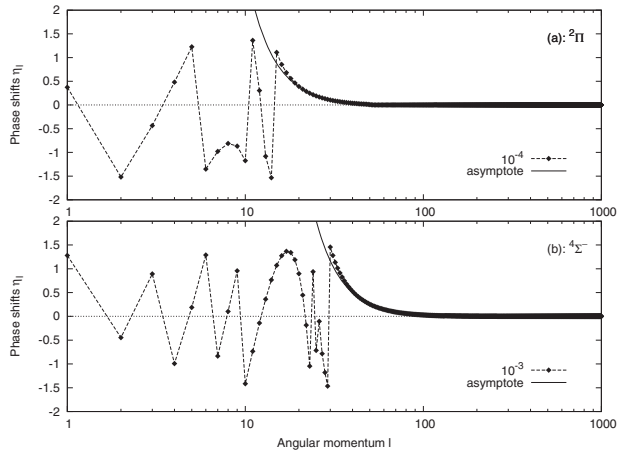

Figure 2. Elastic phase shifts obtained at the energies $\epsilon = 10^{-4}$ and $\epsilon = 10^{-3}$ hartree for the two different C^+He states: (a) $^2\Pi$, and (b) $^4\Sigma^-$. The asymptotic forms are given in full lines.

The accuracy of the phase shifts is highly recommended, since they are determinant in the computation of the requested *quantal* transport cross sections, namely, those effective in *diffusion* [2]

$$Q_d(\kappa) = \frac{4\pi}{\kappa^2} \sum_{l=0}^{\infty} (l+1) \sin^2(\eta_{l+1} - \eta_l), \qquad (7)$$

also known as the *momentum-transfer* cross sections. The individual *doublet* and *quartet* transport cross sections are displayed in Figure 3(a) and 3(b), respectively. At lower energies, where the quantal effects are important, the cross sections exhibit undulations with some regular peaks occurring at orbiting resonances [2]. As pointed out in Refs [1,2], the general behaviour of the transport cross sections depend tightly on the depth of the considered interaction potential, and their decrease becomes smooth and sharp beyond the energies corresponding to the well-depth values D_e. In particular, since the $^4\Sigma^-$ curve represents the deepest potential, the slope change occurs in Figure 3(b) at the highest energy superior to $10^{-2}E_h$. Moreover, if Q_i denotes the momentum-transfer cross section for the individual molecular state i, the *average* transport cross sections are therefore expressed by [1]

$$\overline{Q} = \frac{\sum_i g_i Q_i}{\sum_i g_i}, \qquad (8)$$

where g_i is the multiplicity of the considered state. Accordingly, the average diffusion cross sections $\overline{Q}_d(\kappa)$

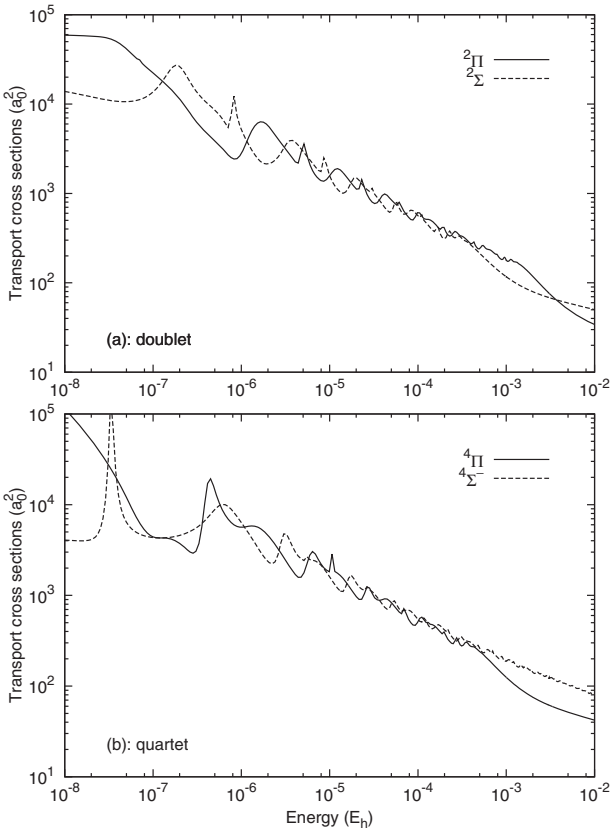

Figure 3. Individual quantal cross sections, effective in diffusion, varying with energy. The cross sections are computed in (a) for doublet states; in (b) for quartet states.

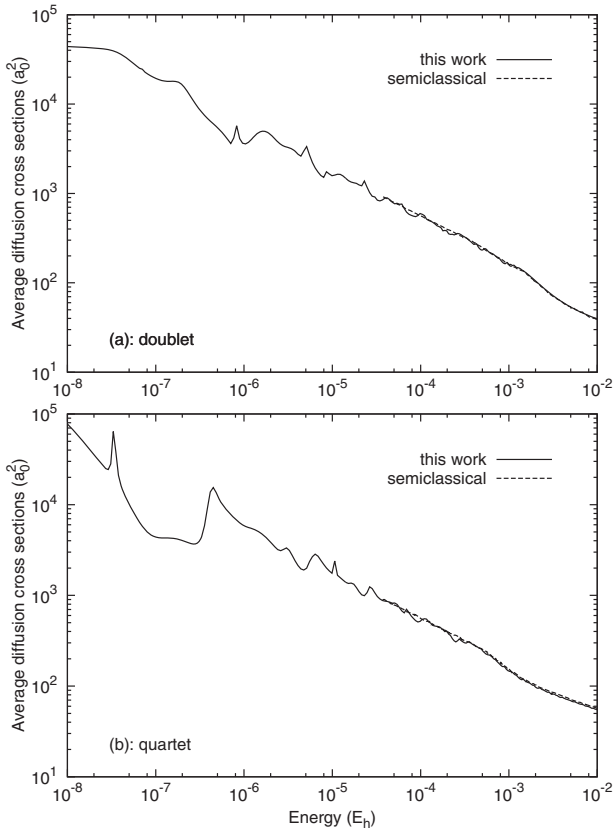

Figure 4. Average diffusion cross sections calculated with Equation (9): in (a) doublet states; in (b) quartet states. Both cross sections are compared with the semiclassical results of Matoba *et al*. [1].

are given by the statistically weighted sum [2]

$$\overline{Q}_d(\kappa) = \frac{1}{3}Q_d^{\Sigma}(\kappa) + \frac{2}{3}Q_d^{\Pi}(\kappa). \tag{9}$$

The average diffusion cross sections relative to the doublet and quartet states are shown in Figure 4(a) and 4(b). They are both compared with the *semiclassical* results of Matoba *et al*. [1], which have linear forms for small energies.

The mean transport cross sections should allow the determination of the temperature-dependent coefficients of diffusion. The knowledge of such measurable parameters may primarily constitute sensitive probes and high-quality assessments for the accuracy of the ion–atom potentials we utilised in the present computations. Indeed, according to the Chapman–Enskog model for the transport theory of *dilute* gases [2], the collision integrals, in connection with the asymptotic separation $C^+(^2P^\circ) + He$ or $C^+(^4P) + He$, are defined as

$$\Omega_d(T) = \frac{1}{2}\int_0^{\infty} \frac{\epsilon^2}{(k_B T)^3}\overline{Q}_d(\epsilon)\exp\left(-\frac{\epsilon}{k_B T}\right)d\epsilon. \tag{10}$$

These integrals lead, in particular, to the *zero-field* diffusion coefficient given by [36]

$$D(T) = \frac{3}{8N}\sqrt{\frac{\pi k_B T}{2\mu}}\frac{1}{\Omega_d(T)}, \tag{11}$$

where k_B denotes Boltzmann's constant and N is the number density of the helium gas. Assuming that the ideal gas law applies, the pressure p of the buffer gas can then be related to N with $p = Nk_B T$. Moreover, the diffusion coefficient allows the calculation of the *zero-field* mobility $K(T)$ of the ions C^+ within the helium buffer gas defined as [36]

$$K(T) = \frac{q}{k_B T}D(T) \tag{12}$$

with q being the electric charge of the atomic ion. Usually, the mobility coefficient is expressed, if p is in torrs and T in kelvins, as

$$K_0(T) = \left(\frac{p}{760}\right)\left(\frac{273.15}{T}\right)K(T), \tag{13}$$

Table 5. Zero-field reduced mobility K_0 and diffusion coefficients D at room temperature $T = 297$ K. The diffusion coefficients are given as D times the pressure $p = 0.250$ torr and the gas density N. The ground-state results are compared with data from Dotan *et al*. [6].

	$C^+(^2P^\circ)$ in He		$C^+(^4P)$ in He
Coefficients	This work	Dotan *et al*. [6]	This work
pD (cm^2 Torr s^{-1})	468	461	463
ND (10^{19} cm^{-1} s^{-1})	1.52	1.50	1.51
K_0 (cm^2 V^{-1} s^{-1})	22.1	21.8 ± 1.1	21.9

known as the *reduced* mobility [2]. Note that, at one temperature T, the integrand appearing in Equation (10) should be a numerically integrable function. Thus, the choice of the whole energy interval, over which the cross sections are computed, should be made to fulfil this requirement.

The results of the diffusion coefficient D, presented in Table 5 as D times the gas pressure $p = 0.250$ *Torr* or times the number density N, are listed for the helium gas temperature $T = 297$ K. Table 5 presents also, in the same conditions, the zero-field reduced mobility K_0 of the $C^+(^2P^\circ)$ and $C^+(^4P)$ ions moving through helium. In particular, our ground theoretical results are compared to the experimental measurements of Dotan, Fehdenfeld, and Albritton [6]. The comparison shows an excellent agreement between the values, which confirms, once again, the good quality of our generated *ab initio* C^+He potentials.

4. Non-zero-field mobility

Knowing the *full* quantum-mechanical cross sections from $\epsilon_{min} = 10^{-8}$ to $\epsilon_{max} = 10^{-2}$, which is roughly equivalent to the temperature interval $10^{-3} \lesssim T \lesssim 10^{+3}$ K, it is now possible to make use of the *three*-temperature theory [2] to output the diffusion and mobility coefficients in the case of a *non-zero* electric field strength **E**.

4.1. Numerical details

With the aim of computing, with a higher level kinetic theory of ions in gases, the mobility of C^+ ions in helium, the *doublet* and *quartet* transport cross sections $\overline{Q}_d(\epsilon)$ have to be introduced into the Fortran code GC.F [10–12]. This code, which relies on the Gram–Charlier series [11], uses the cross sections into three distinctive energy intervals

$$\begin{aligned} \epsilon_{min} &\leqslant \epsilon < \epsilon_c \\ \epsilon_c &\leqslant \epsilon < 3\epsilon_c \\ 3\epsilon_c &\leqslant \epsilon \leqslant \epsilon_{max}, \end{aligned} \tag{14}$$

where ϵ_c is a critical energy at which classical orbiting occurs. Within each interval, the quantum-mechanical cross sections are fitted by means of the Chebyshev expansion coefficients

$$a_i = \frac{2}{\mathcal{N}} \sum_{k=0}^{\mathcal{N}} \widetilde{T}_i \left[\cos\left(\frac{k\pi}{\mathcal{N}}\right) \right] \log\left\{ \overline{Q}_d(\epsilon) \right\}, \tag{15}$$

where $\mathcal{N}$ is the number of energies in each region and the tilde sign above the Chebyshev polynomials T_i indicates that the *first* and *last* terms in the summation are *halved.* The cross sections are rebuilt in GC.F as [37]

$$\log\left\{ \overline{Q}_d(\epsilon) \right\} = \sum_{i=0}^{\mathcal{N}} a_i \widetilde{T}_i \left[\xi(\epsilon) \right], \tag{16}$$

with $|\xi(\epsilon)| \leq +1$ being defined by

$$\xi(\epsilon) = \frac{2\log(\epsilon) - \log(\epsilon_{sup}) - \log(\epsilon_{inf})}{\log(\epsilon_{sup}) - \log(\epsilon_{inf})}, \tag{17}$$

where ϵ_{inf} and ϵ_{sup} are the limits of each of the above energy intervals (14). More numerical details are provided in [37] and in the original Fortran code of Viehland.

4.2. Results and discussion

Before dealing with the reduced mobilities K_0 of ground and metastable-excited C^+ ions in helium at the temperatures of interest 4.3 and 77 K, we have first of all chosen to treat K_0 at room temperature $T = 297$ K. The obtained results, presented as a function of the ratio E/N of the electric field strength to the gas number density, are drawn in solid lines in Figure 5. They are compared in the same figure with a bunch of theoretical and experimental data determined at very close temperatures [6–9,16]. As the ratio E/N goes to zero, the curves show in particular that the lower limits of

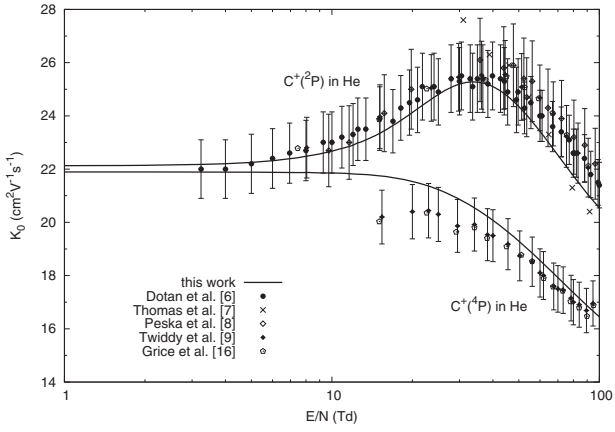

Figure 5. Non-zero-field mobilities of the $C^+(^2P^\circ)$ and $C^+(^4P)$ ions into He as a function of E/N at room temperature $T \simeq 300$ K. They are compared with the published data from [6–9,16].

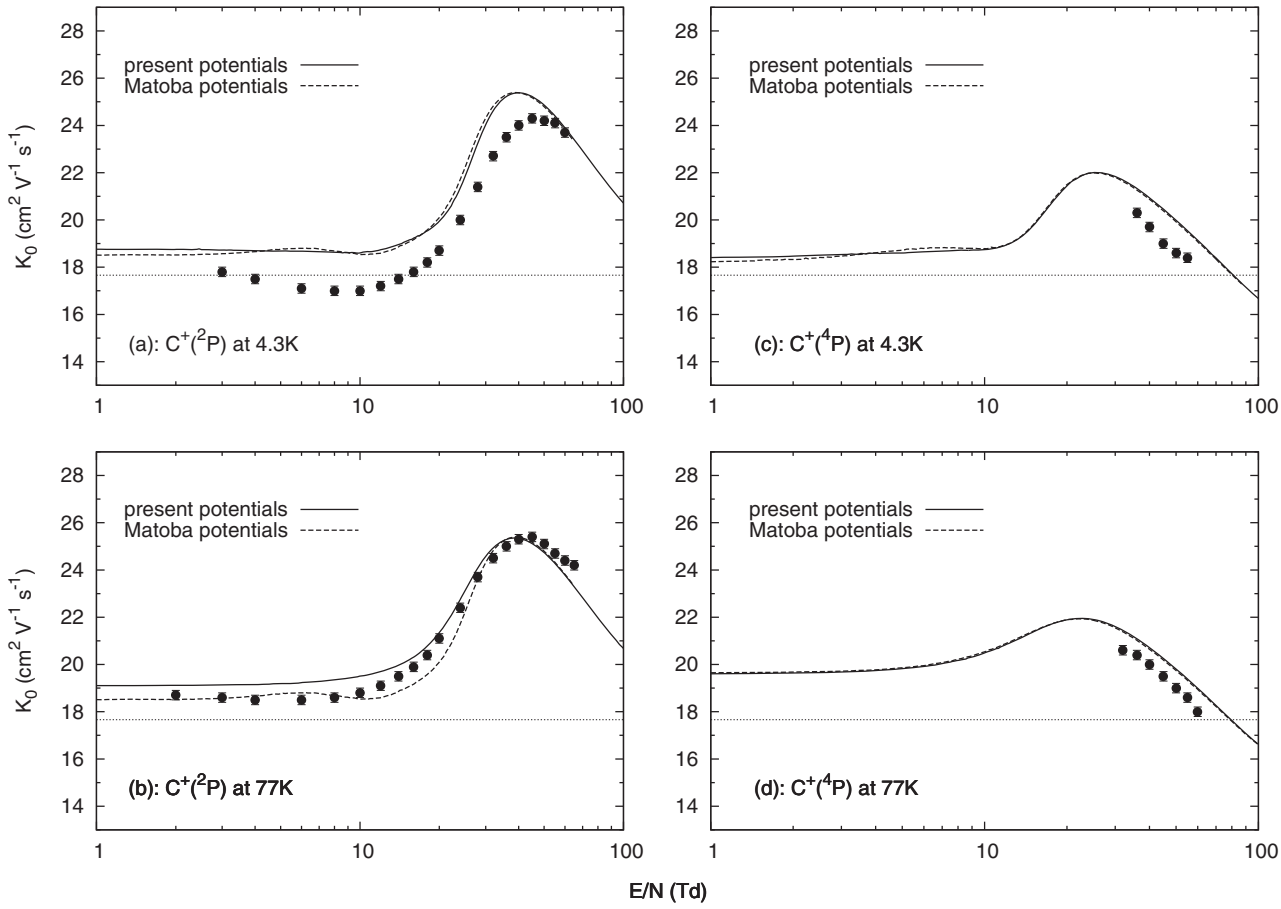

Figure 6. Non-zero-field reduced mobilities at two distinct temperatures: in the upper row at $T = 4.3$ K and in the lower row at $T = 77$ K. Full circles are the measurements of Matoba *et al*. [1], estimated as ± 0.2. The first column is connected with $C^+(^2P^\circ)$ moving through He and the second column with $C^+(^4P)$. The dashed lines represent our calculations with the potentials described in [1]. The horizontal dotted lines represent the polarisation limit $K_{pol} = 17.66\,cm^2\,V^{-1}\,s^{-1}$.

the reduced mobilities agree quite well with the values 22.1 and 21.9 $cm^2\,V^{-1}\,s^{-1}$, also confirmed in Table 5. When the electric field increases in intensity, the present $C^+(^2P^\circ)$ mobility results reach a maximum that lies between 20 and 50 Td (1 Td $= 10^{-21}\,V\,m^2$), which is believed typical for mobilities in helium [8]. In addition, as already emphasised by Dotan *et al*. [6], the zero-field mobilities in He show they are generally substantially different from the polarisation value $K_{pol} \simeq 17.66\,cm^2\,V^{-1}\,s^{-1}$. This fact indicates that the Langevin approximation is a poor one for ions at room temperature in the rather weakly polarisable helium. The polarisation limit is theoretically reached when the gas temperature is low enough, i.e., $T \to 0$ [38].

Being fully satisfied with the reliability and consistency of our C^+He interaction potentials, we have further employed the mathematical three-temperature model of Lin and co-workers [2–5] to generate the mobility of C^+ through He in terms of the ratio E/N at very low temperatures. The results are presented in Figure 6(a)–6(d). The upper and lower graphs illustrate the calculations and measurements at the temperatures 4.3 and 77 K, respectively. The solid curves correspond to those results deduced from the use of the present *ab initio* potentials, whereas the dashed lines represent the mobilities obtained with the potentials described in [1]. The polarisation limit, $K_{pol} \simeq 17.66\,cm^2\,V^{-1}\,s^{-1}$, is shown with horizontal dotted lines. All the present calculations are contrasted with the mobility measurements, known with the accuracy of $\pm 0.2\,cm^2\,V^{-1}\,s^{-1}$, performed at the prescribed temperatures by the TMU group.

Furthermore, the first column of Figure 6 gives the reduced mobility coefficients in connection with the ground $C^+(^2P^\circ)$ ions moving into helium. As the electric field tends to zero, the curves in Figure 6(a) show that the mobility approaches the value $18.8\,cm^2\,V^{-1}\,s^{-1}$, also found from the zero-field analysis based on the Chapman–Enskog model [35,39]. For higher values of the ratio E/N, the experimental data attain their lowest magnitude near 10 Td before they increase again. Unfortunately, the calculations, carried out here with both potential sets, are incapable to

Table 6. Non-zero-field transport properties for the ground state C^+ (2P) in He at (a) 4.3 K and (b) 77 K. These values are calculated with our potentials.

E/N	v_d	K_0	T_L	T_T	D_L	D_T
(Td)	($m\,s^{-1}$)	($cm^2\,V^{-1}\,s^{-1}$)	(K)		($10^{20}\,m^2\,s^{-1}$)	
(1) $T = 4.3$ K						
0.03	0.001	18.76	4.30	4.30	0.187	0.187
1.47	0.553	18.75	5.76	4.88	0.250	0.212
4.46	1.675	18.68	17.71	9.66	0.766	0.418
8.27	3.095	18.63	50.07	22.61	2.160	0.975
12.90	4.881	18.82	118.12	49.83	5.148	2.172
18.40	7.253	19.61	255.62	104.83	11.605	4.759
24.41	10.566	21.53	537.67	217.64	26.803	10.850
29.21	13.941	23.75	932.92	375.74	51.291	20.658
35.61	18.034	25.19	1558.26	625.87	90.896	36.508
42.31	21.553	25.34	2223.74	892.05	130.483	52.343
50.64	25.253	24.81	3051.12	1222.99	175.238	70.241
60.49	29.007	23.86	4024.52	1612.34	222.285	89.054
71.25	32.667	22.81	5102.91	2043.68	269.475	107.923
81.96	36.067	21.89	6219.47	2490.30	315.226	126.218
91.50	39.040	21.23	7286.37	2917.04	358.065	143.349
102.02	42.258	20.61	8536.40	3417.04	407.258	163.022
(2) $T = 77$ K						
0.07	0.006	19.10	77.00	77.00	3.405	3.405
1.39	0.126	19.11	78.37	77.55	3.467	3.431
4.52	0.412	19.16	91.50	82.80	4.060	3.674
8.24	0.758	19.37	126.20	96.68	5.659	4.335
12.96	1.220	19.82	204.28	127.91	9.374	5.870
18.59	1.849	20.94	369.39	193.95	17.905	9.401
24.32	2.640	22.86	673.44	315.57	35.642	16.702
29.41	3.416	24.45	1075.10	476.23	60.848	26.953
35.38	4.247	25.27	1620.04	694.20	94.770	40.609
42.29	5.075	25.27	2280.83	958.51	133.421	56.070
50.74	5.947	24.67	3102.39	1287.12	177.211	73.521
60.61	6.831	23.72	4068.94	1673.73	223.477	91.926
71.33	7.693	22.70	5139.75	2102.04	270.172	110.494
81.92	8.493	21.83	6248.46	2545.51	315.744	128.628
91.40	9.193	21.17	7307.85	2969.25	358.255	145.562
101.77	9.951	20.59	8549.09	3465.74	407.444	165.175

replicate numerically this feature. On the other hand, the agreement of the present results with the experimental data at 77 K is much better for the curves exhibited in Figure 6(b). Accordingly, this leads us to assume that the accuracy of the quantal collision integrals (10) at a higher temperature is good enough. For the same case, as $E/N \to 0$, the reduced mobility appears approaching $K_0 = 19.1\,cm^2\,V^{-1}\,s^{-1}$, which is in conformity with the zero-field value [39]. Table 6 lists in (a) and (b) the most important transport parameters, namely, drift velocity v_d, reduced mobility K_0, parallel T_L and perpendicular T_T temperatures, and parallel D_L and perpendicular D_T diffusion coefficients, that characterise the mobility of $C^+(^2P^\circ)$ in He, as a function of E/N at 4.3 and 77 K, respectively.

The second column displays the dependence, on E/N, of the reduced mobility K_0 relevant to the drift movement of metastable-excited $C^+(^4P)$ ions in helium at the above temperatures. One may observe in Figure 6(c) and 6(d) that, despite the technical complexity of measuring, at low temperatures, the mobility of the metastable-excited ionic species in gases, the experimental data are, in this case, only available for $E/N \gtrsim 30$ Td. The extrapolation of the mobility curves to the zero-field limits ends at the values 18.4 and $19.6\,cm^2\,V^{-1}\,s^{-1}$. We compile in parts (a) and (b) of Table 7, respectively, at 4.3 and 77 K, the main transport coefficients versus the ratio E/N. As remarked above, the computed results with the present and Matoba potentials are capable to better reproduce the measured data.

Once the investigation is complete, it appears that the mobilities are very sensitive to the shape and values of the C^+ He potentials. The calculations revealed in particular that the use, within the three-temperature theory, of the quantal cross sections does not make a notable difference in the results of K_0 if compared to those obtained by Matoba *et al*. [1].

Table 7. Non-zero-field transport properties for the ground state C^+(4P) in He at (a) 4.3 K and (b) 77 K. These values are calculated with our potentials.

E/N	v_d	K_0	T_L	T_T	D_L	D_T
(Td)	($m\,s^{-1}$)	($cm^2\,V^{-1}\,s^{-1}$)	(K)		($10^{20}\,m^2\,s^{-1}$)	
(1) $T = 4.3$ K						
0.03	0.001	18.42	4.30	4.30	0.183	0.183
1.46	0.542	18.44	5.70	4.86	0.243	0.208
4.48	1.675	18.60	17.71	9.66	0.763	0.416
8.22	3.095	18.72	50.07	22.61	2.171	0.980
12.95	4.978	19.12	122.72	51.67	5.432	2.287
18.55	7.851	21.06	298.76	122.08	14.564	5.951
24.38	10.777	21.99	559.22	226.26	28.473	11.520
29.29	12.880	21.88	796.87	321.32	40.363	16.275
35.87	15.392	21.35	1136.28	457.08	56.156	22.589
42.49	17.681	20.70	1497.92	601.73	71.788	28.838
50.69	20.310	19.93	1975.10	792.60	91.142	36.575
60.81	23.330	19.08	2604.73	1044.44	115.092	46.149
71.48	26.273	18.29	3302.28	1323.45	139.802	56.028
82.01	29.007	17.60	4024.52	1612.34	163.949	65.683
91.47	31.399	17.08	4714.62	1888.37	186.391	74.656
101.88	33.987	16.60	5523.20	2211.79	212.220	84.985
(2) $T = 77$ K						
0.00	0.000	19.59	77.00	77.00	3.492	3.492
1.36	0.126	19.62	78.37	77.55	3.560	3.522
4.38	0.412	19.77	91.50	82.80	4.187	3.789
8.22	0.789	20.20	130.25	98.30	6.091	4.597
12.96	1.294	21.02	220.34	134.33	10.723	6.538
18.57	1.923	21.80	393.49	203.59	19.861	10.276
24.37	2.538	21.92	628.02	297.40	31.878	15.096
29.50	3.033	21.65	863.99	391.79	43.300	19.635
35.38	3.554	21.14	1157.37	509.14	56.650	24.921
42.87	4.164	20.44	1560.12	670.23	73.835	31.720
51.05	4.783	19.72	2033.94	859.75	92.870	39.257
61.15	5.494	18.91	2659.14	1109.83	116.435	48.596
71.77	6.187	18.15	3351.78	1386.87	140.825	58.269
82.16	6.831	17.50	4068.94	1673.73	164.881	67.823
91.62	7.394	16.99	4754.20	1947.82	186.991	76.611
101.81	8.003	16.55	5557.08	2268.97	212.917	86.935

5. Conclusion

In this work, motivated by the recommendations of Matoba *et al*.[1], we have applied the three-temperature theory to determine, at $T = 4.3$ and 77 K temperatures, the mobility coefficients of C^+ ions in He and to examine their variation with the ratio E/N. To do so, we have produced with MOLPRO the ground and metastable C^+He potential-energy curves and calculated quantum-mechanically the momentum-transfer cross sections over a wide energy interval. We have further utilised these cross sections to determine the transport parameters and compared them with published measured and computed C^+He mobilities. The agreement has been found fairly good.

Acknowledgements

Special thanks are sent, mainly from one of the authors, Moncef Bouledroua, to Dr Larry A. Viehland, from Chatham University, Pittsburgh, PA, USA, for providing his Fortran codes GRAMCHAR.F and GC.F. The latter program has been used in the main parts of the present calculations.

Disclosure statement

No potential conflict of interest was reported by the authors.

References

[1] S. Matoba, H. Tanuma, and K. Ohtsuki, J. Phys. B **41**, 145205 (2008).
[2] E.A. Mason and E.W. McDaniel, *Transport Properties of Ion in Gases* (John-Wiley, New York, 1988).
[3] L.A. Viehland, Phys. Scripta T **53**, 53 (1994).
[4] S.L. Lin, L.A. Viehland, and E.A. Mason, Chem. Phys. **37**, 411 (1979).
[5] L.A. Viehland and S.L. Lin, Chem. Phys. **43**, 135 (1979).
[6] I. Dotan, F.C. Fehsenfeld, and D.L. Albritton, J. Chem. Phys. **71**, 4762 (1979).
[7] R. Thomas, J. Barassin, and A. Barassin, Int. J. Mass Spectrom. Ion Phys. **31**, 227 (1979).

[8] K. Peska, G. Sejkora, H. Störi, F. Egger, H. Ramler, M. Kriegel, and W. Lindinger, in *3rd Symposium Atomic and Surface Physics*, edited by W. Lindinger, F. Howorka, T.D, Mark, and F. Egger, (Institut für Atomphysik der Universität, Innsbruck, 1982).
[9] N.D. Twiddy, A. Mohebati, and M. Tichy, Int. J. Mass Spectrom. Ion Process. **74**, 251 (1986).
[10] L.A. Viehland (private communication).
[11] L.A. Viehland, Chem. Phys. **179**, 71 (1994).
[12] A. Yousef, S. Shrestha, L.A. Viehland, E.P.F. Lee, B.R. Gray, V.L. Ayles, T.G. Wright, and W.H. Breckenridge, J. Chem. Phys. **127**, 154309 (2007).
[13] D.E. Woon and T.H. Dunning Jr, J. Chem. Phys. **100**, 2975 (1994).
[14] http://www.nist.gov
[15] J.M. Hughes and E.I. von Nagy-Felsobuki, Eur. Phys. J. D **6**, 185 (1999).
[16] S.T. Grice, P.W. Harland, R.G.A.R. MacLagan, and R.W. Simpson, Int. J. Mass Spectrom. Ion Process. **87**, 181 (1989).
[17] H.-J. Werner and P.J. Knowles, J. Chem. Phys. **89**, 5803 (1988).
[18] P.J. Knowles and H.-J. Werner, Chem. Phys. Lett. **145**, 514 (1988).
[19] H.-J. Werner and P.J. Knowles, J. Chem. Phys. **82**, 5053 (1985).
[20] P.J. Knowles and H.-J. Werner, Chem. Phys. Lett. **115**, 259 (1985).
[21] E.R. Davidson and D.W. Silver, Chem. Phys. Lett. **53**, 403 (1977).
[22] S.F. Boys and F. Bernardi, Mol. Phys. **19**, 553 (1970).
[23] H.-J. Werner, P.J. Knowles, R. Lindh, M. Schütz, P. Celani, T. Korona, F.R. Manby, G. Rauhut, R.D. Amos, A. Bernhardsson, A. Berning, D.L. Cooper, M.J.O. Deegan, A.J. Dobbyn, F. Eckert, C. Hampel, G. Hetzer, A.W. Lloyd, S.J. McNicholas, W. Meyer, M.E. Mura, A. Nicklass, P. Palmieri, R. Pitzer, U. Schumann, H. Stoll, A.J. Stone, R. Tarroni, and T. Thorsteinsson, MOLPRO, version 2002.6, a package of *ab initio* programs.
[24] H. Pauly, in *Atom-Molecule Collision Theory*, edited by R.B. Bernstein, (Plenum Press, New York, 1979).
[25] R. Côté and A. Dalgarno, Phys. Rev. A **62**, 012709 (2000).
[26] F. Bouchelaghem and M. Bouledroua, Phys. Chem. Chem. Phys. **16**, 1875 (2014).
[27] G. Łach, B. Jezionski, and K. Szalewicz, Phys. Rev. Lett. **92**, 233001 (2004).
[28] J.W. Schmidt, R.M. Gavioso, E.F. May, and M.R. Moldover, Phys. Rev. Lett. **98**, 254504 (2007).
[29] M. Masili and A.F. Starace, Phys. Rev. A **68**, 012508 (2003).
[30] J. Mitroy, M.S. Safronova, and C.W. Clark, J. Phys. B **43**, 202001 (2010).
[31] S. Kar and Y.K. Ho, Phys. Rev. A **80**, 062511 (2009).
[32] Z.-C. Yan, J.F. Babb, A. Dalgarno, and G.W.F. Drake, Phys. Rev. A **54**, 2824 (1996).
[33] G. Frenking, W. Koch, D. Cremer, J. Gauss, and J.F. Liebman, J. Phys. Chem. **93**, 3397 (1989).
[34] E.D. Jemmis, M.W. Wong, H.-B. Bürgi, and L. Radom, J. Mol. Struct. (Theochem.) **261**, 385 (1992).
[35] N.F. Mott and H.S.W. Massey, *The Theory of Atomic Collisions* (Oxford University Press, Oxford, 1965).
[36] A. Dalgarno, M.R.C. McDowell, and A. Williams, Phil. Trans. R. Soc. London A **250**, 411 (1958).
[37] L.A. Viehland and Y. Chang, Comp. Phys. Com. **181**, 1687 (2010).
[38] L.A. Viehland, Aust. J. Phys. **50**, 671 (1997).
[39] L. Aissaoui and M. Bouledroua, unpublished.

Bibliography

[1] L.A. Viehland and E.A. Mason, Ann. Phys. **91,** 499 (1975).

[2] L.A. Viehland and E.A. Mason, Ann. Phys. **110,** 287 (1978).

[3] S. Matoba, H. Tanuma, and K. Ohtsuki, J. Phys. B **41,** 145205 (2008).

[4] S.L. Lin, L.A. Viehland, and E.A. Mason, Chem. Phys. **37,** 411 (1979).

[5] L.A. Viehland, private communication.

[6] L.A. Viehland, Chem. Phys. **179,** 71 (1994).

[7] A. Yousef, S. Shrestha, L.A. Viehland, E.P.F. Lee, B.R. Gray, V.L. Ayles, T.G. Wright, and W.H. Breckenridge, J. Chem. Phys. **127,** 154309 (2007).

[8] E.W. McDaniel and E.A. Mason, *The Mobility and Diffusion of Ions in Gases,* (Wiley, New York, 1973).

[9] E.A. Mason and E.W. McDaniel, *Transport Properties of Ions in Gases,* (Wiley, New York, 1988).

[10] L.A. Viehland and D.E. Goeringer, J. Phys. B **38,** 3987 (2005).

[11] L.A. Viehland, D.M. Danailov, and D.E. Goeringer, J. Phys. B **39,** 3993 (2006).

[12] L.A. Viehland and W.F. Siems, J. Am. Soc. Mass Spectrom. **23,** 1841 (2012).

[13] D. Burnett, Proc. Lond. Math. Soc. **39,** 385 (1935).

[14] D. Burnett, Proc. Lond. Math. Soc. **40,** 382 (1935).

[15] M.J. Bastian, C.P. Lauenstein, V.M. Bierbaum, and S.R. Leone, J. Chem. Phys. **98,** 9496 (1993).

[16] P.W. Harland and B.J. McIntosh, Int. J. Mass Spec. Ion Proc. **54,** 217 (1983).

[17] P.W. Harland and B.J. Mcintosh, Int. J. Mass Spec. Ion Proc. **57,** 283 (1984).

[18] L.A. Viehland and E.A. Mason, At. Data Nucl. Data Tables **16,** 495 (1975).

[19] M. Waldman and E.A. Mason, Chem. Phys. **58,** 121 (1981).

[20] H.W. Ellis, M.G. Thackston, E.W. McDaniel, and E.A. Mason, At. Data Nucl. Data Tables **31,** 113 (1984).

[21] H. Pauly, in *Atom-Molecule Collision Theory,* edited by R.B. Bernstein, (Plenum Press, New York, 1979).

[22] D.E. Woon and T.H. Dunning Jr., J. Chem. Phys. **100,** 2975 (1994).

[23] `http://www.nist.gov.`

[24] J.M. Hughes and E.I. von Nagy-Felsobuki, Eur. Phys. J. D **6,** 185 (1999).

[25] H.-J. Werner and P.J. Knowles, J. Chem. Phys. **89,** 5803 (1988).

[26] P.J. Knowles and H.-J. Werner, Chem. Phys. Lett. **145,** 514 (1988).

[27] H.-J. Werner and P.J. Knowles, J. Chem. Phys. **82,** 5053 (1985).

[28] P.J. Knowles and H.-J. Werner, Chem. Phys. Lett. **115,** 259 (1985).

[29] E.R. Davidson and D.W. Silver, Chem. Phys. Lett. **53,** 403 (1977).

[30] S.F. Boys and F. Bernardi, Mol. Phys. **19,** 553 (1970).

[31] H. -J. Werner, P. J. Knowles, R. Lindh, F.R. Manby, M. Schütz, P. Celani, T. Korona, G. Rauhut, R.D. Amos, A. Bernhardsson, A. Berning, D.L. Cooper, M.J.O. Deegan, A.J. Dobbyn, F. Eckert, C. Hampel, G. Hetzer, A.W. Lloyd, S.J. McNicholas, W. Meyer, M.E. Mura, A. Nicklass, P. Palmieri, R. Pitzer, U. Schumann, H. Stoll, A.J. Stone, R. Tarroni, T. Thorsteinsson, MOLPRO, version 2002.6, a package of *ab initio* programs.

[32] R. Côté and A. Dalgarno, Phys. Rev. A **62,** 012709 (2000).

[33] F. Bouchelaghem and M. Bouledroua, Phys. Chem. Chem. Phys. **16,** 1875 (2014).

[34] G. Łach, B. Jezionski, and K. Szalewicz, Phys. Rev. Lett. **92,** 233001 (2004).

[35] J.W. Schmidt, R.M. Gavioso, E.F. May, and M.R. Moldover, Phys. Rev. Lett. **98,** 254504 (2007).

[36] M. Masili and A.F. Starace, Phys. Rev. A **68,** 012508 (2003).

[37] J. Mitroy, M.S. Safronova, and C.W. Clark, J. Phys. B **43,** 202001 (2010).

[38] S. Kar and Y.K. Ho, Phys. Rev. A **80,** 062511 (2009).

[39] Z.-C. Yan, J.F. Babb, A. Dalgarno, and G.W.F. Drake, Phys. Rev. A **54,** 2824 (1996).

[40] S.T. Grice, P.W. Harland and R.G.A.R. MacLagan, Int. J. Mass Spectrom. Ion Processes **87,** 181 (1989).

[41] G. Frenking, W. Koch, D. Cremer, J. Gauss, and J.F. Liebman, J. Phys. Chem. **93,** 3397 (1989).

[42] E.D. Jemmis, M.W. Wong, H.-B. Bürgi, and L. Radom, J. Mol. Struct. (Theochem.) **261,** 385 (1992).

[43] L.A. Viehland and Y. Chang, Comput. Phys. Commun. **181,** 1687 (2010).

[44] H. O'Hara and F.J. Smith, J. Comput. Phys. **5,** 328 (1970).

[45] J.C. Rainwater, P.M. Holland, and L. Biolsi, J. Chem. Phys. **77,** 434 (1982).

[46] H. Jeffreys, Proc. Lond. Math. Soc. **23,** 428 (1942).

[47] R.J. Munn, E.A. Mason, and F.J. Smith, J. Chem. Phys. **41,** 3978 (1964).

[48] A. Dalgarno, M.R.C. McDowell, and A. Williams, Proc. Phys. Soc. A. **250,** 411 (1958).

[49] N.F. Mott and H.S.W. Massey, *The Theory of Atomic Collisions,* (Oxford University Press, Oxford, 1965).

[50] H.W. Ellis, E.W. McDaniel, D.L. Albritton, L.A. Viehland, S.L. Lin, and E.A. Mason, At. Data Nucl. Data Tables **22,** 179 (1978).

[51] H.W. Ellis, R.Y. Pai, E.W. McDaniel, E.A. Mason, and L.A. Viehland, At. Data Nucl. Data Tables **17,** 177 (1976).

[52] R.W. Simpson, R.G.A.R. Maclagan, and P.W. Harland, J. Chem. Phys. **87,** 419 (1987).

[53] I. Dotan, F.C. Fehsenfeld, and D.L. Albritton, J. Chem. Phys. **71,** 4762 (1979).

[54] R. Thomas, J. Barassin, and A. Barassin, Int. J. Mass Spectrom. Ion Phys. **31,** 227 (1979).

[55] K. Peska, G. Sejkora, H. Störi, F. Egger, H. Ramler, M. Kriegel, and W. Lindinger, in *3rd Symposium Atomic and Surface Physics,* W. Lindinger, F. Howorka, T.D. Mark, F. Egger, Eds, (Innsbruck, 1982), p. 318.

[56] N.D. Twiddy, A. Mohebati, and M. Tichy, Int. J. Mass Spectrom. Ion Processes **74,** 251 (1986).

[57] L.A. Viehland, Aust. J. Phys. **50,** 671 (1997).